The University Of Sheffield.

Investigating the role of myosin 7a in mechanotransduction

Anna Underhill

The University of Sheffield

Faculty of Science

Department of Biosciences

June 2022

Acknowledgements

First and foremost, I would like to thank my supervisor, Walter Marcotti, for sharing his passion for hearing research and electrophysiology. For his always challenging me to improve, for his advice and insight and for always being around to help solve a patching question or talk through any problems. I have learnt so much during this PhD and that is all down to Walters excellent supervision.

To Hubashia, Piece and Fanbo who started the PhD at the same time as me. Thank you for sharing this journey and always being there to celebrate the successes and commiserate the losses. To Adam, Stuart and Ginny for helping with so many of my experiments and patiently answering my endless questions. And to everyone else, all the past and present lab members for the cake, trips to the pub and always being willing to lend a hand. This lab has been such an amazing and supportive place to work over the last four years.

Next, I would like to thank my parents, all my family and Bella and Belinda and for giving me the support to be able to complete my PhD. I truly wouldn't have been able to do anything that I have achieved without them. They have always supported everything I do I would particularly like to thank them for their unending backing of my dream to cure deaf mice.

Lastly my thanks to Scott for listening to all my complaints, talking through all the problems and for learning an impressive amount about hearing research and electrophysiology. Thank you for always being there for me.

Declaration

I, the author, confirm that the Thesis is my own work, except in cases where it is clearly specified in the text and outlined below. All work that is not my own was reproduced with consent. I am aware of the University's Guidance on the Use of Unfair Means (www.sheffield.ac.uk/ssid/unfair-means). This work has not previously been presented for an award at this, or any other, university.

All ABR and DPOAE work was carried out by Walter Marcotti

All inner hair cell recordings were carried out by Adam Carlton

Abstract

In the auditory system, sound waves are translated into electrical signals through a process called mechanoelectrical transduction (MET). Myosin 7a is believed to be integral to mechanoelectrical transduction, in particular, to the gating of the MET channel (Grati and Kachar, 2011). In humans, mutations to myosin 7a causes a disease known as Usher syndrome type 1B, which causes profound deafness, blindness and vestibular dysfunction (Well *et al.*, 1995). Understanding the role of myosin 7a would provide more information on the process of mechanotransduction as a whole. It would also provide insight into how myosin 7a could be targeted for treatment in Usher syndrome.

To better understand the role of myosin 7a in mechanoelectrical transduction, two different mouse models were used. One was a conditional knockout of myosin 7a and the other was a point mutation of myosin 7a (known as the *Shaker-1* mouse). Electrophysiological recordings were performed to investigate the MET current biophysical characteristics. Scanning electron microscopy and immunostaining was used to investigate the morphology of the hair bundle.

The results from my project show that myosin 7a is required for mechanoelectrical transduction and hearing. Both mouse models were deaf and showed a decline in size of the MET current. In the *Shaker-1* mouse model there were morphological changes to the hair bundle in early ages. However, this was not seen in the conditional knockout model, suggesting that myosin 7a has two roles in the hair cell. One in early development of the hair bundle, and one later on in maintaining the MET current of the cell.

This work has provided greater information on the role of myosin 7a and shown that it is vital for the proper development and maintenance of the hair cell. However, the precise role that myosin 7a plays in the hair cell is still unknown.

Table of Contents

Figure list

Table list

List of Abbreviations

6N	C57BL/6NTac
ABR	Auditory Brain stem responses
ADP	Adenosine di-phosphate
ANOVA	Analysis of variance
ATP	Adenosine triphosphate
BAPTA	1,2-bis(*o*-aminophenoxy)ethane-*N*,*N*,*N'*,*N'*-tetra acetic acid
BK	Big potassium channel
CIB1	Calcium and integrin binding family member 1
cKO	Conditional knock-out
CLRN2	Clarin-2
DAPI	4',6-diamidino-2-phenylindole
DNA	Deoxyribonucleic Acid
DPOAE	Distortion product otoacoustic emissions
EDTA	Ethylenediaminetetraacetic acid
ENU	N-ethyl-N-nitrosourea
EP	Endocochlear potential
FERM	4.1 protein, ezrin, radixin, moesin
I_{Ca}	Calcium current
ICS	Intracellular solution
IHC	Inner hair cell
I_K	Potassium current
I_{Na}	Sodium current
KCNJ10	ATP-sensitive inward rectifier potassium channel 10
KCNQ1	Potassium voltage-gated channel subfamily Q member 1
KCNQ4	Potassium voltage-gated channel subfamily Q member 4
KO	Knock-out
LHFPL5	Lipoma HMGIC fusion partner-like 5 gene
LOC	Lateral olivary complex
LRTOMT	Leucine rich transmembrane and O-methyl transferase domain

MET	Mechanoelectrical transduction
MOC	Medial olivocochlear neurons
MYO7A	Myosin 7a
NMDA	N-methyl-D-aspartate
OHC	Outer hair cell
P(X)	Post-natal day
PBS	Phospho-buffered saline
PBST	Phosphate-buffered saline/tween
PCDH15	Protocadherin-15
PCR	Polymerase chain reaction
PFA	Paraformaldehyde
PGK	Phosphoglycerate kinase
PIP_2	Phosphatidylinositol 4,5-bisphosphate
PMCA	Plasma membrane Ca^{2+}-ATPase pump
RNA	Ribonucleic acid
SEM	Scanning electron microscopy
SGN	Spiral ganglion neuron
SH3	Sarcoma Homology 3 domain
SLC26A6	Solute carrier family 26 member 6
SLC26Q5	Solute carrier family 26 member 5
SPL	Sound pressure level
TCH	Thiocarbohydrazide
TECTA	Tectorin-A
TM	Tectorial membrane
TMC	Trans-membrane channel-like protein
TMIE	Trans-membrane inner ear
TOMT	Transmembrane O-Methyl transferase
TRPV1	Transient receptor potential cation channel subfamily v member 1
USH1B	Usher syndrome type 1B
USH3A	Usher syndrome type 3A
VLGR1	Very large G protein-coupled receptor 1

Chapter 1 -General introduction

1.1 Mammalian auditory system

Sound waves are collected from the world around us and are focused into the ear canal by the external part of the ear, called the pinna. The structure of the external, middle and inner ear is shown in Figure 1.1. As sound waves enter the ear canal they push against the eardrum. The eardrum is a membrane that separates the external and middle ear. The vibrations from the sound waves are transmitted along the middle ear to the inner ear by three small bones called the malleus, stapes and incus. These three bones allow impedance matching from sound waves in the air to the fluid filled cochlea. When sound waves in the air reach a liquid most of the energy is reflected. The bones in the middle ear concentrate the pressure from the sound vibrations so less energy is lost. They do this in two ways; one is that the area of the eardrum is much larger than the footplate of the stapes, which connects to the oval window in the cochlea, this concentrates the sound pressure to a much smaller area. The second is that the three bones act as a lever, to further increase the pressure on the oval window.

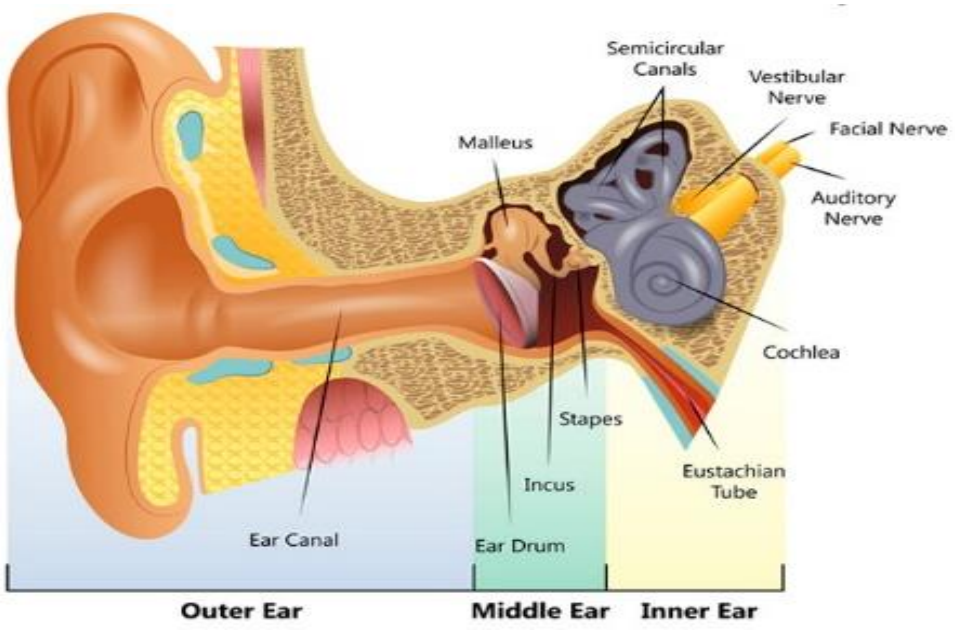

Figure 1.1- Diagram showing the anatomy of the ear

There are three parts to the ear, the outer ear, the middle ear and the inner ear. The outer ear is made up of the pinna and the ear canal. In the middle ear there are three small bones, the malleus, incus and stapes. The inner ear contains the cochlea, semi-circular canals and nerve fibres (Hearing link, 2018).

The inner ear is made up of two parts, the cochlea which is responsible for detecting sound, and the vestibular system which is involved in maintaining balance. The cochlea is a coiled structure encased in bone. There are two openings in the bony shell around the cochlea, the oval and round window. Vibrations of the stapes pushes on the oval window and increases the pressure in the fluid filled cochlea. In response to the increase in pressure the round window bulges outwards. Through the cochlea runs a membrane of varying width and stiffness, called the basilar membrane. Sound waves move along the basilar membrane in a travelling wave, with the area of greatest membrane displacement dependant on the frequency of the sound (Figure 1.2). As the basilar membrane is widest and least stiff at the apex of the cochlea, low frequency sounds cause the largest displacement at the apex and high frequency sounds cause the largest displacement at the base of the cochlea. The frequency of sound that a section of membrane is most sensitive to is known as its characteristic frequency.

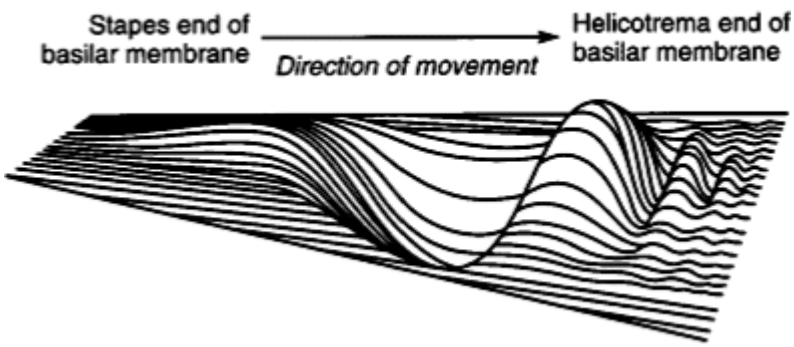

Figure 1.2- Diagram showing the travelling wave moving along the basilar membrane

Changes in pressure in the cochlea, caused by sound waves, elicits a travelling wave along the basilar membrane (Scottish Sensory Centre, 2010).

Within the cochlea, below the basilar membrane, is a smaller structure called the organ of Corti. The organ of Corti is comprised of a tectorial membrane that sits on top of three rows of outer hair cells (OHC) and one row of inner hair cells (IHC). As the travelling wave moves along the basilar membrane the tectorial membrane in the organ of Corti moves up and down and causes deflection of stereocilia on top of the inner and outer hair cells. The tallest row of outer hair cell stereocilia connects directly to the tectorial membrane, whereas the stereocilia

on top on IHCs are not connected and are free-floating and they are moved by fluid motion beneath the tectorial membrane.

In mammalian hair cells there are 20-300 stereocilia on top of each hair cell arranged in three rows of increasing height. The stereocilia are made up of packs of actin filaments that are inserted in the cuticular plate at the apical end of the cell. Connecting each row of stereocilia are tip links which are connected to ion channels on top of the two shorter rows of stereocilia, known as mechanoelectrical transducer (MET) channels. When the stereocilia are deflected the tip links stretch and open the MET channels, allowing K^+ and Ca^{2+} ions to enter the cell. The influx of K^+ ions depolarises the hair cell (Goutman et al., 2015). A graded receptor potential is generated that can modulate the fusion of synaptic vesicles and glutamate release from ribbon synapses (Glowatzki & Fuchs, 2002).

Spiral ganglion neurons synapse onto the inner and outer hair cells and carry the information to the brain. The axons from the spiral ganglion neurons form the axon of the auditory nerve fibre. This nerve fibre then innervates the three sections of the cochlea nucleus complex: the anteroventral, posteroventral and dorsal cochlea nucleus. The cochlea nucleus complex is organised tonotopically with fibres from different areas of the cochlea innervating different sections. The tonotopic arrangement is shown in Figure 1.3. Fibres from the basal areas innervate the ventral regions and fibres from the apical areas innervate the dorsal regions (Kandler et al., 2009).

Some fibres from the ventral and dorsal cochlea nuclei travel to the inferior colliculus and some travel to the superior olivary complex. The superior olivary complex (SOC) is involved in the localisation of sound. The SOC contains the lateral superior olive (LSO), medial superior olive (MSO) and the medial nucleus of the trapezoid body (MNTB) (Masterton et al., 1967). All the input then converges in the inferior colliculus which integrates information about sound identification and sound localisation. This then projects to the medial geniculate nucleus in the thalamus and finally projects to the primary auditory cortex located in the cerebral cortex. There is also tonotopic arrangement of input in the primary auditory cortex (Kelly & Sally, 1988; Pickles, 2015).

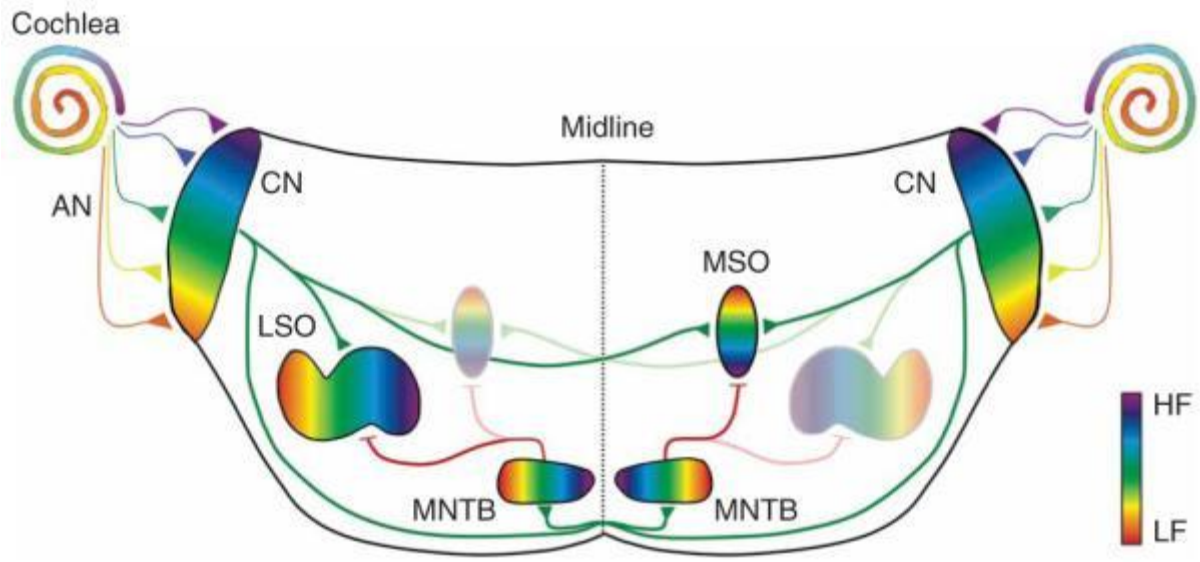

Figure 1.3- Diagram showing the pathway of auditory signals in the brainstem

Schematic of auditory circuits in the brainstem showing tonotopic organisation of input. Excitatory connections are shown in green, and inhibitory connections are shown in red. A colour gradient from high to low frequency shows the tonotopic arrangement of the brain stem. CN- cochlea nucleus, LSO- lateral superior olive, MSO- medial superior olive, MNTB- medial nucleus of the trapezoid body, AN- auditory nerve, HF- high frequency, LF- low frequency (Kandler et al., 2009)

1.1.1 General structure of the inner ear

The cochlea is located in the temporal bone at the base of the skull. In mice it is 0.2 mm in diameter with a length of 6 mm, compared to a length of 35 mm in humans. There are two and half turns of the cochlea in mice and humans, although this varies in other species (Fettiplace, 2017).

Figure 1.4 shows a cross section of the cochlea. The cochlea is split into three main chambers: the scala vestibuli, the scala media and the scala tympani. The solutions inside the three chambers are markedly different. Inside the scala vestibuli and scala tympani is fluid known as perilymph, which has an ionic composition similar to normal extracellular solution. The fluid inside the scala media is more similar to intracellular solution and is known as endolymph. The scala vestibuli is connected with the scala tympani via an opening called the helicotrema.

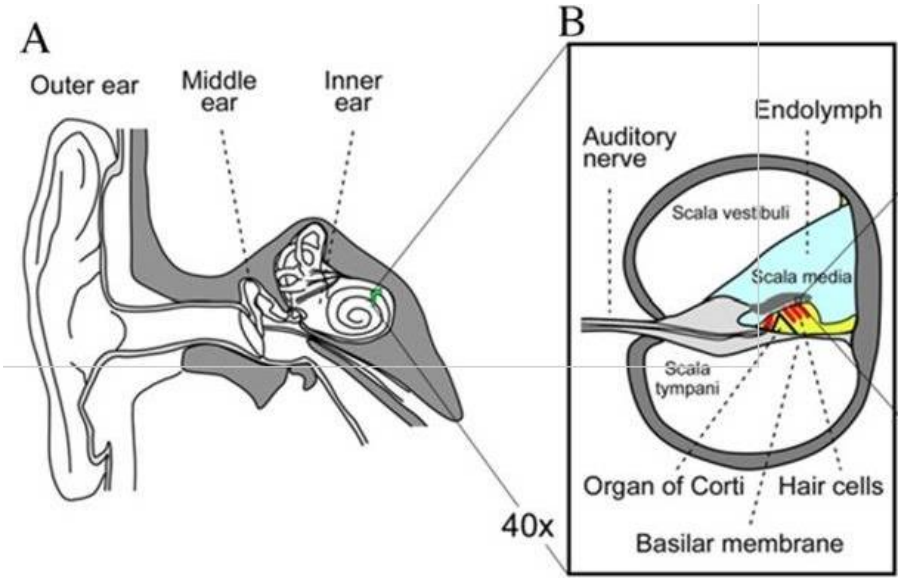

Figure 1.4- A cross-section of the cochlea

(A) Cross section of ear showing the outer ear, middle ear and inner ear. (B) Cross section of cochlea showing the three sections of the cochlea and location of the organ of corti. The scala media contains a solution known as endolymph (Elliott and Shera, 2012).

The scala vestibuli is located at the top of the cochlea and is separated from the scala media by the Reissner's membrane. This membrane is made up of two cell layers and separates the fluid in the scala media (endolymph) from the fluid in the scala vestibuli (perilymph) (Duvall & Rhodes, 1967). The Reissner's membrane acts as an ionic barrier to ions and might be involved in the regulation of the ionic composition of endolymph and perilymph by selectively pumping ions across the membrane (Raphael & Altschuler, 2003).

The scala tympani is located at the bottom and is separated from the scala media by the basilar membrane (Elliott & Shera, 2012). At the end of the scala tympani is the oval window, where sound vibrations are transmitted to the cochlea. The fluid in the cochlea is continuous with the saccule, utricle and the three semi-circular canals that make up the vestibular system (Fettiplace, 2017).

In the cochlea there are sensory hair cells that are responsible for detecting and transmitting sound information to the brain. Underneath the apical membrane of the hair cell is the cuticular plate. The role of the cuticular plate is to support and anchor the base of the

stereocilia (Raphael & Altschuler, 2003). There are also supporting cells that surround the hair cells and support their function. The IHCs are surrounded by inner pharyngeal and border cells. The OHCs are surrounded by Deiter cells. There are also inner and outer pillar cells that form the tunnel of Corti and separate the two domains of inner and outer hair cells (Basch et al., 2016).

Supporting cells link to each other and to hair cells via tight and adherens junctions. They also communicate with other supporting cells via gap junctions. The supporting cells have many roles in the cochlea. For example, they have a rigid cytoskeleton that helps to maintain the structural integrity of the cochlea during movement of the head or sound stimulation. They also generate some of the components for the tectorial membrane in the organ of Corti (Wan et al., 2013).

1.1.2 Perilymph and Endolymph

The ionic composition of the solutions that surround the hair cells is vitally important for their function (see Table 1.1). The endolymph is the solution that bathes the apical surface and stereocilia of the hair cells. The endolymph has an unusually high K^+ (157 mM) and low Na^+ (1mM) concentration. The perilymph bathes the basolateral side of the hair cells and has low levels of K^+ (4mM) (Wangemann & Schacht, 1996). Tight junctions between the supporting cells and hair cells separate the endolymph and perilymph (Ben-Yosef et al., 2003). Tight junctions are intracellular adhesion complexes that form size and charge selective gates in epithelia and endothelia. Tight junctions regulate the diffusion of ions and solutes across epithelia (Farquhar & Palade, 1963).

This difference in ionic composition between the two solutions means the endolymph has an endocochlear potential (EP) of +80mV relative to the perilymph. This EP is the driving force that forces K^+ ions into the hair cell through open MET channels (Adachi et al., 2013).

Ion	Perilymph (mM)	Endolymph (mM)
Na^+	148	1.3
K^+	4	157
Ca^{2+}	1.3	0.02
Cl^-	119	132
HCO_3^-	21	31

Table 1.1-The ionic composition of endolymph and perilymph

The table details the ionic composition of the perilymph and endolymph solutions (Wangemann and Schacht., 1996).

The ionic composition of the endolymph is maintained by a K^+ ion recycling pathway (this pathway is demonstrated in Figure 1.5) (Tasaki & Spyropoulos, 1959). The EP drives K^+ ions from the endolymph into the hair cells through MET channels on top of stereocilia, then out of the hair cell and into the perilymph, across the basolateral membrane of the cell. From the perilymph, K^+ is taken up by fibrocytes that make up the spiral ligament. K^+ then diffuses into strial intermediate cells via the KCNJ10 K^+ channels (Marcus et al., 2002). From here K^+ is taken up by the strial marginal cells and secreted back into the endolymph (Wangemann et al., 1995).

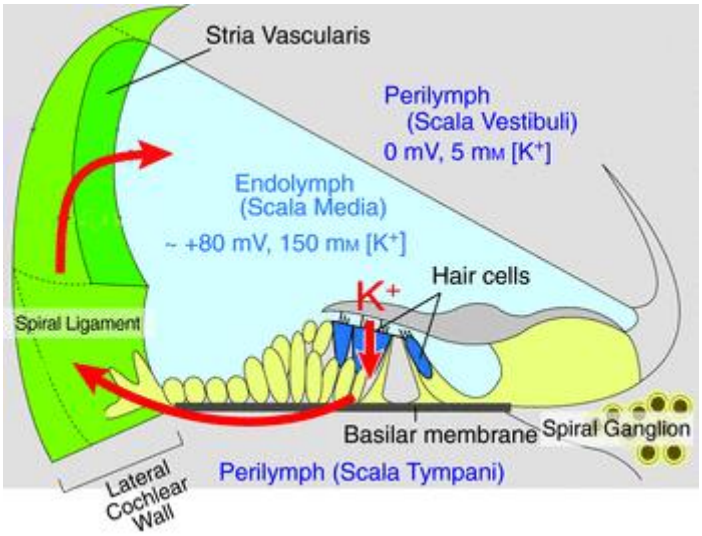

Figure 1.5- Diagram demonstrating the recycling of potassium ions from the perilymph, back to the endolymph

The endocochlear potential drives potassium ions into the hair cells from the endolymph, then out of the cell into the perilymph. Potassium ions are then recycled back into the endolymph by the spiral ligament (Image modified from Adachi et al., 2013).

The calcium ion concentration in the endolymph is also unusual in that it is very low compared to the perilymph. In mice, the calcium ion concentration in the endolymph is only 20-40 µM, compared to 1.3 mM in the perilymph (Wangemann & Schacht, 1996). Ca^{2+} ions enter the hair cells cytoplasm through the MET and voltage sensitive Ca^{2+} channels. The plasma membrane Ca^{2+}-ATPase pump (PMCA), that is located on the stereocilia, actively pumps Ca^{2+} ions that have accumulated in the cytoplasm back into the endolymph (Beurg et al., 2010). This pump is highly expressed in the hair bundle of the OHCs and IHCs, as well as in vestibular hair cells (Dumont et al., 2001).

1.1.3 Hair cell structure and function

On top of each hair cell is an array of connected stereocilia that contain MET channels, known as the hair bundle (Figure 1.6). Stereocilia are made up of actin filaments arranged in parallel and cross-linked by cross-linking proteins such as fimbrin. Hair cells possess a dense core of

actin filaments that they use to extend the stereocilia (A. Flock & Cheung, 1977; Sobin & Flock, 1983).

The hair bundle is arranged in two or more rows of stereocilia of increasing height connected by tip links (Fettiplace, 2017). Tip links are extracellular filaments that connect the MET channel on the tip of shorter rows of stereocilia to the lateral wall of taller stereocilia (Pickles et al., 1984).

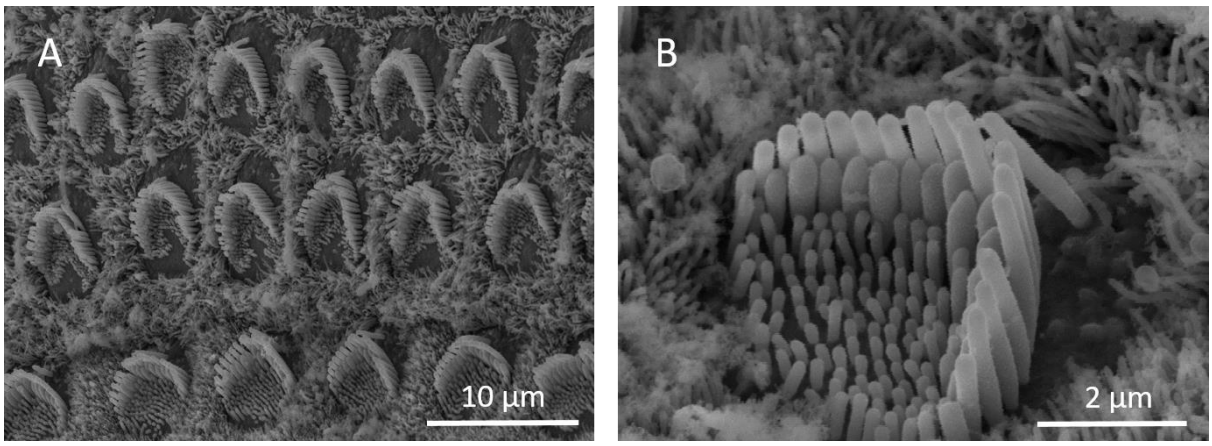

Figure 1.6- Scanning electron microscopy image of P4 mouse outer hair cells

(A) SEM image of OHCs in an apical section of a P4 mouse cochlea. (B) Close up image of a hair cell showing the three main rows of stereocilia. At this immature stage there are many small stereocilia around the hair bundle that disappear as the hair bundle matures (Image taken by Anna Underhill)

The IHCs are the primary sensory cells and are responsible for detecting sound and sending the information to the brain. IHCs are pear-shaped and have a round nucleus located in the centre of the cell body (Raphael & Altschuler, 2003). Each IHC has anywhere between twenty and a few hundred stereocilia arranged in three rows of increasing height and inserted into the cuticular plate (Purves et al., 2001). The OHCs are responsible for the mechanical amplification process and the fine tuning and sensitivity of the ear (Goutman et al., 2015; Schnupp et al., 2011).

The properties of the hair cells change along the cochlea. For example, at the apex of the cochlea, where the lowest frequency sounds are encoded, the hair bundles on top of the IHCs

are longer than they are at the base and less stiff. Also, the OHCs at the apex are bigger than they are at the base (Fettiplace & Hackney, 2006).

There are several other lateral links between stereocilia that are not involved in mechanotransduction (see Figure 1.7). There are horizontal tip connectors, shaft connectors and ankle links (Goodyear et al., 2005). These lateral links could be involved in maintaining the integrity of the hair bundle or transmitting force throughout the bundle (Gowri D. et al., 2007).

The lateral links present in stereocilia varies throughout development. Early in development transient lateral links connect adjacent stereocilia and kinociliary links connect the kinocilium to stereocilia next to it. As the hair bundle develops, ankle links appear at the base and tip links appear at the tips of stereocilia. As the hair bundle matures the kinociliary links, transient lateral links and ankle links disappear in the cochlea hair bundle, although some lateral links remain in the vestibular system (Goodyear et al., 2005).

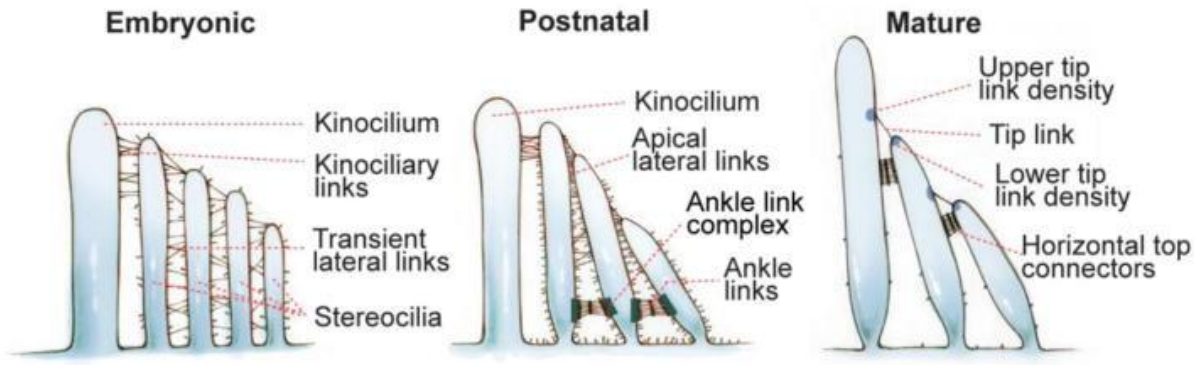

Figure 1.7- Cross-section of the stereocilia bundle showing lateral links between stereocilia throughout development

The presence of lateral links between stereocilia change between embryonic, postnatal and mature hair cells. (Mathur and Yang, 2015).

1.1.4 Electromotility

The role of the OHCs is to amplify the signal to the IHCs by augmenting the movement of the basilar membrane. They achieve this by contracting or elongating their cell body. The OHCs can be made to change their length by changing the membrane potential; this ability is known

as electromotility (Brownell et al., 1985). The molecule in the OHC that is responsible for electromotility is known as prestin. Prestin is part of the SLC26Q5 anion transporter family and is abundant in the lateral membranes of OHCs (see Figure 1.8 for location of prestin) (Lohi et al., 2000).

Movement and mobility of prestin is voltage dependent (Dallos et al., 2006; Karniski et al., 1998). Prestin is an incomplete transporter that behaves as a mechanoenzyme as part of its transport cycle, however this cycle is not complete. Binding of an intracellular chloride ion causes a conformational change in the protein that increases the length of the OHCs (Ashmore, 2019). When the hair bundle is deflected, ions enter the cell from the endolymph and depolarise the cell. Depolarization of the hair cell causes a decrease in Cl^- binding to prestin and contraction of the cell (Homma & Dallos, 2011).

Contraction and elongation of the hair cell can augment displacement of the basilar membrane by 1000X (Ren et al., 2011). Augmenting displacement of the basilar membrane at the characteristic frequency can sharpen the tuning curve and improve frequency selection (Oghalai, 2004). When prestin was mutated to be inactive, the sharp tuning of the basilar membrane was lost. Frequency selectivity and cochlea sensitivity were also reduced (Dallos et al., 2008).

The sensing of basilar membrane movement means the OHCs can be involved in a feedback loop that controls tuning of the basilar membrane (Ashmore, 2019). Negative feedback from the efferent nerve fibres can be used to reduce movement of the basilar membrane and protect the cochlea from overstimulation (Oghalai, 2004).

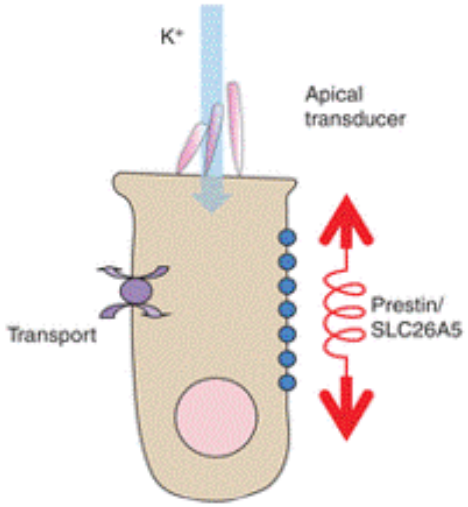

Figure 1.8- Diagram showing the location of prestin in an outer hair cell

Diagram showing the location of prestin in OHCs. Prestin is located in the lateral wall of OHCs and generates longitudinal forces (Ashmore, 2019).

1.1.5 Innervation of hair cells

In the cochlea, spiral ganglion neurons (SGN) innervate the hair cells and synapse onto cochlea neurons in the brain stem. Innervation to the cochlea differs between the inner and outer hair cells. Type I SGN's synapse onto IHCs and type II SGN's synapse onto OHCs. In the adult cochlea, OHCs have both efferent and afferent connections, in contrast, IHCs only have afferent connections. OHCs receive input from medial olivocochlear neurons (MOC) directly onto their cell bodies (Ashmore, 1994; Patuzzi & Robertson, 1988).

Hair cells and SGN's are connected by glutamatergic ribbon synapses. Ribbon synapses are characterised by an electron dense structure and possess specialised organelles called ribbons. Ribbon synapses hold vesicles close to the active zone and convey information by continuously changing the rate that glutamate is released. This allows for fast and sustained neurotransmission (Coate et al., 2019; Odermatt & Lagnado, 2009).

Type I spiral ganglion neurons (SGN) are bipolar, unbranched neurons that each contact with one IHC. Each IHC can contact 6-20 type I SGN's (Meyer et al., 2009). The type I SGN's are all myelinated and their role is to carry sound information from the IHCs to the brain (Spoendlin, 1981). Efferent connections from the lateral olivary complex (LOC) synapse with type I SGN's just below the IHCs and can be branched or unbranched. Their function is unknown but as

they have an inhibitory input it could be that they have a protective role (M. Frank & Goodrich, 2018).

Type II SGN's are branched, unmyelinated fibres and each one can contact 3-10 OHCs (Berglund & Ryugo, 1987; Spoendlin, 1981). The role of the type II SGN's is so far unclear as they don't seem to respond to sound. It is possible that these neurons protect against overstimulation and their role is related to nociception sensing (C. Liu et al., 2015).

In the rest of the body, noxious stimuli are detected by somatosensory neurons, however these neurons are not present in the cochlea. Therefore, it is unclear how the cochlea detects noxious sounds and tissue damage. There are several pieces of evidence that OHCs are involved in nociception sensing. Loud noises cause damage to hair cells, particularly to OHCs. To investigate the role of OHCs a mouse model was created where the canonical auditory pathway was silenced. This pathway consists of glutamate release by the IHCs that activates type I spiral ganglion neurons. In this mouse model there was no activity in the cochlea nuclei at lower sound levels (80dB), but very loud sounds (120dB) did trigger activity. This suggests there is an alternative noxious sound sensing pathway in the cochlea. As this response originated in the cochlea it seems likely that this pathway is mediated by the type II spiral ganglion neurons (Flores et al., 2015).

It is also thought that the type II afferent fibres are involved in the medial olivocochlear reflex suppression of the cochlear amplifier. The cochlear amplifier works to amplify vibrations in a particular region of the cochlea. Suppression of this amplifier helps to hear specific sounds in a noisy room, with sound localisation and protects against over-stimulation. In a mouse model with no type II SGN innervation of OHCs and normal IHC innervation, there was no suppression of the cochlear amplifier (Froud et al., 2015).

Efferent connections to OHCs from the MOC are branched and can form large inhibitory complexes with many OHCs (Warr & Guinan, 1979). The MOC efferent reduces amplification in the cochlea via the OHCs (M. M. Frank & Goodrich, 2018). The medial olivocochlear neurons control conductance of the hair cell to K^+, this leads to hyperpolarisation of the cell and reduction of cochlea sensitivity (Ashmore, 1994).

1.1.6 Development of the cochlea

The organ of Corti is derived from the pro-sensory domain of $Sox2^{+}$ progenitor cells (Jacques et al., 2012). From embryonic day 10-12 (E10-12) the cochlea undergoes an initial period of proliferation and elongation (Basch et al., 2016). After this, from E12-E14.5, the cyclin dependent kinase inhibitor $p27^{kip1}$ is upregulated and the hair cells start to enter terminal mitosis (Lee et al., 2006). The cells at the apex start terminal mitosis first, then moving down the cochlea, with cells at the base entering terminal mitosis last.

The cyclin dependent kinase inhibitors $p21^{cip1}$ and $p19^{ink4d}$ are also needed to maintain the viability of the cells and the post-mitotic state. One of the roles of cyclin dependent kinases is to promote the progression of the normal cell cycle. Therefore, inhibiting cyclin dependent kinases prevents the hair cell entering the cell division cycle and keeps the cell in a post-mitotic state (Laine et al., 2007).

From E13.5 the proneural gene, Atoh1, starts to be expressed and leads to differentiation of the hair cells. Atoh1 is needed for the formation of mechanoreceptors and photoreceptors (Jarman et al., 1994). Without Atoh1 the prosensory cells can't form hair cells or supporting cells and cell death occurs (N. Pan et al., 2011). Differentiation of the hair cells starts in the mid-basal region of the cochlea duct and spreads down to the base and up to the apex over the next 3-4 days (Basch et al., 2016).

Figure 1.9A shows the changes in channel expression in inner and outer hair cells from E14.5 to adulthood. In terms of their biophysical properties, inner and outer hair cells are very similar from E14.5 up to birth. The inner and outer hair cells start to deviate from each other from birth onwards.

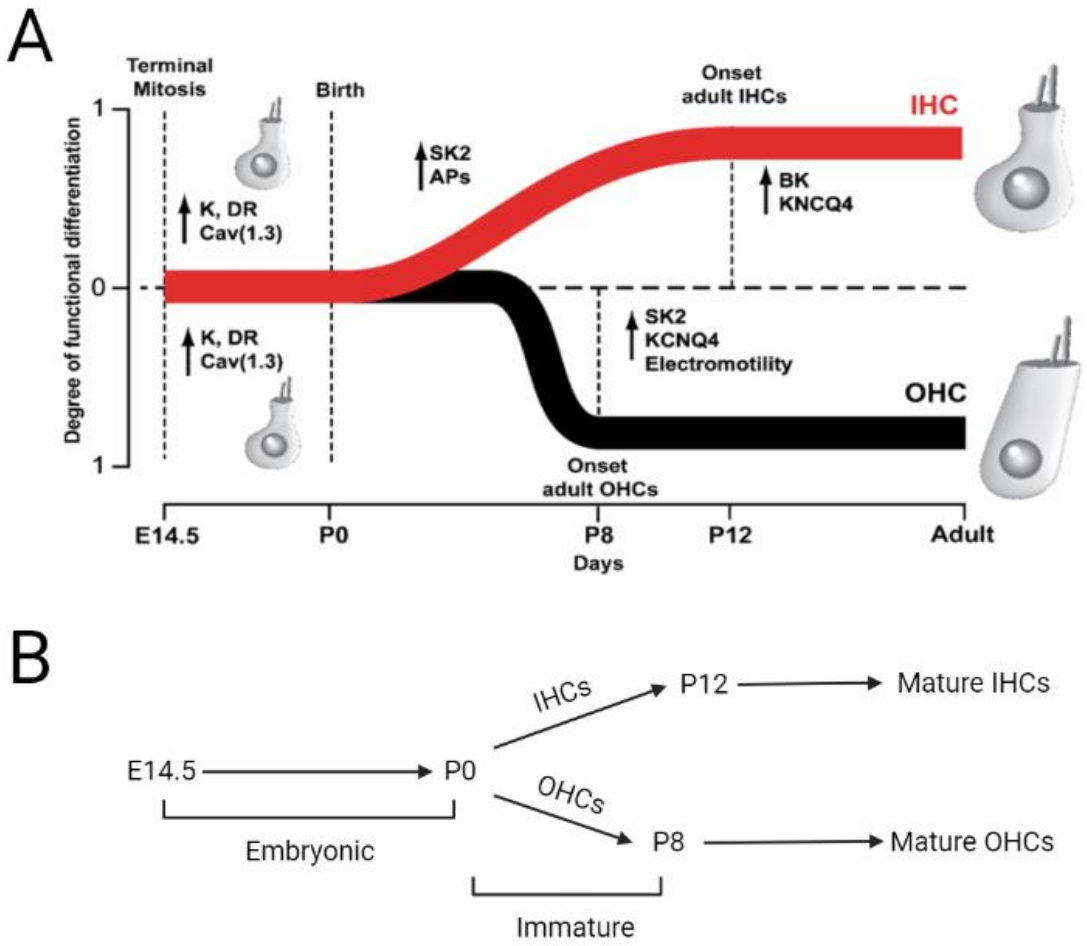

Figure 1.9- Development of ion channels in the inner and outer hair cells

(A) This diagram shows the process of maturation of ion channels in the inner and outer hair cells from embryonic day 14.5 to adulthood. The IHCs reach functional maturity at around P12. OHCs start to differentiate after IHCs but reach functional maturity earlier, at P8 (Marcotti, 2012). (B) Diagram showing the relationship between E/P number and maturity of inner and outer hair cells.

The IHCs start to differentiate first and reach functional maturity after OHCs. One of the characteristics of immature IHCs is the occurrence of spontaneous action potentials. Slow and repetitive spontaneous action potentials start at E18.5. These change to rapid spontaneous action potentials in the first postnatal week. This is needed to develop the connections in the auditory system and causes pruning of the highly branched afferent fibres to one to one contact with inner hair cells (Johnson et al., 2011). The OHCs start differentiating later and are functionally mature by postnatal day 8 (P8). Immature OHCs also show spontaneous

action potentials that disappear once they reach maturity. Maturity of outer hair cells is characterised by electromotility, presence of a delayed rectifying K^+ current ($IK_{,n}$) and the sensitivity to the neurotransmitter acetylcholine (Housley et al., 2006).

The structure of the hair bundle is important to the function of the cell and its development is tightly regulated. Most of the studies into how the stereocilia develop has been carried out using avian hair cells. A diagram showing the development of the hair bundles is shown in Figure 1.10. At the beginning of development, the apical surface of the hair cells is covered in microvilli and in the centre is a single cilium known as the kinocilium. The microvilli then start to extend to form stereocilia of a similar height. The kinocilium moves to the edge of the apical surface and the stereocilia next to the kinocilium start to extend. Following this the stereocilia in the next adjacent row begin to extend. The stereocilia stop growing upwards and start to add actin filaments to increase their width and extend basally to form rootlets into the apical surface. Finally, the stereocilia grow to their final length. In mammalian cells, once the hair cell has matured the kinocilium is lost (Schwander et al., 2010; Tilney et al., 1992).

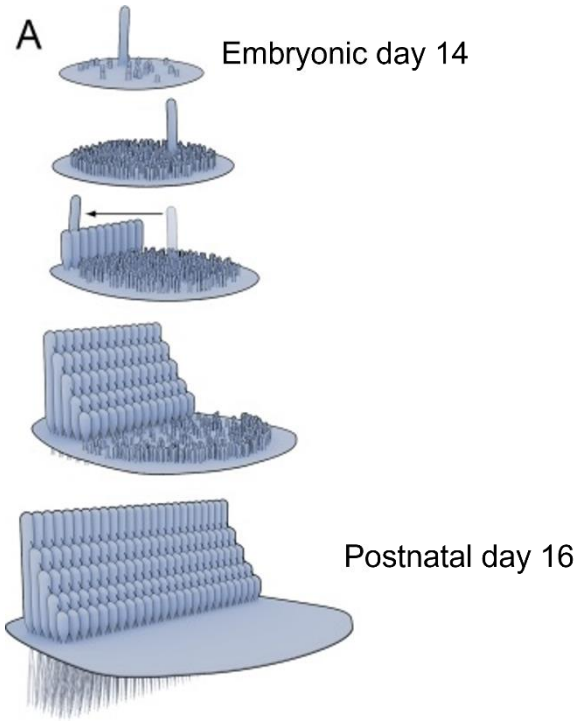

Figure 1.10- Diagram showing the development of the hair bundle

Diagram showing the development of the hair bundle from E14 to P16. At the start of the development of the hair bundle there are many small stereocilia and one large kinocilium. The kinocilium then moves to the edge of the cell and the stereocilia start to extend to form rows of increasing height. The extra, short stereocilia then disappear, leaving the fully developed hair bundle (Schwander et al., 2010).

1.1.7 Development of hair cell ion channels

Immature IHCs and OHCs possess a similar complement of ion channels. Both have an outward potassium current ($I_{K,neo}$) and an inward rectifier potassium current (I_{K1}), a calcium current and a sodium current. However, in the OHCs, all of these currents are a lot smaller. The resting potential in the immature inner and outer hair cells is around -60 mV and these cells fire spontaneous action potentials. When the cells are functionally mature the resting membrane potential changes to be around -70 mV and there are no spontaneous action potentials (Kros et al., 1998). The changes to ion channels through development is shown in Figure 1.11.

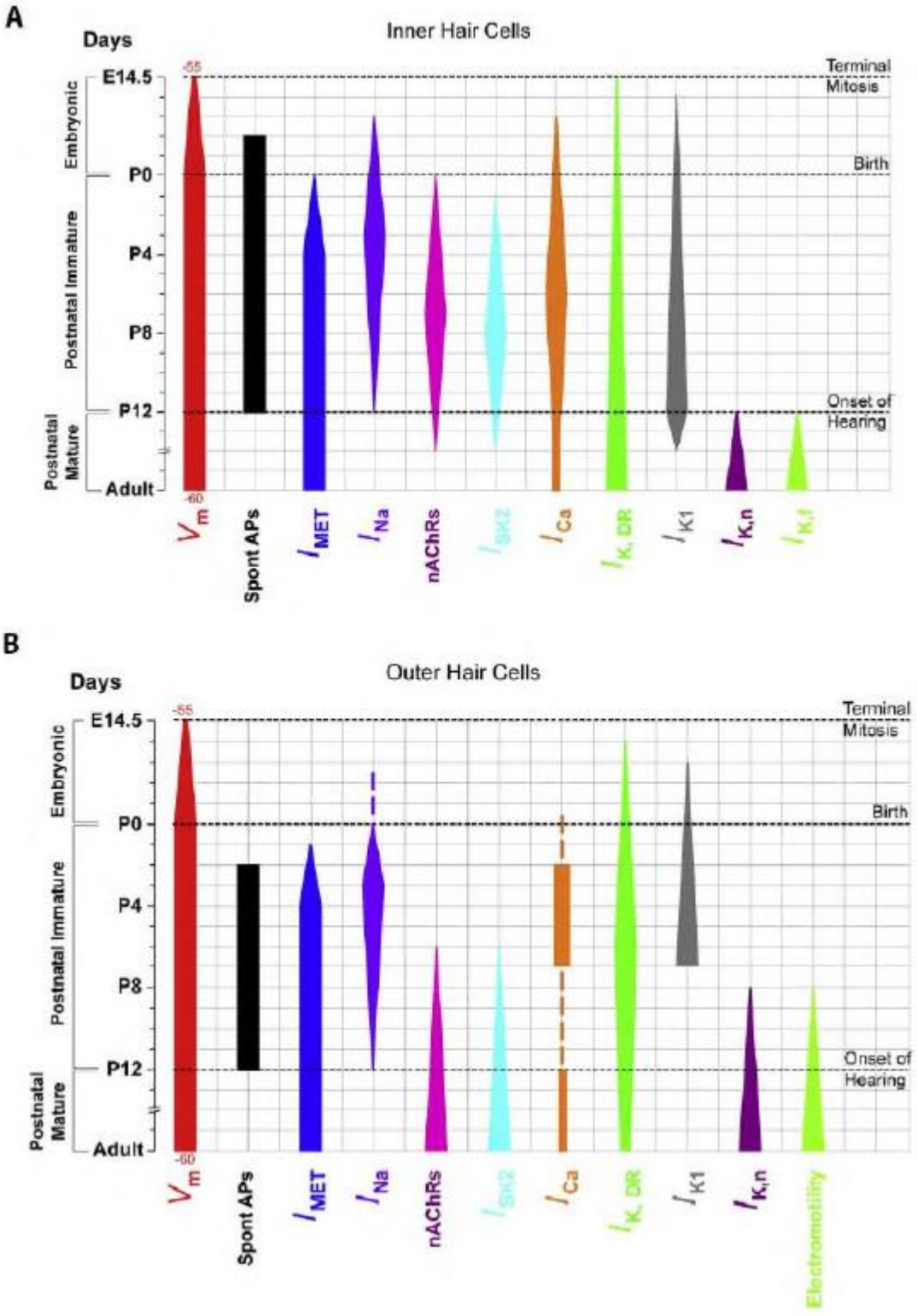

Figure 1.11- Changes to ion channels and hair cell activity throughout development

This diagram illustrates the changes in channel activity that IHCs and OHCs go through, from terminal mitosis up to adulthood (Corns et al., 2014)

In the immature IHCs and OHCs spontaneous action potentials are mainly fired in the first postnatal week. This is because the resting membrane potential is around -50 to -60 mV, which is close to the action potential threshold (Marcotti et al., 2003). There is an inward Ca^{2+} current (I_{Ca}) and a slowly activating delayed rectifier current ($I_{K,neo}$) current that allows for the generation of spontaneous action potentials (Kros et al., 1998). I_{Ca} is activated close to the resting membrane potential of the cell (-65mV) and, together with the immature K^+ currents, speeds up the depolarisation phase of the action potential spike. I_{Ca} decreases the time it takes for the cell to reach threshold and decreases the width of the spike (Marcotti et al., 2003).

When extracellular Ca^{2+} was depleted, no spikes could be elicited (Marcotti, Johnson, Rusch, et al., 2003). The I_{Ca} is carried by voltage dependent L-type Ca^{2+} channels that contains the $Ca_v1.3$ subunit (Michna et al., 2003). $Ca_v1.3$ subunits make up slowly activating L-type Ca^{2+} channels that can activate at more negative potentials (Koschak et al., 2001). This channel begins to be activated at -65 mV and reaches its maximum inward current at about -19 mV (Marcotti, Johnson, Rusch, et al., 2003).

$I_{K,neo}$ activates near -50 mV and shows slow inactivation. This current is believed to be the main route of outward current flow in the basolateral membrane in immature hair cells and is responsible for the repolarisation phase of spontaneous action potentials (Marcotti, Johnson, Holley, et al., 2003; Marcotti & Kros, 1999).

In embryonic and neonatal inner hair cells there is an inward Na^+ current. This current is activated at -60 mV. It is possible that I_{Na} is carried by $Na_v1.7$ voltage gated Na^+ channels (Marcotti, Johnson, Rusch, et al., 2003). Although the I_{Na} current is not involved in generating the spontaneous action potential, it is possible that it reduces the time it takes to reach the threshold for spiking and helps to set the frequency of spikes.

Moving to the second postnatal week, the membrane potential becomes more hyperpolarised and there are fewer spontaneous action potentials. This is due to the inward rectifier K^+ current (I_{K1}) having a bigger role. I_{K1} is the main contributor to the resting membrane potential of the inner hair cells (Marcotti & Kros, 1999).

In IHCs and OHCs, from P12 and P8 respectively, the negatively activated delayed rectifier K^+ current ($I_{K,n}$) begins to be seen. It is thought that this current is involved in the functional

maturation of the hair cells. The $I_{K,n}$ current is carried by the K^+ voltage gated channel that contains KCNQ4 subunits. $I_{K,n}$ is activated above -100 mV and is almost completely open at -60mV. $I_{K,n}$ contributes to the resting membrane potential and helps to prevent spontaneous activity in the mature hair cells by lowering the resting membrane potential to -80 mV (Marcotti, Johnson, Holley, et al., 2003; Marcotti & Kros, 1999).

From the onset of hearing at P12 the IHCs also gain the rapidly activating large conductance Ca^{2+} activated K^+ current ($I_{K,f}$). The $I_{K,f}$ and $I_{K,n}$ currents prevent any spontaneous action potentials in the cell (Kros et al., 1998; Marcotti, Johnson, Holley, et al., 2003). Around P8 in the OHCs, and P12 in the IHCs, $I_{K,neo}$ started to be downregulated and there is increased expression of $I_{K,n}$.

Before the onset of hearing in the IHCs there is a small outward delayed rectifier current ($I_{K,DR}$). However, from P13 the cells acquire a fast component that is largely responsible for the increase in total current ($I_{K,f}$). It was discovered that the fast K^+ current is carried by large conductance Ca^{2+} activated K^+ channels (BK) (Marcotti *et al.*, 2004b). These channels are activated when the cell depolarises. The outward current then repolarises the cell (Kros et al., 1998).

In the immature inner hair cells and mature outer hair cells there is an apamin sensitive small conductance Ca^{2+} activated K^+ current (I_{SK}). This channel is activated by a rise in intracellular Ca^{2+} concentration, either through Ca^{2+} channels or through nicotinic acetylcholine receptors. Efferent stimulation via the nAchR's causes an increase in intracellular calcium that activates the I_{SK} channel and causes an outflow of K^+ that hyperpolarises the cell (Marcotti et al., 2004a). This plays a role in sustaining repetitive spiking in immature inner hair cells by making the repolarisation phase of the action potential more robust. Blocking I_{SK} meant the repolarisation phase became less efficient and it eventually failed altogether (Marcotti et al., 2004b).

1.2 Introduction to Usher syndrome

Around 250 million people around the world are affected by hearing loss and about half of these cases are caused by genetic mutations. A genetic condition that causes 3-6% of cases of childhood deafness is called Usher syndrome (Pan et al., 2017). Usher syndrome is an

autosomal recessive disorder that is genetically heterogeneous. The genes that are mutated in Usher syndrome are spread throughout the genome (Koffler et al., 2015).

There are three forms of Usher syndrome. Type 1 causes profound deafness, vestibular dysfunction and progressive blindness in the first decade of life. The proteins involved in Usher syndrome type 1 are: myosin 7a, harmonin, cadherin23, protocadherin15, sans and calcium and integrin binding protein 2 (Lefèvre et al., 2008). All of these proteins are involved in the mechanotransduction machinery (Giese et al., 2017; Koffler et al., 2015). The most common form of type 1 Usher syndrome is type 1B. 75% of Usher syndrome type 1 patients are included in the type 1B category. Usher syndrome type 1B is caused by mutations to the myosin 7a protein (Sun et al., 2001; Well et al., 1995).

Type 2 causes moderate hearing loss, normal vestibular function and blindness in the second decade of life. In Usher syndrome type 2 the proteins involved are usherin, VLGR1 and whirlin. All of these proteins are involved in the ankle link complexes at the base of stereocilia (Koffler et al., 2015).

Type 3 causes progressive, variable and sporadic onset of hearing loss, blindness and vestibular dysfunction (Mathur & Yang, 2015). In Usher syndrome type 3 there is thought to be only one protein involved: clarin-1. Clarin-1 is suspected to be involved in the function of the MET channel, however the role of clarin-1 in mechanotransduction is still unclear (Ogun & Zallocchi, 2014).

All the Usher protein mutations cause defective development of the stereocilliary hair bundle. In some cases, there are still three rows of stereocilia, as normal, but the length of stereocilia is variable and appear to be splayed. In other cases, the orientation, length and number of stereocilia is affected. This led to the hypothesis that the Usher proteins have a role in the development of hair cell bundles (Cosgrove & Zallocchi, 2014).

1.2.1 Myosin 7a

The Usher protein that this work focuses on is myosin 7a. The human genome contains 39 different myosin genes (Berg et al., 2001). These molecules generate movement and force that is powered by hydrolysis of ATP (Houdusse & Sweeney, 2016). Myosin is a type of

cytoskeletal molecular motor that is involved in muscle contraction, cell division, cell adhesion, phagocytosis and transport of cargo (A. Xiong et al., 2018). Myosin proteins are also involved in the maintenance and formation of actin bundles in filopodia, enterocyte brush border microvilli and hair cell stereocilia (Siththanandan & Sellers, 2011).

All myosin proteins have a motor domain, neck region and tail region. The motor domain is the binding site for nucleotides and actin. The neck region is made up of IQ motifs and binds calmodulin and members of the calmodulin protein family. The number of IQ domains determines the length of the neck and size of the power stroke. Lastly is the tail domain, this is the most diverse domain of the protein. In the tail domain can be found other functional domains, such as; MyTH4-FERM (myosin tail homology 4- 4.1 protein, ezrin, radixin, moesin) domains, PH (pleckstrin homology) domains and SH3 (SRC homology 3) domains (Siththanandan & Sellers, 2011; L. Wu et al., 2011).

Of the 12 classes of myosin, class 7 myosin's are one of the most widely produced (Berg et al., 2001; Wolfrum et al., 1998). The activity of myosin 7a is regulated by interaction between the tip of the tail and the motor domain (Yang et al., 2009). During embryonic development myosin 7a is expressed exclusively in epithelial cells which possess microvilli, for example; sensory hair cells in the cochlea, retinal pigment epithelial cells, olfactory receptor neurons and epithelial cells of the intestine and kidney (Sahly et al., 1997; Self et al., 1998). In the stereocilia myosin 7a forms a complex with sans and harmonin, which then interacts with the proteins that make up the tip links (Figure 1.12). Expression of myosin 7a coincides with the appearance of microvilli on these cell types. This expression pattern could suggest that myosin 7a has a role in the elongation of microvilli/stereocilia during development (Sahly et al., 1997).

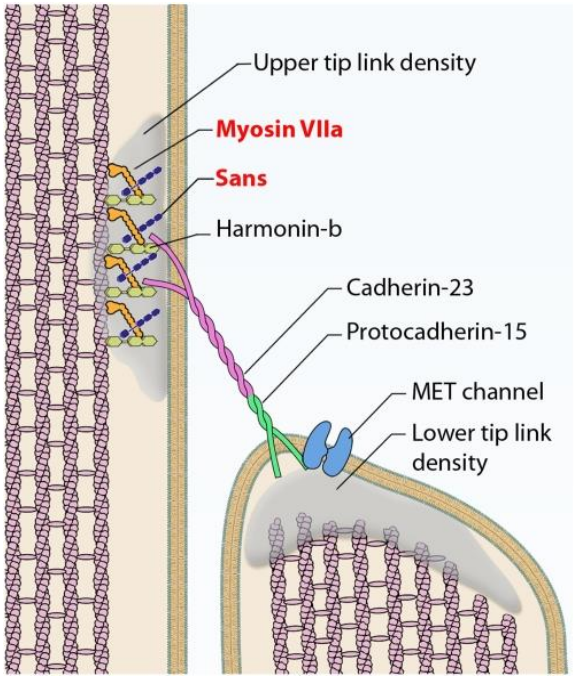

Figure 1.12- -Structural and molecular component of stereocilia tip links

The upper tip link density contains myosin 7a, sans and harmonin. These three proteins form a complex that interacts with the tip link. The tip link is made up of cadherin-23 and protocadherin-15. The tip link interacts with the MET channel in the lower tip link density (Grati and Kachar, 2011).

The myosin 7a protein has a motor domain, 5 IQ motifs and a complex tail domain containing two MyTH4-FERM domains separated by a SH3 domain (Chen *et al.*, 1996; Wu *et al.*, 2011). These two domains appear to be vitally important for the function of the protein. In these two domains there are more than twenty-six truncation/deletion mutations and forty missense mutations that cause disease. It has also been found that a truncation mutation in the second MyTH4-FERM domain decreases the stability of the motor protein (Schwander *et al.*, 2009).

There are several mutations of myosin 7a that are linked to deafness phenotypes. Many of the key deafness mutations are detailed in Figure 1.13. Two that have been investigated are myosin $7a^{6J}$ and myosin $7a^{4626SB}$. In the 6J mutant there are lower levels of myosin 7a although it is still detectable, and it is presumed that myosin 7a is dysfunctional. In the 4626SB mutant the level of myosin 7a expression is very low and these mice have a more severe phenotype than the 6J mouse. The protein level for each mouse was measured and reported as relative

to the WT level of 1. The 6J mutant had a protein level of 0.21 and the 4626SB mutant had a protein level of 0.0072 (Kros et al., 2002; Mburu et al., 1997).

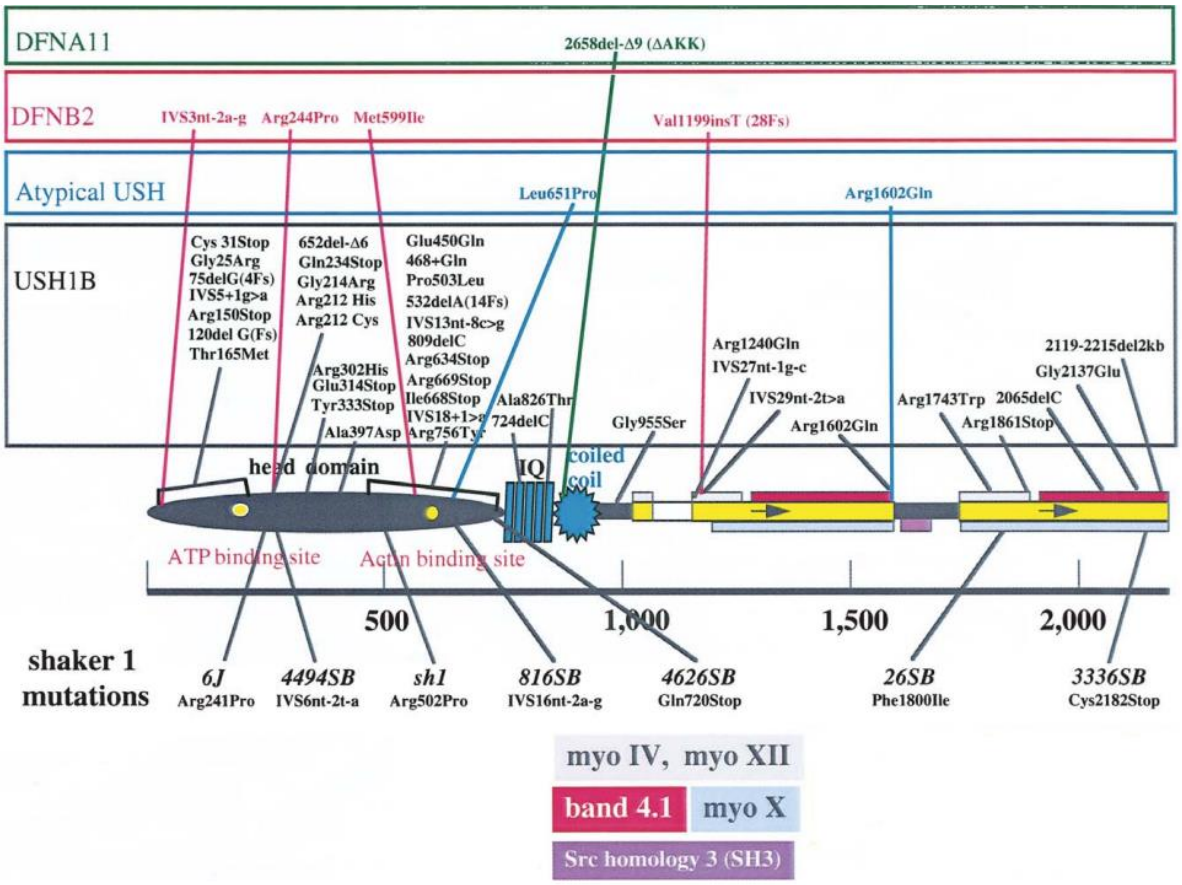

Figure 1.13- Diagram showing the key deafness mutations to myosin 7a

This diagram illustrates the mutations that are linked to usher syndrome type 1B, atypical usher syndromic deafness, recessive non-syndromic deafness (DFNB2) and dominant non-syndromic deafness (DFNA11). Seven shaker-1 alleles are also shown, along with homology domains in the myosin 7a tail (Adapted from X. Z. Liu et al., 1998).

From P3, in the 6J mutant, the hair bundles are disorganised, and the normal V shape is lost. In the remaining clusters of hair cells, the height of the stereocilia is normal and the tip links remain intact. In the 4626SB mice the disorganisation of the bundle is even greater (Kros et al., 2002). This disorganisation suggests that myosin 7a is needed for proper organisation of the hair bundle.

A paper by Lefevre *et al.* also used the Myo7a^{4626SB} mutant mouse to look at the morphology of the hair bundle. During development they found that there was increased growth of the stereocilia. This is different to what they found in other usher 1 mouse knockout models, where there was decreased growth in the stereocilia. They suggested that myosin 7a could have a role in transporting actin polymerization regulators along stereocilia (Lefèvre et al., 2008).

It seems likely that myosin 7a is a motor protein that maintains the tension in the tip links. In the homozygous myosin 7a mutant mouse there was a large MET current that was comparable to the current seen in heterozygous control mice. However, the resting open probability was zero at hyperpolarising potentials. This suggests that the tip links are slack, as tip link tension is needed to keep the MET channel open at rest. Also, a very large displacement was needed to elicit a current, much more than was needed in the heterozygous mice. This suggests that a functional myosin 7a protein is needed for normal transducer current gating. It is unlikely in this case that the phenotype seen is due to deterioration of the bundle as there are still normal resting potentials and voltage gated K^+ and Ca^{2+} currents (Kros et al., 2002).

1.3 Clarin-2

Part of this project aimed to compare the phenotypes seen in a constitutive and conditional knockout of myosin 7a. It was thought that the constitutive knockout would affect the initial development and formation of the hair bundle, and this would make it harder to determine the role of myosin 7a in mechanotransduction.

It was hypothesised that this would also be the case for constitutive knockouts of other deafness related proteins. To investigate this a different conditional and constitutive knockout mouse model were used. These mouse models have a knockout of the deafness-related gene, clarin-2. This work could provide a greater understanding into whether MET channel properties can be accurately determined from constitutive knockouts, or whether the disorganisation of the hair bundle caused by the constitutive knockout confuses interpretation of results.

Previously, Dunbar et al. (2019) characterised the morphological and MET channel properties of the clarin-2 constitutive knockout mouse. This thesis aimed to characterize the MET current of the conditional knockout, so it could be compared to the constitutive knockout. The conditional knockout uses myosin 15-cre to knockout out clarin-2 at around P4 in the hair cells. The constitutive knockout has a smaller MET current at P6-8, so it was hypothesised that clarin-2 has a role in mechanotransduction (Dunbar et al., 2019). However, very little is known about this protein and what its possible role in the hair cell could be.

1.4 Mechanotransduction

Hearing requires the conversion of a physical stimuli (sound waves) into an electrical signal that is sent to the brain. This process of converting a physical force into a biological signal is called mechanoelectrical transduction (Paluch et al., 2015). In the mouse, development of the hair bundle and mechanoelectrical transduction happens in the first two postnatal weeks (Pujol et al., 1998). Onset of the MET current is around P2 and reaches its maximal amplitude towards the end of the second postnatal week (K. X. Kim & Fettiplace, 2013). The onset of hearing occurs at about postnatal day 12 but the auditory system continues to develop and refine for another few weeks.

As described in section 1.1.3, the stereocilia are connected via tip links. Tip links connect the tips of shorter stereocilia to the sides of longer stereocilia (Mathur & Yang, 2015). When the movement of the tectorial membrane deflects the stereocilia towards the excitatory direction, it creates tension in the tip links which opens ion channels at the ends of the two shorter rows of stereocilia and allows potassium and calcium ions to flow into the cell (Beurg et al., 2009).

The endolymph is 80-100 mV more positive than the perilymph, this combined with a membrane potential of around -70 mV in the cell creates a voltage difference. This voltage difference is the driving force behind potassium ions entering the hair cell through the MET channel and generating the MET current (Steel & Barkway, 1989).

Mechanoelectrical transduction at the hair bundle is very sensitive, with a maximum response achieved over a tenth of a micrometre (Fettiplace, 2017). Deflection towards the tallest

stereocilia opens the MET channels and increases the MET current, while deflection in the other direction decreases the current (Goutman et al., 2015).

In the absence of sound stimulation, there is still a small amount of tension on the tip-links to allow the cell to respond to both excitatory and inhibitory stimuli with high sensitivity. This increases the open probability of the channels and means that Ca^{2+} and K^{+} ions are continuously entering the cell (Vélez-Ortega et al., 2017).

1.4.1 MET channel

For each stereocilia there are 1-2 MET channels located at the tip of the shorter stereocilium (Beurg et al., 2009). In OHCs in mice above P4 there was a 1.5 fold increase in MET current from the apex to the base, this is not seen in the IHCs (K. X. Kim & Fettiplace, 2013). Before P6 in OHCs the calcium permeability of the MET channel decreases from the apex to the base. This is not seen in IHCs, or after P7 in OHCs (Beurg et al., 2006; K. X. Kim & Fettiplace, 2013). The channel is very permeable to Ca^{2+} ions, the permeability to Na^{+} and K^{+} ions is about a quarter of the calcium permeability (Beurg et al., 2006).

Identifying the components of the MET channel has proven to be difficult and it is still disputed which proteins are involved. The number of hair cells and the amount of protein that could be involved in the MET channel is very low and isolating enough protein to identify which proteins are involved in the MET channel is a challenge. Most of the information that we have about the MET channel comes from genetically modified mouse models of deafness (Fettiplace, 2017).

There are four criteria that a protein must meet to be considered as one of the components of the MET channel.

- The protein must be expressed in the right place and at the right time
- It must be required for mechanosensitivity in the hair cells.
- A mutation to the protein should affect the properties of the mechanical response
- Expression of the protein should cause mechanical sensitivity in a cell that is normally insensitive (Cunningham & Müller, 2019).

Figure 1.14 illustrates the proteins and interactions thought to be involved in the MET transducer apparatus. The tip links are made up of two homodimers: two molecules of protocadherin-15 and two of cadherin-23. They both have long extracellular domains that interact at their N-termini to form a 150nm long link. This interaction is Ca^{2+} dependent (Furness et al., 2008; A. Xiong et al., 2018). Protocadherin-15 interacts with the proteins suspected to form the MET channel; TMC1, LHFPL5 and TMIE (Cunningham et al., 2017).

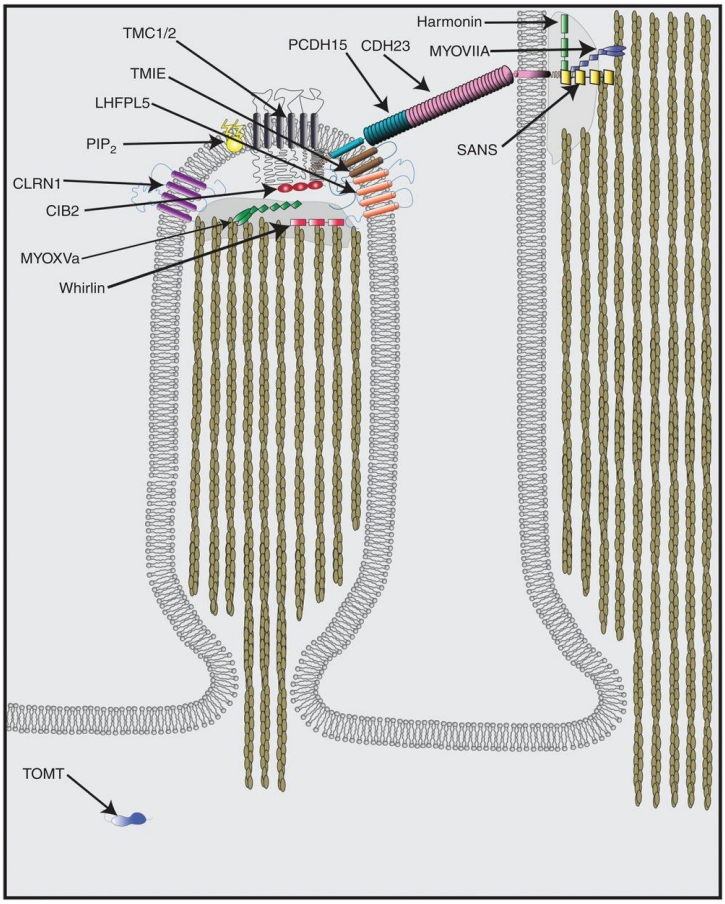

Figure 1.14- Diagram showing the potential interactions of proteins involved in mechanoelectrical transduction in the hair cells

There are many proteins that are suspected to be involved in the mechanotransduction machinery. Harmonin, myosin 7a and sans make up the upper tip link density. Cadherin-23 and protocadherin-15 make up the tip link. TMC1/2, TMIE and LHFPL5 are all candidates for MET channel proteins. The other proteins shown here are all associated with the MET channel but are not thought to make up the channel itself (Cunningham and Muller, 2019).

At the upper tip link density there is a complex of three proteins (harmonin, myosin 7a and sans) that link the tip link to the lateral side of the stereocilia. A knockout of any of these proteins causes deafness, demonstrating that they are essential for hearing. Cadherin-23 interacts with harmonin, which then interacts with the scaffolding protein, sans. Sans interacts with the MyTH4-FERM domains in the tail region of the myosin 7a protein, harmonin also binds weakly to the MyTH4-FERM domain of myosin 7a (Yu et al., 2017). It has been shown *in vitro* that cadherin-23 interacts directly with the tail domain of the myosin 7a protein (Bahloul et al., 2010; Boëda et al., 2002).

Harmonin links the cadherin-23 protein to the F-actin that makes up the stereocilia core. When harmonin is knocked out there is no mechanotransduction, even though the tip links are still intact (Grillet et al., 2009). The interactions between harmonin, sans, myosin 7a and cadherin-23 are seen in Figure 1.15.

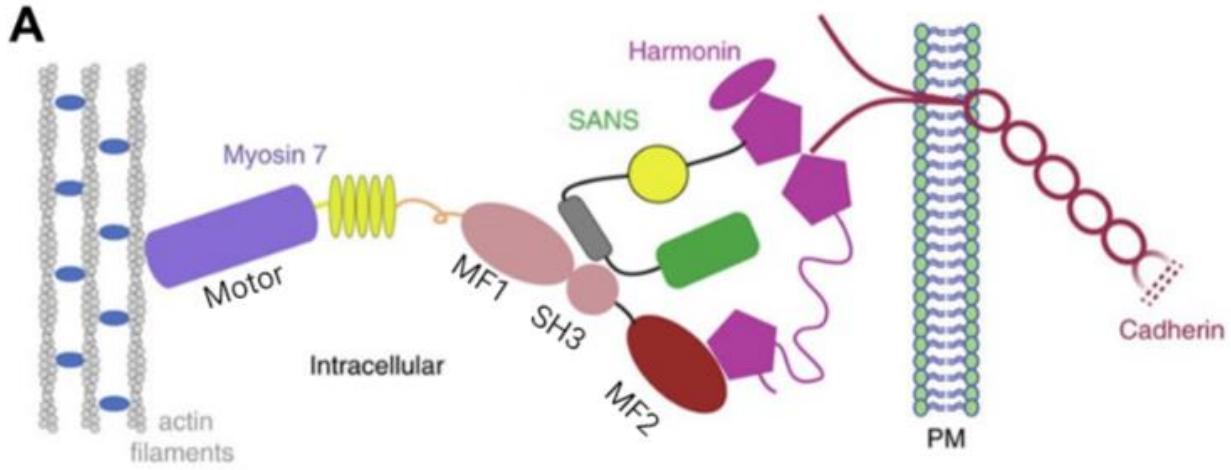

Figure 1.15- Illustration showing the interactions between myosin 7a, sans, harmonin and cadherin-23

Myosin 7a, sans and harmonin all interact to form a complex at the upper tip link density. Harmonin then interacts with cadherin-23, which makes up the upper part of the tip link. MF1- Myth4-FERM domain 1, SH3- sarcoma homology 3 domain, MF2- Myth4-FERM domain 2 (Adapted from Yu et al., 2017)

There are three main candidates for the components of the MET channels: TMC1, TMIE and LHFPL5.

The first candidate for a MET channel component is transmembrane channel-like 1/2 (TMC1/2). There are 35 TMC1 mutations that cause deafness in humans. The mRNA for *Tmc2* is expressed first and it starts to appear from birth and lasts until P10. *Tmc1* mRNA appears from P3 and levels increase into adulthood (Kawashima et al., 2011). From P5, TMC1 was localised to the tips of shorter stereocilia. TMC1/2 can interact with PCDH-15 but doesn't interact with LHFPL5 or TMIE (Beurg et al., 2015).

In the double Tmc1/2 mutant mice there is no MET current, despite there still being tip links present. In the TMC1 KO mice there is a reduced MET current with some residual current being carried by TMC2 for the first few days. After this the current starts to drop and eventually disappears. This suggests that TMC1 alone is needed for the MET current at the later stages of development (Cunningham & Müller, 2019; Kawashima et al., 2011).

Mutations to the TMC1/2 protein affects the properties of the MET channel. The Beethoven mutation to TMC1 causes there to be an extra positive residue in one of the extracellular loops (Vreugde et al., 2002). This mutation caused a decrease in unitary conductance and calcium permeability of the MET channels in the OHCs and IHCs (Corns et al., 2016; B. Pan et al., 2013). This suggests that TMC1/2 could form part of the MET channel pore, although it is still possible that they are accessory proteins for the MET channel proteins (Cunningham & Müller, 2019).

The next candidate is the TMIE protein. There are several mutations to TMIE that are linked to deafness in humans and mouse models of this protein are deaf (Naz et al., 2002). mRNA of TMIE was found in the cochlea and the protein is localised to the tips of the shorter stereocilia. The protein binds to protocadherin-15 (PCDH15) and LHFPL5. PCDH15 makes up part of the tip link and LHFPL5 is another candidate for a MET channel protein (Zhao et al., 2014).

In the TMIE knockout mouse the morphology of the hair bundle is normal but there is no MET current. However, the MET current can be rescued with expression of TMIE. In the TMIE knockout mouse the localisation of the other MET channel components is normal, suggesting that TMIE doesn't have a role in transporting these proteins (Zhao et al., 2014).

The last candidate is the LHFPL5 protein. The LHFPL5 protein is predicted to have four transmembrane domains (Cunningham & Müller, 2019). It is localised throughout the stereocilia with some concentrated at the tip links and it binds to PCDH15 (Beurg et al., 2015; Mahendrasingam et al., 2017). mRNA of LHFPL5 starts to be expressed at the same time as the appearance of the MET current and continues throughout adulthood (Scheffer et al., 2015).

Knockout mouse models of LHFPL5 are deaf and the MET current is reduced by 90% (Beurg et al., 2015; W. Xiong et al., 2012). The reduction could be partly due to the reduction in the number of tip links. However, the conductance of the MET channels is also reduced, there is slowed activation of the channels and impaired fast activation. As there is still a current present it is unlikely that LHFPL5 is a component of the channel pore. It is possible that the LHFPL5 protein helps to modulate the function of the MET channel instead (Xiong et al., 2012).

Another hypothesis it that LHFPL5 is involved in the proper localisation and transport of TMC1. In the LHFPL5 deficient mice there is no TMC1 at the tips of the stereocilia. Also, there is no tonotopic gradient of MET conductance in the LHFPL5 deficient mice, this is also seen in the *Tmc1*$^{-/-}$ mice (Beurg et al., 2015).

There are several other proteins that are thought to be associated with the MET channel. The structure of these proteins is not similar to the structure of other ion channels so it is unlikely that they form part of the channel pore (Cunningham & Müller, 2019).

The first of these proteins in the calcium and integrin binding protein (CIB2). Mutations to this protein have been linked to deafness in humans and mutations have been shown to abolish the MET current in hair cells (Giese et al., 2017; Riazuddin et al., 2012). CIB2 is correctly located in the stereocilia of hair cells (Riazuddin et al., 2012). CIB2 has 3 EF hand domains that are believed to mediate intracellular calcium signalling. The second and third EF hand domain in CIB2 bind to calcium (Blazejczyk et al., 2009; Gentry et al., 2005).

CIB2 is known to interact with whirlin, myosin 7a and TMC1/2, but not LHFPL5 or TMIE (Riazuddin et al., 2012). Some of the mutations that are linked to deafness weaken CIB2's interaction with TMC1/2. The other MET proteins are all localised correctly in the CIB2 mutant, suggesting this protein is not involved in the transport of MET-related proteins (Giese et al., 2017).

The next protein is TOMT (also known as LRTOMT in humans). Mutations to TMOT causes deafness in humans and mice. The mRNA of TOMT is localised to the hair cells and the protein was found in the cell bodies of hair cells (Ahmed et al., 2008; Cunningham et al., 2017). Mutating TMOT abolished the MET current in hair cells, and this could be partially rescued with TMOT expression. TOMT interacts with PCDH15, TMIE, LHFPL5 and TMC1/2. In TOMT mutants TMC1/2 is not localised correctly, suggesting TOMT has a role in TMC1/2 transport to the cell membrane. In heterologous cells TOMT alone is not enough to transport TMC1/2, suggesting it works with other, so far unidentified proteins, to carry out his function (Cunningham et al., 2017).

The last protein covered here is PIP_2. PIP_2 is a phospholipid component of all cell membranes. It has been shown that changing PIP_2 can alter the function of ion channels (Borbiro et al., 2015). In rat hair cells the depletion of PIP_2 had many effects on the MET channel. The fast adaption component was lost, there was a decrease in MET single-channel conductance, a change in ion selectivity, slower activation of the channels, a decrease in the calcium pore block and increased open probability of ion channels (Effertz et al., 2017). This demonstrates that the properties of the ion channel can be affected by factors outside of the channel (Cunningham & Müller, 2019).

Although all these proteins have been linked to the MET channel and have been shown to be vital to the MET current there is still no clear evidence to show which proteins make up the MET channel pore.

1.4.2 Adaptation

In response to a step deflection of the hair bundle, the activation of the MET current is followed by a decline in current over time, even though the stimulus is still present, and the open probability also reduces. This is thought to be adaptation rather than inactivation as the current can be recovered by increasing the amplitude of the stimulus (Stauffer & Holt, 2007). Adaptation of the MET current response is an important mechanism to prevent saturation of the response and optimise sensitivity. There are two phases of adaptation; the first is fast adaptation that happens within a millisecond time scale, then there is slow adaptation that happens over tens of milliseconds (Wu et al., 1999).

It is thought that slow adaptation involves changes in the point where the tip link attaches to the stereocilia. Positive deflection of the bundle and calcium entry through the MET channel causes the motor protein that links the tip link to the stereocilia to slip downwards and reduce the tension on the tip link, causing the MET channel to close and reducing the open probability (Gillespie & Cyr, 2004; Howard & Hudspeth, 1987).

There are several pieces of evidence that point to myosin being the motor protein responsible for slow adaptation. First, slow adaptation takes place in stereocilia that are rich in actin, and myosin is the only protein that is known to interact with actin (Flock et al., 1981). Slow adaptation requires calcium and calmodulin, both of which can control the activity of unconventional myosin proteins (Walker & Hudspeth, 1996). Also, myosin inhibitors (ADP and phosphate inhibitors) are known to block slow adaptation (Gillespie & Hudspeth, 1993; Yamoah & Gillespie, 1996). There are several proteins that have been suggested as candidates for the myosin protein responsible for slow adaptation. Two of these are myosin 1c and myosin 7a (Li et al., 2020).

The amount of myosin 1c protein present in the stereocilia is enough for it to be responsible for adaptation and it has been localised to the tips of the stereocilia (Gillespie et al., 1993). To investigate whether myosin 1c was involved in slow adaptation a mutation was introduced into the protein that increased its sensitivity to N^6- mediated nucleotides. When these inhibitory nucleotides were introduced adaptation was blocked (Holt et al., 2002).

Latest information suggests that myosin 7a is a more likely candidate for maintaining tip link tension. Localisation studies found that around eight myosin 7a protein molecules gather at the upper tip link densities which suggests they are involved in tip link tension (Grati & Kachar, 2011). Studies into the motor properties of myosin 7a found that the protein can move more efficiently on parallel bundled actin. This motor property makes myosin 7a suitable for moving proteins up actin bundles in hair cell stereocilia and as a tip-link tensor (Sato et al., 2017).

It has been suggested that fast adaptation is caused by the influx of calcium ions. When ions enter the MET channels calcium ions bind either to the pore of the channel or a protein associated with the channel which causes the channel to close (Howard & Hudspeth, 1988). Work in low frequency hair cells, such as those in the bullfrog saccule, showed that fast

adaptation is regulated by the influx of calcium ions (Cheung & Corey, 2006). Whether this is the same in mammalian cochlea hair cells is still disputed.

There are several pieces of evidence for the idea that adaptation is regulated by Ca^{2+}. Corns *et al.* found that applying the calcium chelator, BAPTA (1,2-bis(o-aminophenoxy)ethane-N,N,N',N'-tetra acetic acid), or preventing calcium entry into MET channels removed or strongly reduced all forms of adaptation (Corns et al., 2014). Also, when the extracellular concentration is lowered, the time constant of fast adaptation (time taken for current to decline during a sustained deflection of the hair bundle) is reduced. The current-displacement curve is sensitive to extracellular Ca^{2+} concentration and buffering by intracellular Ca^{2+} concentration (Ricci et al., 1998). A current-displacement curve is generated by measuring the MET current over time in response to a series of saturating excitatory stimuli. Lastly, preventing Ca^{2+} entry by depolarizing the cell to -80mV, prevents adaptation (Crawford et al., 1991).

A study by Goldring *et al.* used mice with mutated forms of TMC1/2 to investigate the mechanisms of adaptation. Goldring *et al.* found that the time constant and extent of adaptation depends on the isoform of TMC that is present (Goldring et al., 2019). TMC2 is replaced by TMC1 at the stereocilia tip at the end of the first postnatal week (Kawashima et al., 2011). Adaptation was faster and occurred to a greater extent with the TMC1 isoform, when compared to the TMC2 isoform. This was despite TMC2 being more permeable to calcium. Also, when they mutated TMC1 to make it less permeable to calcium they suggested the extent of adaptation occurring was greater. They used a reduced resting open probability in the mutated TMC1 mouse to imply that the extent of adaptation was stronger, however, resting open probability can be influenced by other processes (Goldring et al., 2019).

1.4.3 Role of MET current in hair cell maintenance

The MET current has a key role in the development and maintenance of the IHC functions. In the second postnatal week, before the onset of hearing, the open MET channels keep the membrane potential of the IHCs at the threshold necessary for Ca^{2+} action potentials. These action potentials are needed for functional differentiation of the IHCs into mature sensory

receptors. Without these action potentials the IHCs regress into a more immature state (Corns et al., 2018).

Corns et al. used a Myo7a$^{fl/fl}$:Myo15cre$^{+/-}$ mouse model to look at the role of myosin 7a in mechanotransduction. In this mouse model myosin 7a is knocked out. Myosin 7a is one of the proteins involved in the MET current machinery. The inner hair cell MET current was absent in these mice after the onset of hearing. The IHCs started to display the characteristics of an immature hair cell. There was re-innervation by cholinergic efferent fibres, down-regulation of adult-like ion channels in the basolateral membrane and the hair cells regained the ability to fire action potentials (Corns et al., 2018).

There is also evidence that the MET current is needed to maintain the structure of the hair bundles. When the MET current was blocked, by either breaking the tip links or using chemical blockers, there was remodelling at the tips of the stereocilia and eventually retraction of the stereocilia. This was only observed in the two shorter rows of stereocilia, where the MET channels are located, and not the tallest row. These experiments were carried out in young post-natal mice so it is not known whether the same thing would be seen in the adult mouse (Vélez-Ortega et al., 2017).

Changing the concentration of intracellular or extracellular Ca^{2+} also caused remodelling of stereocilia and shortening of the second and third rows of stereocilia. This could suggest that the influx of Ca^{2+} is important in maintaining stereocilia structure (Vélez-Ortega *et al.*, 2017).

1.5 Hypothesis and Aims

The main aim of this project was to understand how myosin 7a is involved in mechanotransduction. In particular, how a point mutation to myosin 7a can affect mechanotransduction and hair bundle morphology in the *Shaker-1* mouse. A greater understanding of the function of myosin 7a would help understand the mechanotransduction machinery and how it is affected in deafness.

This project used three mouse models to investigate mechanotransduction. Two models looked at the role of myosin 7a, the Shaker-1 mouse and a conditional knockout of myosin 7a. Using these two models together allowed us to see how myosin 7a is involved in both development of hair cells and maintenance once the hair bundle has developed. The last model looked at another Usher protein, clarin-2. This model allowed us to look more broadly at the study of mechanotransduction and whether using a conditional knockout mouse gives a more accurate picture of the role of usher proteins than a constitutive model.

The aims of the project are detailed below:

1. **Investigate how a point mutation in myosin 7a causes deafness in the *Shaker-1* mouse model**

It was hypothesised that the point mutation to myosin 7a would decrease the size of the MET current by affecting gating of the MET channel and cause the hair bundle to degenerate by affecting the development of the hair bundle.

2. **Compare the physiological properties and morphology of hair cells in a conditional myosin 7a knockout to a constitutive knockout**

It was hypothesised that the conditional knockout would affect the size of the MET current and resting open probability by affecting tensioning of the tip links and gating of the MET channel. Also, that the morphology of the hair bundle would be affected, though possible less severely than in the constitutive myosin 7a knockout.

3. Investigate the electrophysiological properties of another usher protein; clarin-2

It was hypothesised that the conditional knockout of clarin-2 would affect the size of the MET current, but not the resting open probability, possibly by affecting trafficking of the MET channel. This is in line with the results seen in the constitutive clarin-2 knockout mouse.

Chapter 2 - General Methods

2.1 Ethics

All animal studies were performed in the UK and licenced by the Home Office under the Animals (Scientific Procedures) Act 1986. All work was approved by the University of Sheffield Ethical Review Committee.

2.2 Animals

The animals used in this study were *CLRN2$^{fl/fl}$:Myo15-cre$^{+/-}$*, *Myo-7a$^{fl/fl}$:Myo15-cre$^{+/-}$*, *Tecta$^{-/-}$:Myo-7a$^{fl/fl}$:Myo15-cre$^{+/-}$* and the *Shaker-1* mouse (more information on each strain can be found in Table 2.1). Myosin 15-cre heterozygous mice crossed with myosin 15 wild type mice to generate litters that were 50% heterozygous and 50% wild type. This allowed littermate mice to be used as controls for experiments.

Mouse Model	Description
Shaker-1	• Point mutation to myosin 7a • Similar to human Usher syndrome type 1B
Myo-7a$^{fl/fl}$:Myo15-cre$^{+/-}$	• Conditional knockout of myosin 7a in hair cells • Myosin 7a is knocked out at P4 • Allows investigation of myosin 7a without widespread disorganisation of hair bundle
Tecta$^{-/-}$:Myo-7a$^{fl/fl}$:Myo15-cre$^{+/-}$	• Conditional knockout of myosin 7a • Missing tectorial membrane • Allows patch clamping of OHCs >P12
CLRN2$^{fl/fl}$: Myo15-cre$^{+/-}$	• Conditional knockout of clarin-2 in hair cells • Clarin-2 is knocked out at P4 • Allows investigation of clarin-2 without degeneration of hair bundle

Table 2.1- Table detailing mouse models used and a brief description of each one

The background strain for all mice used was C57BL/6N. Mice were held at the University of Sheffield under Home Office guidelines. All mice were maintained in a 12-hour light/dark cycle. For this project, all mice were culled using cervical dislocation. For *in vivo* hearing

measurements mice were anaesthetised using an intraperitoneal (IP) injection of ketamine (100mg/kg) and xylazine (10mg/kg). Animals were culled by a schedule 1 home office method for tissue (*ex vivo* experiments) or at the end of procedures (*in vivo* experiments).

In order to generate the *Myo7a$^{fl/fl}$:Myo15-cre$^{+/-}$* mouse model, exons 10 and 11 in the myosin 7a protein were floxed. The cre-LoxP system works by using a cre-recombinase protein that recognises the *lox*P DNA sequence. The cre-recombinase then deletes the DNA sequence located between two *lox*P sites. For this system two mouse strains were used; one that had cre-recombinase expressed by a promotor for myosin-15 cre, and one strain that has two *lox*P sites flanking the DNA sequence of myosin 7a (Kim et al., 2018). Myosin-15 is a hair cell specific protein that starts to be expressed from ~P4. The later expression of myosin-15, and the associated cre protein, allows the hair bundle to develop normally before the knockout of myosin-7a.

The CLRN2$^{fl/fl}$:Myo15-cre$^{+/-}$ mouse was obtained from Harwell, UK. This mouse model was generated by deleting exon 2 from the *clrn2* gene. A single strand oligodonor was then added with exon 2 flanked by loxP sites. The floxed CLRN2 mouse was crossed with the myosin 15-cre mouse.

The Shaker-1 mutation (R502P) is a spontaneous mutation that was obtained from Harwell, UK.

2.3 Genotyping

CLRN2$^{fl/fl}$:Myo15-cre$^{+/-}$, *Myo-7a$^{fl/fl}$:Myo15-cre$^{+/-}$*, *Tecta$^{-/-}$:Myo-7a$^{fl/fl}$:Myo15-cre$^{+/-}$* were genotyped using polymeric chain reaction (PCR) to amplify the DNA. The PCR product was run on a gel and the genotype could be determined by the band size seen in the gel image (band sizes are detailed in Table 2.2).

As the *Shaker-1* mice have a point mutation they could not be genotyped using PCR. The *Shaker-1* mice were genotyped by amplifying the DNA using PCR, the PCR product from the *Shaker-1* mice was then sequenced.

For the PCR reaction DNA was extracted from either ear clips or tail sample using a lysis buffer (25mM NaOH+0.2mM EDTA (Ethylenediamine tetra acetic acid)) and incubated at 95°C for 1 hour. 40mM of TrisHCL was then added to each sample.

The PCR reaction was set up with 1 µl forward primer, 1 µl reverse primer, 10 µl 2xGoTaq master mix, 7 µl dH_2O and 1 µl of either DNA or water (negative control). PCR primers and protocols for each genotype are detailed in Table 2.2. The PCR products were then run on a 2% agarose gel for 50 minutes at 120 V.

Strain	Primer	Primer sequence 5'-3'	Protocol	Expected bands
CLRN2	WTF3	ACTCTGCCAAGCCAATGCC	1) 95°C 5 min 2) 95°C 30 sec 3) 60°C 30 sec 4) 72°C 45 sec (repeat 2-4 X35) 5) 72°C 7 min 6) 12°C hold	WT 670bp MUT 749bp
	WTR3	CTTCCAGACTGCAATAAAAGTGC		
	LoxP_F	ATCCGGGGGTACCGCGTCGAG		
	LoxP_R	ACTGATGGCGAGCTCAGACC		
Tecta	MGGF1	CTCCCTGATAACCTACACTTC	1) 95°C 5 min 2) 95°C 30 sec 3) 60°C 30 sec 4) 72°C 30 sec (repeat 2-4 X35) 5) 72°C 5 min 6) 12°C hold	WT 350bp MUT 350bp
	EX1R1	GAGCATGCTGATCAAGAGCTGTAGG		
	MGGR1	AACACAAGGATGACATCTGC		
Myosin-7a	Myo7a F	GGGAGAGAAAGCAGGGTGTG	1) 95°C 5 min 2) 95°C 30 sec 3) 65°C 30 sec 4) 72°C 45 sec (repeat 2-4 X35) 5) 72°C 7 min 6) 12°C hold	WT 360bp MUT 510bp
	Myo7a R	AAGCTGGACTCTCTGGTGGC		
Myosin-15 cre	P1	AGGGACCTGACTCCACTTTGGG	1) 95°C 5 min 2) 95°C 30 sec 3) 65°C 30 sec 4) 72°C 45 sec (repeat 2-4 X35) 5) 72°C 7 min 6) 12°C hold	WT no band MUT 500bp
	P2	TGGTGCACAGTCAGCAGGTTGG		
Shaker-1	Sh1_F	GAGCATCGACTGGTTGCACA	1) 95°C 5 min 2) 95°C 30 sec 3) 60°C 30 sec 4) 72°C 30 sec (repeat 2-4 X35) 5) 72°C 5 min 6) 12°C hold	WT and MUT 130bp
	Sh1_R	CCACCTTGGGGAACTTGCTC		

Table 2.2- Primers and protocols used for PCR reactions

2.4 Auditory brain stem responses

Auditory brainstem responses (ABRs) are measured as a series of electrical waves. These waves represent the activity of different populations of neurons along the auditory pathway. The first wave is generated by the auditory nerve and consists mainly of responses from the IHCs. The ABR threshold is determined to be the lowest sound level that is required to elicit a response in the auditory brain stem and is used as a readout for IHC function (J.-Y. Jeng et al., 2021).

ABRs were recorded from knockout or mutant mice and their littermate controls between P18 and P35. This age range was chosen as this was where we saw a decrease in the size of MET current. For ABR recordings mice were anaesthetised (as described in section 2.2). The depth of anaesthesia was measured as loss of retraction reflex to a toe pinch. To record the

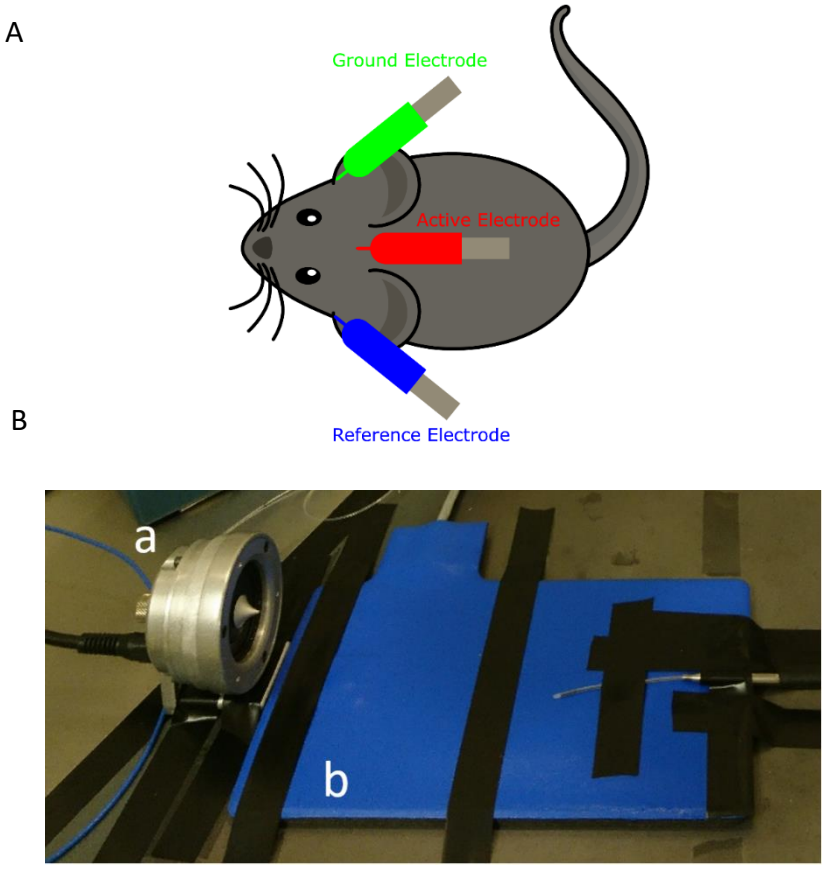

Figure 2.1- Set up for recording open field auditory brainstem responses

A- Position of electrodes on mouse. Active electrode placed on vertex (red), reference electrode on left bulla (blue) and ground electrode on right bulla (green). B- set up of ABR recording chamber with the speaker (a) and hearing pad (b).

ABR thresholds the mice were placed in a sound-proof chamber (MAC-3 Acoustic Chamber, IAC Acoustic UK) on a heating pad at 37°C. A calibrated loud-speaker (MF1-S Multi Field Speaker, Tucker-Davis Technologies, USA) was placed 10 cm away from the mouse to deliver the stimuli.

Two electrodes (reference and ground electrode) were placed subcutaneously under the skin behind each pinna and one active electrode was placed subcutaneously on the vertex (Figure 2.1) (Ingham *et al.*, 2011). The stimuli given was tone bursts at 3, 6, 12, 18, 24 and 30kHz and clicks at 0.01ms. The stimuli sound pressure level increased in steps of 5 dB SPL, up to 95 dB SPL. Tone bursts lasted 5 ms with a 1 ms on/off ramp time and were presented at a rate of 42.6 s^{-1}.

Evoked responses were amplified, then digitized and bandpass filtered between 300-3,300Hz. The ABR's were recorded as an average of 256 presentations of each stimulus. The hearing threshold was determined as the lowest stimulus intensity that generated an ABR waveform.

2.5 Distortion Product Otoacoustic Emissions

Distortion product optoacoustic emissions (DPOAEs) are the sounds generated when the cochlea is stimulated by two pure tones (f1 and f2). These tones produce a distortion of sounds in the cochlea, this generates acoustic signals at a lower frequency. This acoustic signal is related to the electromotility of OHCs and is a good indication of OHC function (Michna et al., 2003).

Mice were anesthetised for DPOAEs as described above and placed in a soundproof chamber. Two pure tones were presented directly into the left ear canal of the mouse using 3cm plastic tubes connected to two calibrated loudspeakers. The tones were presented at a ratio of f2/f1=1.2. The f2 tones were presented at 6, 12, 18 and 24kHz at an increasing range of decibels from 0-65 dB SPL in steps of 5dBs. The amplitude of the f1 tone was set to be equal to the f2 tone.

The DPOAE threshold was determined to be at the lowest stimuli level that evoked a 2f1-f2 response that was two standard deviations above the mean noise level (J.-Y. Jeng et al., 2021).

2.6 Tissue dissection

For the dissection mice were culled by cervical dislocation and the cochlea was removed from the temporal bone. All dissections were carried out in cold extracellular solution (Table 2.3) under a dissecting microscope. The bone surrounding the cochlea was then removed using forceps to expose the spiral shaped cochlea inside. The stria vascularis was then removed, revealing the organ of Corti along the edge of the spiral. The apical coil was removed from the modiolus and transferred to a chamber filled with extracellular solution. In the chamber the cochlea was fixed in place under a nylon mesh. Lastly the tectorial membrane was removed to allow access to hair cells underneath.

2.7 Single cell electrophysiology

After dissection, the cochlea was placed in a specially designed chamber and the cochlea was fixed in place with a nylon mesh. The chamber was placed on a rotating stage attached to an upright microscope (LEICA DM LFS, Leica Instruments, UK.). The microscope was on an anti-vibration table (TMC, USA) contained in a Faraday cage to prevent electrical noise interfering with the electrophysiological recordings.

Solution flowed over the chamber at 8ml/min controlled using a pump (Cole-Parmer, USA). The position of the recording pipette was controlled using a micromanipulator (PatchStar, Scientifica, UK). Position of electrodes and pipettes used can be seen in Figure 2.2.

All recordings were carried out at room temperature (20-22°C). To access the hair cells the surrounding supporting cells were removed with positive and negative pressure applied by the cleaning pipette. A patch pipette was positioned in the chamber, near to the hair cells. The patch pipette was filled with intracellular solution. The composition of the intracellular solution depended on the experiment being carried out (intracellular solution compositions are detailed in Table 2.4, Table 2.5, Table 2.6 and Table 2.7). Once the pipette was close enough to the targeted cell, a negative pressure was applied to form a seal with the cell membrane. The resistance of the seal was around 1 GΩ. The cells were maintained at a holding potential of -80 mV.

All recordings were taken in the whole cell patching configuration. For whole-cell recordings light suction was applied to break the section of cell membrane attached to the pipette. Breaking the membrane meant the inside of the pipette was continuous with the cytoplasm of the cell, and currents from the entire cell could be measured.

Acquisition of data was controlled by pCLAMP software (Molecular Devices, USA) using Digidata 1440A. The membrane potential was corrected for voltage drop across series resistance after compensation of 60-80%. The recordings were low-pass filtered at 0.5 or 1kHz with a Bessel low-pass filter and sampled at 5 kHz. Data was then stored on a computer for off-line access.

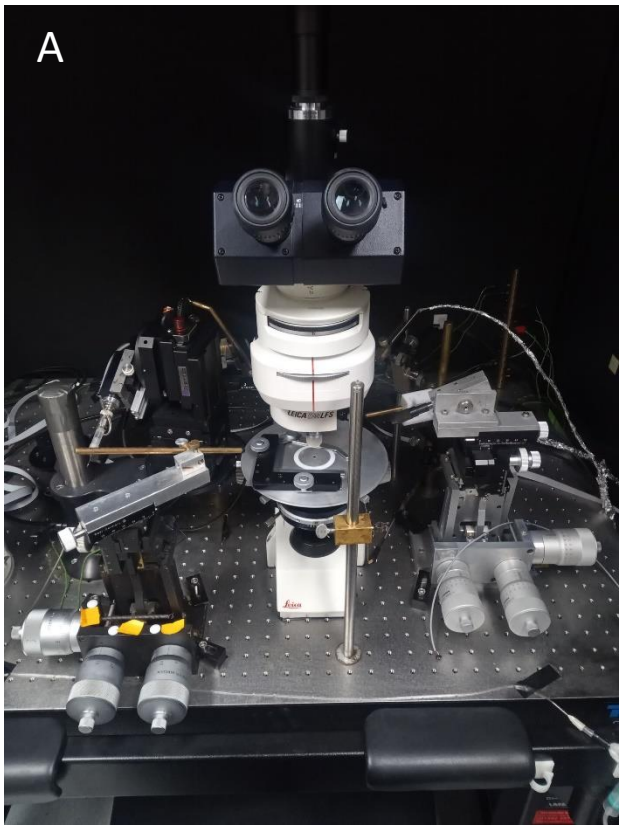

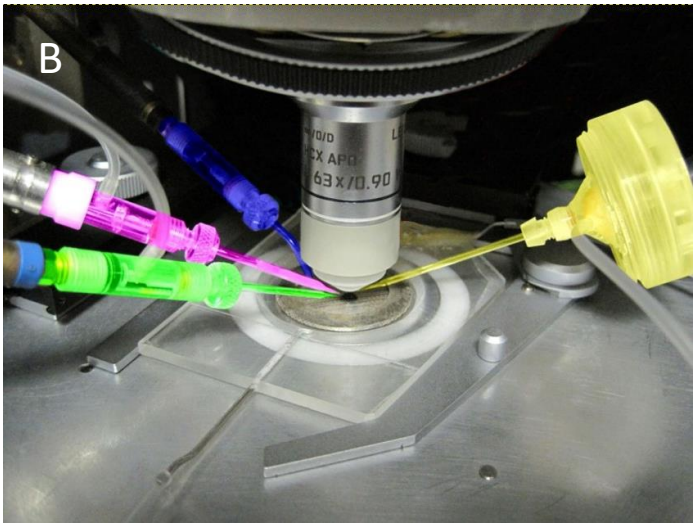

Figure 2.2- Set-up used for electrophysiological recordings

A, Microscope and micromanipulators used for patch-clamping.

B, Close up view of electrodes and pipettes. Patch pipette (pink), ground electrode (blue), cleaning pipette (green), fluid jet (yellow).

2.7.1 Recording pipette

Patch pipettes were pulled from soda glass capillaries (1413027, Hilgenberg, Germany) using a pipette puller (Narishige Instruments, Japan). Pipettes were coated with wax (Mr Zoggs SexWax, USA) to reduce fast electrode capacitance transients. The resistance of the pipettes was between 3-4 MΩ. For experiments pipettes were filled with intracellular solution (Table 2.4, Table 2.5, Table 2.6, Table 2.7).

2.7.2 Cleaning pipette

Cleaning pipettes were pulled from borosilicate capillary glass (30-0062, Harvard Apparatus, UK) using a pipette puller. The diameter of the cleaning pipettes was about 10µm. The pipettes were filled with extracellular solution (Table 2.3) then attached to a syringe to apply suction and clean the cells. Cells around the target hair cell were removed by the cleaning pipette to allow the recording pipette access to the cell.

2.7.3 MET recording

For MET recordings a fluid jet was used to stimulate the hair bundle. The fluid jet was comprised of a borosilicate glass pipette (10µm diameter) driven by a piezo-electric disk (Kros *et al.*, 1992). The fluid jet was filled with extracellular solution (Table 2.3) and positioned above the modiolar side of the cochlea, around 10 µm from the hair bundle. For all MET current experiments, the recording pipette was filled with a CsCl intracellular solution (Table 2.4). Once the patch pipette was in a whole cell configuration, stimuli was applied as a 45Hz sinusoid (filtered at 0.5kHz) with a driving voltage of ±40V.

Positive pressure from the fluid jet pushed the stereocilia towards the tallest row and opened the MET channels, mimicking an *in vivo* excitatory stimulus. Negative pressure sucked fluid into the pipette and pulled the stereocilia in an inhibitory direction, closing the MET channels.

2.7.4 Solutions

Extracellular solutions were made to be similar to the physiological solution that bathes the basolateral membrane of the hair cell. This solution was used for dissection of the cochlea

and bathing the cochlea during electrophysiological experiments. The composition of the extracellular solution is shown below in Table 2.3. Amino acids (50X) (11130-036, Gibco, USA) and vitamins (100X) (11120-037, Gibco, USA) were added to the extracellular solution as a supplement. The pH of the solution was adjusted as required using 1M NaOH. The final osmolality of the solution was between 304-309mOsm/kg H_2O.

Chemical	Final mM
NaCl 1M	135
$CaCl_2$ 1M	1.3
KCl	5.8
$MgCl_2$ 1M	0.9
HEPES	10
Glucose	5.6
NaH_2PO_4	0.7
NaPyruvate	2
pH	7.48
Osmolality	308mOsm/kg H_20

Table 2.3- Composition of extracellular solution

For MET current recordings a CsCl-based intracellular solution was used to reduce the contribution of potassium currents. Caesium blocks the large BK potassium current, allowing the MET current to be seen more clearly. The composition of the solution is detailed below in Table 2.4. The pH of the solution was adjusted using 1M CsOH. The solutions final osmolality was 288-292mOsm/kg H_2O.

Chemical	Final mM
CsCl	131
Na_2Phosphocreatinine	10
$MgCl_2$	3
Na_2ATP	5
HEPES	5
CsOH-EGTA 0.1M	1
pH	7.29
Osmolality	290mOsm/kg H_20

Table 2.4- Composition of CsCl intracellular solution

To measure the basolateral current, the patch pipette was filled with KCl intracellular solution (see Table 2.5). The pH of the solution was adjusted using 1M KOH. The final osmolality of the solution was between 290-294mOsm/kg H_2O.

Chemical	Final mM
KCl	131
Na_2Phosphocreatinine	10
$MgCl_2$	3
Na_2ATP	5
HEPES	5
KOH-EGTA 0.1M	1
pH	7.28
Osmolality	293mOsm/kg H_20

Table 2.5- Composition of KCl intracellular solution

To measure the MET channel's sensitivity to calcium, the patch pipette was filled with a CsCl intracellular solution containing either 0.1mM (Table 2.6) or 5mM (Table 2.7) BAPTA. BAPTA is a calcium chelator and was used to remove calcium from the intracellular environment of the cell. The pH of the solution was adjusted using 1M CsOH. The final osmolality of the solution was either 292mOsm/kg H_2O (5mM) or 293mOsm/kg H_2O (0.1mM).

Chemical	Final mM
CsCl	131
Na_2Phosphocreatinine	10
$MgCl_2$	3
Na_2ATP	5
HEPES	5
K_4BAPTA	0.1
pH	7.28
Osmolality	292mOsm/kg H_20

Table 2.6- Composition of CsCl intracellular solution with 0.1mM BAPTA

Chemical	Final mM
CsCl	122
Na_2Phosphocreatinine	10
$MgCl_2$	3
Na_2ATP	5
HEPES	5
K_4BAPTA	5
pH	7.28
Osmolality	293mOsm/kg H_20

Table 2.7- Composition of CsCl intracellular solution with 5mM BAPTA

2.7.5 Data analysis

All data was analysed using Clampfit software (Molecular Devices, USA) and OriginPro (OriginLab, USA). The holding current was analysed in Clampfit, whereas MET current size, resting open probability, total steady state current, $I_{K,n}$ and I_K current were all analysed using OriginPro. The total steady current was measured between 145-165ms from onset of depolarising voltage steps. The $I_{K,n}$ current was measured as the difference between the peak current and the steady-state current at -124mV (Marcotti & Kros, 1999). The I_K current is measured as the difference between the size of the steady-state outward K^+ current at 0mV and the holding potential of -84mV (Jeng et al., 2021). For the MET current recordings the resting open probability was obtained by measuring the difference in current size during the saturated inhibitory stimuli and at rest. This was then taken as a percentage of the total current size. All the membrane potentials were corrected for the liquid junction potential of -4mV for chloride based intracellular solutions.

Statistical analysis was carried out using Prism software (GraphPad Software, USA). Statistical comparisons between data sets were made using students t-tests and two-way ANOVA followed by Šídák multiple comparisons post-test, where $P<0.05$ indicated statistical significance. Two-way ANOVA was used for comparisons between genotype and age group.

2.8 Immunofluorescence microscopy

Cochleae were dissected from the skull of mice older than P8 and were perfused with 100µl of 4% PFA (paraformaldehyde), to improve the efficiency of fixation. Small holes were made in the apex of the cochlea and PFA was gently pushed through the round and oval window using a pipette tip. The sample was then fixed in 4% PFA for twenty minutes at room temperature.

The sample was then washed three times in 1X PBS at room temperature for 10 minutes each. Once the cochlea was dissected out of the bony shell it was transferred to an Eppendorf cap filled with 200µl of 1X PBS. The PBS was replaced with PBST (0.5% Triton X-100 in PBS) supplemented with 5% normal goat serum (#31873, Invitrogen) and incubated for one hour at room temperature.

The blocking solution was replaced with 100µl of primary antibody diluted in PBST containing 1% of serum and incubated overnight at 37°C (for concentrations see Table 2.8). The primary antibody was replaced with secondary antibody for one hour at 37°C (for concentrations used see Table 2.9). The sample was washed three times with 1X PBS for 10 minutes.

The samples were mounted with VECTASHIELD (H-1000, VECTOR Labs). Confocal images were obtained using the Zeiss LSM 880 Airyscan confocal microscope. Images were processed using Fiji ImageJ software.

Primary antibody	Source-Isotype	Concentration	Serial number
CDH-23	Rabbit	1:50	Gifted by Guy Richardson
Myosin 7a	Rabbit	1:500	Proteus BioSciences 25-6790
Harmonin	Rabbit	1:200	Gift from Saaid Safieddine

Table 2.8- Concentration of primary antibodies

Secondary antibody	Concentration	Serial number
Goat anti-rabbit Texas Red	1:1000	A21245
Goat anti-rabbit Alexa 488	1:1000	Thermo Fisher A11034
Goat anti-rabbit Pacific blue	1:1000	Thermo Fisher P10994
Phalloidin Texas red	1:400	Thermo Fisher T7471
Phalloidin Alexa 488	1:400	Thermo Fisher A12379
DAPI	1:1000	Merck Sigma 10236276001

Table 2.9- Concentration of secondary antibodies

2.9 Scanning electron microscopy

Cochlea were removed from the skull then fixed for two hours in 2.5% glutaraldehyde, 0.1 M sodium cacodylate buffer and 2mM CaCl. To improve efficiency of fixation, cochlea from mice older than P8 were perfused with fixative through the round and oval window. The samples were then washed in 0.25% glutaraldehyde three times for 10 minutes. The bone and stria vascularis were removed to expose the hair cells.

1% osmium solution was made by diluting 0.1g of osmium in 10ml 0.1M Na cacodylate/2mM CaCl solution. The sample was incubated in osmium for 1 hour then washed three times in Na cacodylate for five minutes. Then incubated in a 95% saturated solution of thiocarbohydrozide (TCH) in distilled water for 20 minutes then washed six times in distilled water for three minutes. Incubated in osmium for two hours then washed six times in distilled water for three minutes. Incubated in TCH for 20 minutes then washed six times in distilled water for three minutes. Incubated in osmium for two hours then washed six times in distilled water for three minutes. The sample was then left in 75% ethanol overnight (Furness & Hackney, 1986).

The next day the sample was dehydrated through an ethanol series (80%, 90%, 100%, 100% dry). The sample was left for 10 minutes in each ethanol concentration. Then the sample was dried with a Leica EM CPD300 critical point dryer and imaged at 10kv with a Tescan Vega3 LMU electron microscope.

Chapter 3 - Electrophysiological properties and morphology of hair cells in the *Shaker-1* mouse

3.1 Introduction

One mouse model that has been widely used to understand the role of myosin 7a is the *Shaker-1* mouse. The *Shaker-1* mouse was first described in the 1920's by Lord and Gates. These mouse show deafness, hyper-activity, head-tossing and circling, which are all characteristics associated with a defect in the inner-ear. They noted that the head-tossing began a few days after birth. The mice started to become deaf at 22-30 days old, although this was only measured with a startle test, which is a very crude way to assess hearing function (Lord & Gates, 1929).

The *Shaker-1* mouse has a mutation in the gene orthologous to the human myosin 7a gene and the *Shaker-1* mouse replicates many of the symptoms of Usher syndrome. However, in the *Shaker-1* mouse there is no degeneration of the retina (Hasson, Gillespie, et al., 1997; Self et al., 1998), which is present in humans affected by the mutation (Mathur & Yang, 2015). The absence of retinal degeneration in the *Shaker-1* mouse can be explained by differences in myosin 7a expression in the visual system between mice and primates. In humans and macaques, myosin 7a is expressed in the inner segment of photoreceptors. Whereas, in mice, myosin 7a is mainly expressed in the retinal epithelial pigment (Calabro et al., 2019; El-Amraoui et al., 1996).

In the *Shaker-1* mouse there is a R502P missense mutation in the myosin 7a protein (see Figure 3.1) (Gibson et al., 1995). The Arg-502 residue is located in the activation loop of the protein, between the Q and R helices. The activation loop is located in the motor domain of myosin 7a (Xiong et al., 2018). The motor domain contains the actin binding site and ATPase activity of myosin 7a (Doran & Lehman, 2021). The activation loop interacts with the N-terminal of actin and is thought to be involved in initiating force generation on the actin filament (Várkuti et al., 2012). It is likely that the *Shaker-1* mutation changes the conformation of the activation loop, and that changing the conformation of the activation loop affects its movement and its ability to hydrolyse ATP (Coureux et al., 2004; A. Xiong et al., 2018).

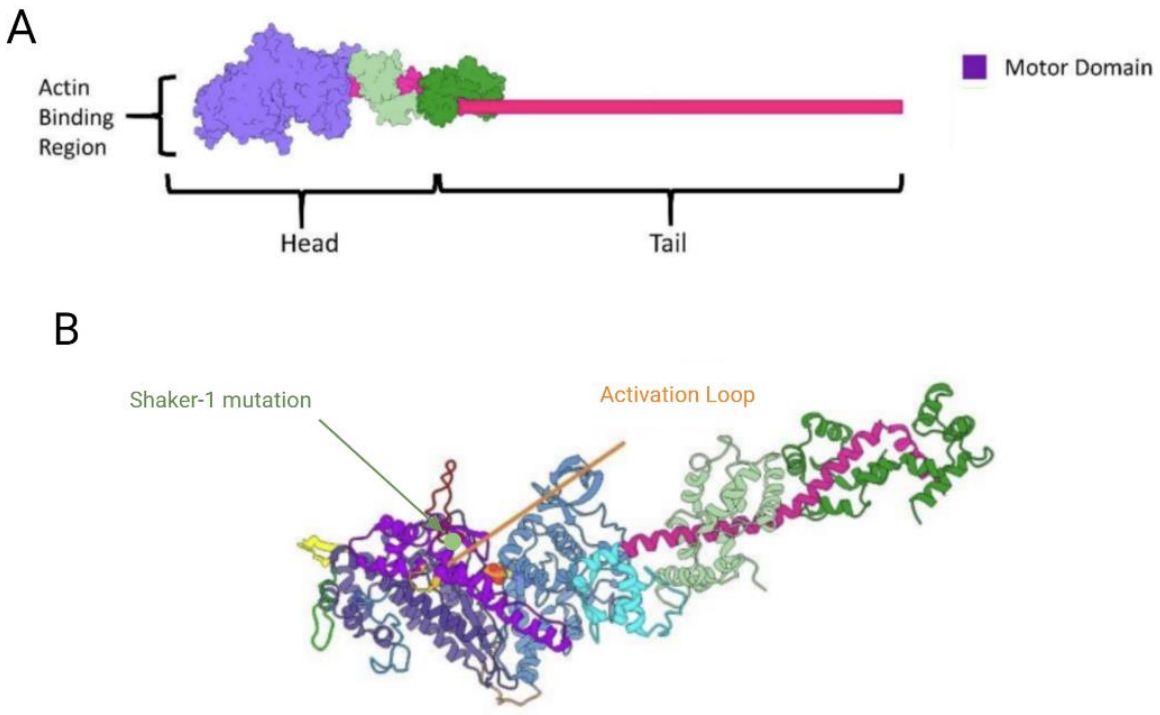

Figure 3.1- Location of Shaker-1 mutation on myosin 7a

This diagram shows the location of the *Shaker-1* mutation in the myosin 7a protein. (A) The motor domain of myosin 7a contains the actin binding region. (B) Structure of the myosin 7a motor domain showing the approximate location of the Arg-502 residue in the activation loop (shown in green) (Modified from Doran and Lehman, 2021).

Hasson *et al.* (1997) looked at how the *Shaker-1* mutation affected mRNA and protein expression of myosin 7a in one- to three-month-old mice. As the sensory epithelium in the inner ear was completely degenerated at this age, it was not possible to measure myosin 7a levels in this tissue. Therefore, they used tissue from the kidney and testis, as they also express myosin 7a. The mRNA and protein expression in the *Shaker-1* mouse was equivalent to wild type levels, suggesting that the hearing loss is not due to a lack of protein (Hasson, Walsh, et al., 1997).

Self *et al.* (1998) used SEM to look at the structure of the stereocilia bundle from 3-15 days' post birth (see Figure 3.2). They showed that up to 15 days old in the *Shaker-1* mouse the stereocilia develop normally and there is no disorganisation, however there were only two rows of stereocilia rather than the usual three rows (Self et al., 1998). The loss of the third

row of stereocilia could be caused by reduced tension in the tip links. At the lower tip link density, it is possible that the MET machinery and the actin regulators share some molecular components and the reduced tension in the tip link causes the shortening and loss of shorter rows of stereocilia seen in the *Shaker-1* mice (Lefèvre et al., 2008; Manor & Kachar, 2008).

Morphological studies of the cochlea, carried out by Deol (1996), showed that the structure of the cochlea was normal until P12 and then it began to degenerate. After the onset of hearing, the hair cells began to shrink, and the supporting cells lost their shape. Deol also noted that the tectorial membrane started to curl up. Degeneration of the stria vascularis was only noticed after degeneration of the cochlea (Deol, 1956). Even though the stria was damaged it was still able to maintain the endocochlear potential in the deaf *Shaker-1* mice (Brown & Ruben, 1969).

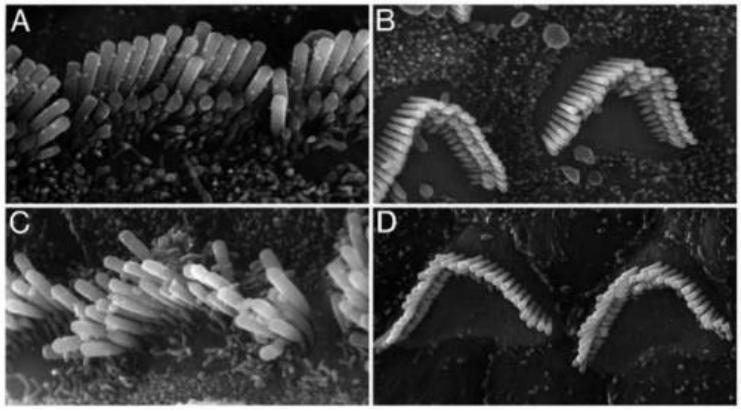

Figure 3.2- Scanning electron microscopy image showing morphology of the *Shaker-1* hair bundle at 15 days old

SEM of inner (left column) and outer (right column) hair cells at P15. (A,B) control hair cells showing three rows of stereocilia in the IHCs and OHCs, (C,D) *Shaker-1* hair bundles showing the loss of the third row of stereocilia in the IHCs and OHCs (Self et al., 1998).

A different study also found that hearing and the hair bundle develops normally for the first few days then from 12 days postnatal the hair cells rapidly deteriorate (Saw Jr. et al., 1997). Shnerson *et al*. (1983) used low magnification EM to look at how the *Shaker-1* mutation affects maturation of the organ of Corti in older mice. They found that maturation of the organ of Corti was delayed and there was early degeneration. Also, the afferent innervation

of the IHCs showed advanced degeneration and by day 18 most of the afferent fibres had degenerated (Shnerson et al., 1983). Kikuchi and Hilding (1965) also saw degeneration of the hair cells from day 12 and by 7 weeks old all of the hair cells had degenerated (Kikuchi & Hilding, 1965).

Self *et al.* (1998) looked at cochlea function at P15 and P20 and found that the *Shaker-1* mice can still generate cochlea microphonic (CM) responses and summating potentials (SP). The CM mimics the waveform of the sound stimuli and is proportional to the displacement of the basilar membrane. SP is the direct current response of hair cells as they move with the basilar membrane. This suggests that some the hair cells are still able to depolarise in response to sound and that mutant myosin 7a is sufficient for the stereocilia to develop normally initially.

The CM was nearly normal, despite lacking one row of OHC stereocilia. However, the SP response could only be elicited at high sound intensities, and the compound action potential (CAP) was abnormal. The CAP represents synchronous firing of cochlea neurons. This suggests that myosin 7a is needed for normal function of the hair cells (Self et al., 1998).

It was thought that myosin 7a played a role in transporting the sans and harmonin protein to the upper tip link density and the reason the *Shaker-1* mouse is deaf is that these proteins are not localised correctly. However, in the *Shaker-1* mouse, staining for myosin 7a, harmonin and sans shows that all three proteins are correctly located to the upper tip link density at P12-13 (Figure 3.3). This suggests that either the *Shaker-1* mutation doesn't affect cargo transporting ability of myosin 7a or there is another protein that is also responsible for transporting these proteins (Grati & Kachar, 2011).

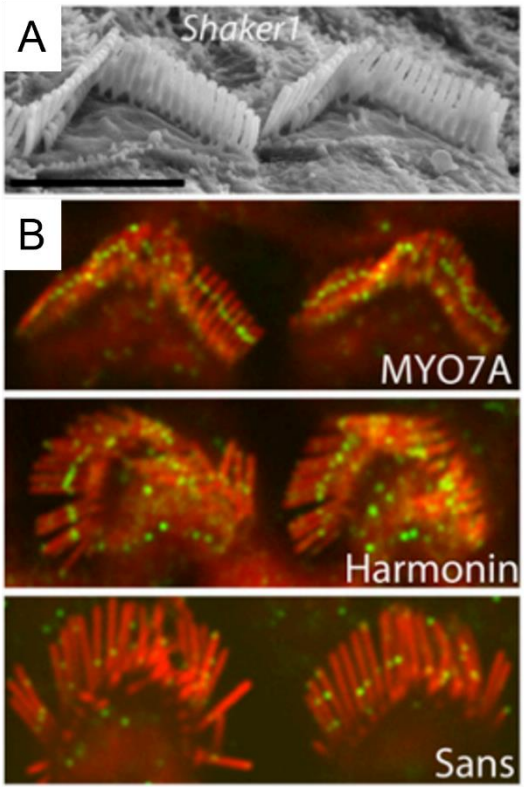

Figure 3.3- Immunostaining for Myo7a, harmonin and sans protein in a *Shaker-1* mouse

(A) SEM image of P12-13 *Shaker-1* mouse OHC showing the loss of the third row of stereocilia. (B) Immunostaining of P12-13 *Shaker-1* OHCs for myosin 7a, harmonin and sans, showing that these three proteins still localise to the upper tip link density in the *Shaker-1* mouse (Grati and Kachar, 2011).

Another proposed hypothesis for the *Shaker-1* mouse deafness is that the mutation affects the hydrolysis of ATP by myosin 7a. Xiong *et al.* (2018) found that ATP hydrolysis in the *Shaker-1* mouse is two hundred times slower that in the wild type and this hampers the motor function of the protein. However, as the ATP binding site is on the opposite side of the protein to the point mutation it is unclear how this mutation would affect ATP binding (Xiong et al., 2018).

This chapter explores how the *Shaker-1* mutation affects the function and morphology of the hair bundle and what this can tell us about the role of myosin 7a in mechanotransduction.

3.2 Results

3.2.1 The *Shaker-1* mutation affects hearing thresholds

To measure the impact of the *Shaker-1* mutation on hearing thresholds, ABR recordings were taken from *Shaker-1*$^{+/-}$ and *Shaker 1*$^{-/-}$ mice at P18 (Figure 3.4). At P18 the *Shaker 1*$^{-/-}$ mutant mice show a severe hearing impairment at all frequencies tested (P<0.05, 2-way ANOVA, Šidák post-test), however they still have hearing at the higher dB SPL levels. This shows that the *Shaker 1*$^{-/-}$ mutation is affecting hearing in this mouse model.

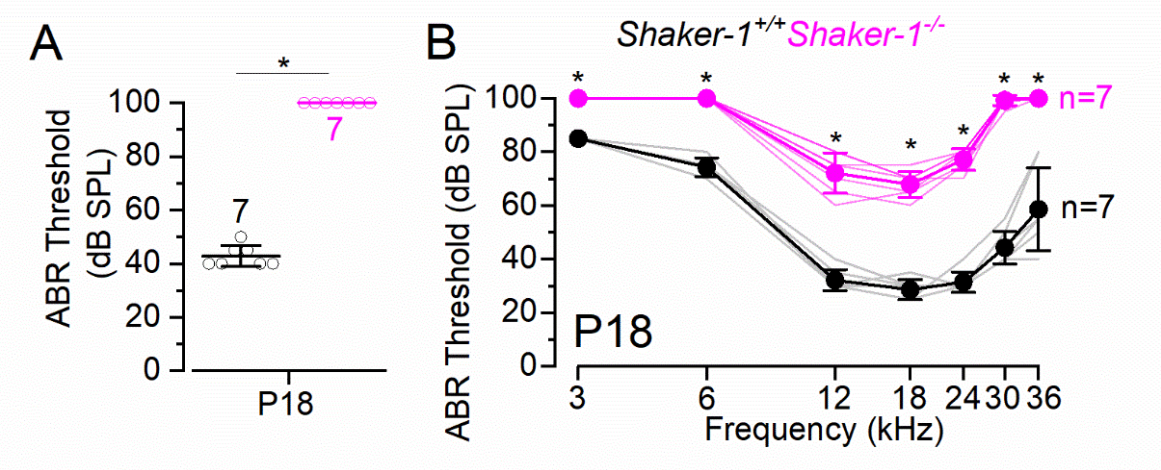

Figure 3.4- ABR recordings from the *Shaker-1* mice at P18

(A) Mean ABR thresholds for clicks from control *Shaker-1*$^{+/-}$ (n=7) and littermate *Shaker 1*$^{-/-}$ mice (n=7) at P18. (B) ABR thresholds for frequency-specific pure tone stimulation from 3kHz to 30kHz from control *Shaker-1*$^{+/-}$ and littermate *Shaker-1*$^{-/-}$ mice. In the *Shaker-1*$^{-/-}$ mouse the hearing threshold is increased at all frequencies tested. Values are mean ± S.D. P<0.05, post-hoc Sidak's test following two-way ANOVA, and students t-test, (n=animals). *Shaker-1*$^{+/-}$ control (black), *Shaker 1*$^{-/-}$ (pink). Experiment carried out by Walter Marcotti and reproduced with consent.

3.2.2 The *Shaker-1* mutation affects the morphology of the hair bundle

To determine at which point the hair bundle starts to lose the third row of stereocilia, SEM was carried out on *Shaker-1* mice at P6, P12 and P29-32. At P6 it is apparent that both the third and second row of OHC stereocilia is shorter in the *Shaker-1* mice than in the control mice. For the IHCs, there was no discernible shortening of hair bundle stereocilia at this age

(Figure 3.5). This shows that the shortening of stereocilia in the OHC hair bundle starts at a very early age. There is currently no accurate way to measure the length of stereocilia using SEM. To get a precise measurement of the length and width of stereocilia, they would need to be examined with transmission electron microscopy (TEM). Therefore, this experiment can only indicate large changes in bundle morphology.

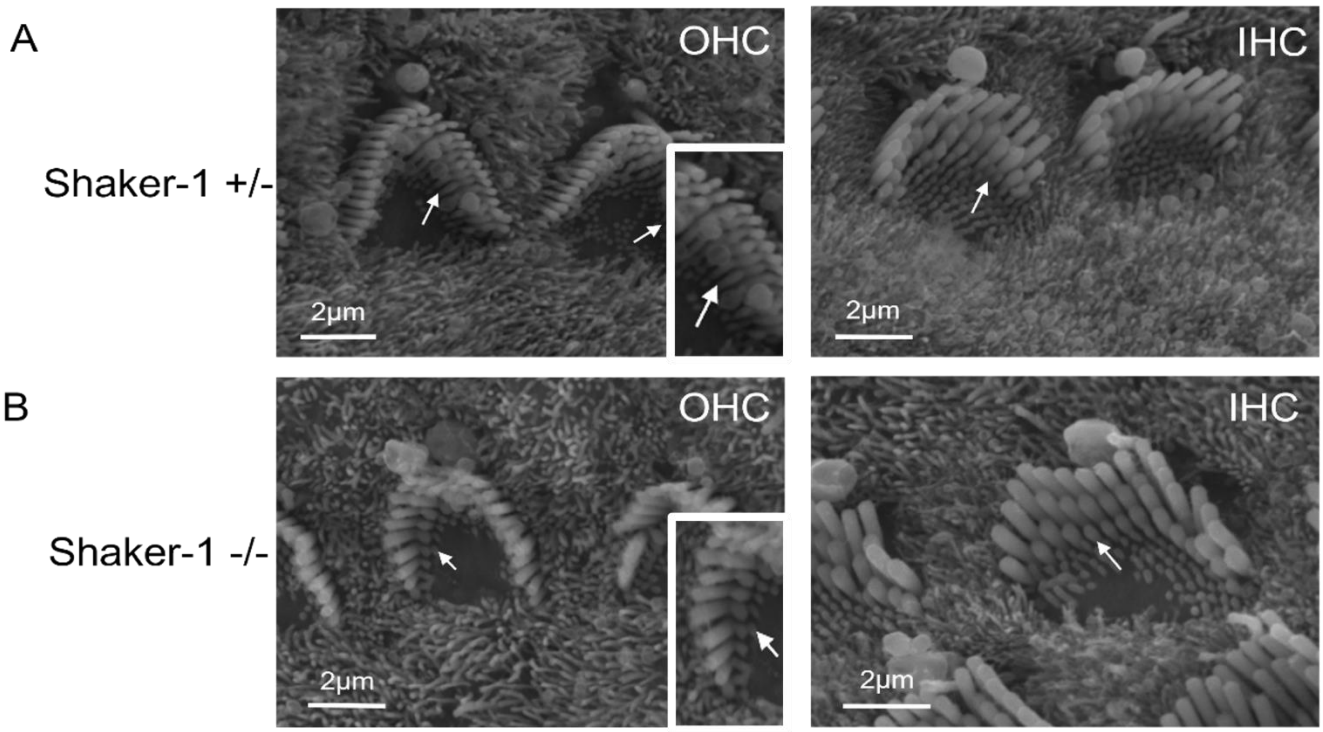

Figure 3.5- SEM of apical section of P6 *Shaker-1* cochlea

Scanning electron micrographs showing the IHCs and OHCs from the apical coil of a (A) control *Shaker-1*$^{+/-}$ (n=3) and (B) littermate *Shaker 1*$^{-/-}$ mice at P6 (n=3). In the control *Shaker-1* mouse the arrows indicate the presence of the third row of stereocilia. In the *Shaker 1*$^{-/-}$ mouse the arrows shows the missing row of stereocilia in the OHC hair bundle. For the IHCs the arrows show the normal bundle morphology and presence of all rows of stereocilia. (n=animals).

At P12, as shown by Self *et al.*, (1998), the third row of stereocilia in the OHCs has completely disappeared. For the IHCs, most hair bundles show no abnormalities, but a few show some disorganisation (Figure 3.6).

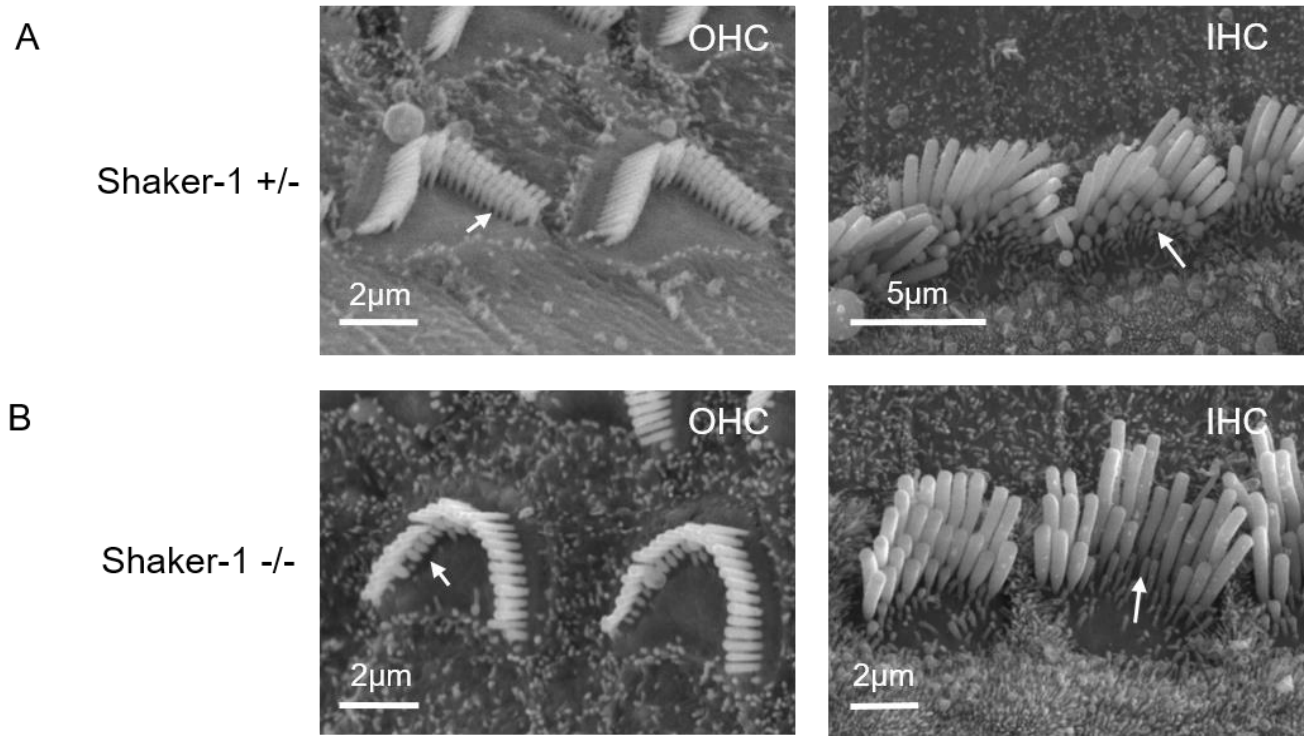

Figure 3.6- SEM of apical section of P12 *Shaker-1* cochlea

Scanning electron micrographs showing the IHCs and OHCs from the apical coil of a (A) control *Shaker-1*$^{+/-}$ (n=5) and (B) littermate *Shaker 1*$^{-/-}$ mice at P12 (n=6). The arrows in the control images show the normal bundle morphology with all three rows of stereocilia present. The arrows in the *Shaker 1*$^{-/-}$ OHC image indicates the loss of the third row of stereocilia. The arrow in the *Shaker 1*$^{-/-}$ IHC image shows the presence of disorganisation in some hair bundles.

To investigate whether the stereocilia loss continues as the mouse ages, further SEM was done at P29-32 (Figure 3.7). At this age, the OHC hair bundle looks similar to the P12 *shaker 1*$^{-/-}$mouse, in that there are still two rows of stereocilia that look to be a similar length. However, in the IHCs there was a marked difference compared to those at P12, with the third and second row of stereocilia disappearing. This suggests that, in the *shaker 1*$^{-/-}$ mouse, myosin 7a is needed for the maintenance of the hair bundle from an early age and loss of IHC stereocilia happens after loss of OHC stereocilia.

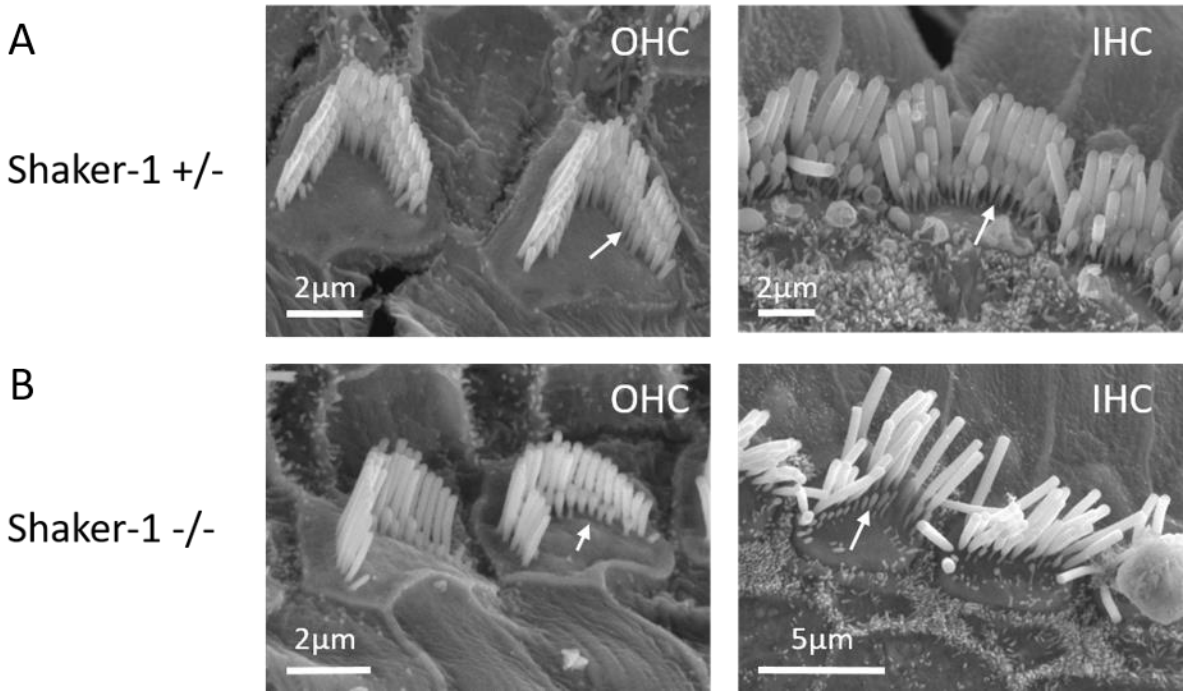

Figure 3.7- SEM of apical coil of a P29-32 *Shaker-1* cochlea

Scanning electron micrographs showing the IHCs and OHCs from the apical coil of a (A) control *Shaker-1*$^{+/-}$ (n=2) and (B) littermate *Shaker 1*$^{-/-}$ mice at P29-32 (n=3). In the control images the arrows show the normal morphology of the hair bundle with all three rows of stereocilia. In the *Shaker 1*$^{-/-}$ images the arrows indicate the missing rows of stereocilia.

3.2.3 OHC MET current and resting open probability is affect by the *Shaker-1* mutation

As in the conditional knockout of myosin 7a, we investigated the function of the MET channel in the *Shaker-1* model by measuring the MET current as the hair bundle is being displaced by a piezo driven fluid jet (see Methods). When the bundles are displaced towards the excitatory direction (towards the tallest stereocilia) there is a large inward current when a negative membrane potential is applied. When the bundle is displaced towards the inhibitory direction the channels open at rest are closed, removing the resting open probability. As the OHCs are depolarised, the MET current decreases in size as the electrochemical gradient driving ions through the MET channel reduces. Due to the non-selective permeability of the MET channel to cations, the current reverses around 0mV. The current then becomes outwards and there is a larger resting open probability at the positive membrane potentials (Corns et al., 2014). Current-voltage curves were obtained by stimulated the hair bundles while stepping the membrane potential from -124mV to +99mV in 20mV steps.

For this experiment the MET current was measured at a range of ages from P5-P10. At P5, P7 and P8 the MET current in the *shaker 1*$^{-/-}$ mouse is comparable to the control mouse (Figure 3.9).

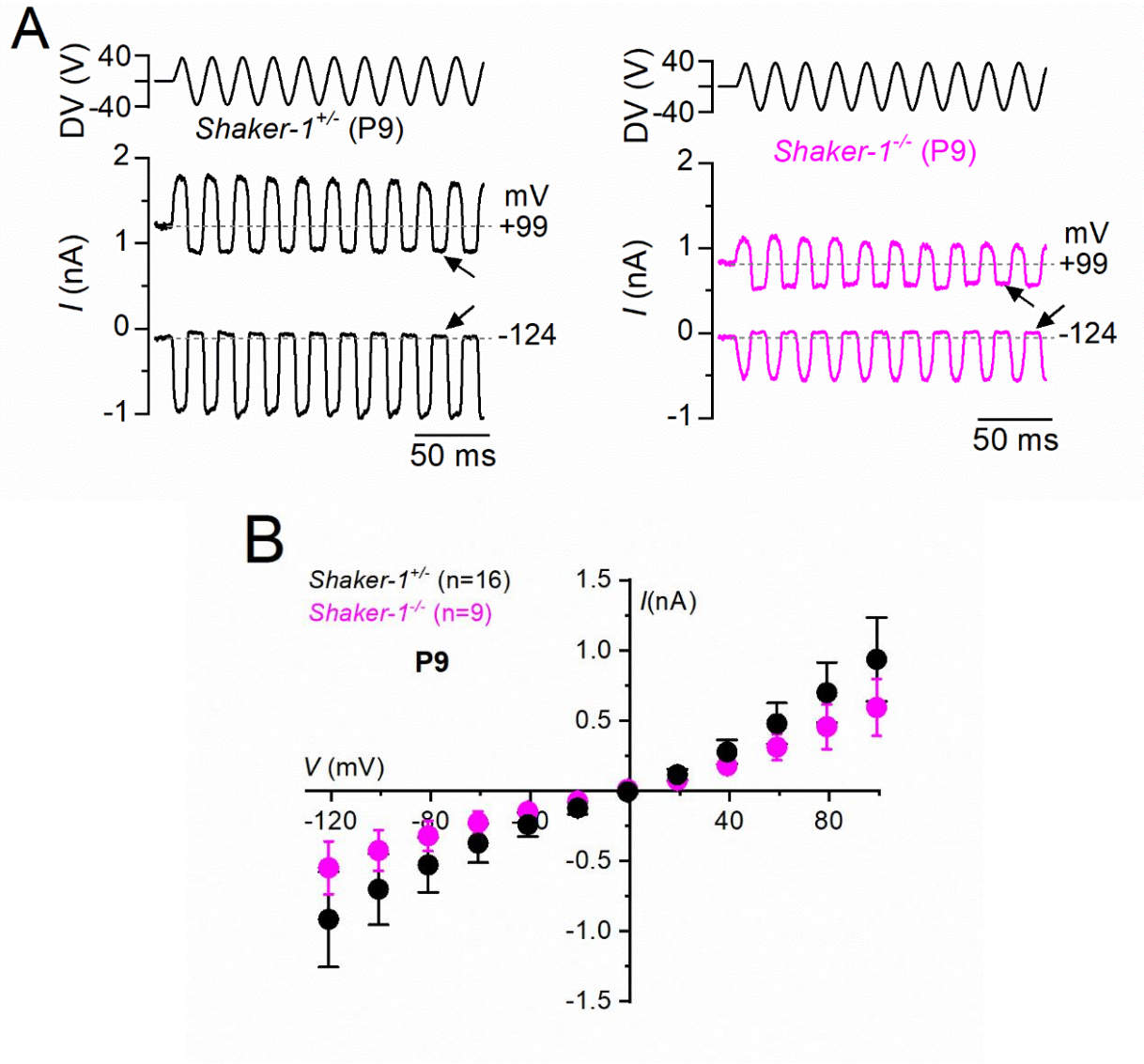

Figure 3.8- MET current in *Shaker-1* OHCs at P9

(A) saturating MET current in apical coil OHCs from P9 control *Shaker-1*$^{+/-}$ and littermate P9 *Shaker 1*$^{-/-}$ mice in response to the sine wave stimuli at -124mV and +99mV. (B) average MET current-voltage curves from P9 control *Shaker-1*$^{+/-}$ (n=16 (10)) and littermate *Shaker 1*$^{-/-}$ (n=9 (7)) mice. Current-voltage curves were obtained by stimulated the hair bundles while stepping the membrane potential from -124mV to +99mV in 20mV steps. Values are mean ± S.D, (n=cells (animals)). *Shaker-1*$^{+/-}$ control (black),

From P9 onwards there was a steady decrease in the size of the MET current, which is significantly smaller at P9 and P10 in the *shaker 1*$^{-/-}$ mouse compared to the control mouse (Figure 3.8). Figure 3.10 shows the steady decline in the size of the MET current from P5 (P=0.77, 2-way ANOVA, Šidák post-test) to P9 (P=0.01, 2-way ANOVA, Šidák post-test) and P10 (P=0.01, 2-way ANOVA, Šidák post-test). This demonstrates that the *Shaker-1* mutation to myosin 7a disrupts the normal function of the MET channel.

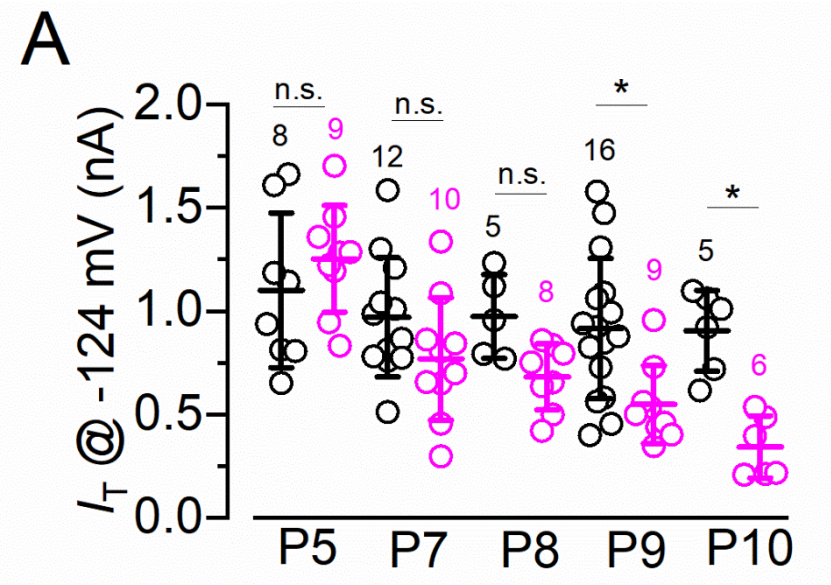

Figure 3.10- Average MET current in *Shaker-1* OHCs from P5-P10

(A) maximal size of the MET current in control *Shaker-1*$^{+/-}$ and littermate *Shaker 1*$^{-/-}$ mice at -124mV at P5 and P7-P10. At P5, P7 and P8 the size of the MET current in the *Shaker 1*$^{-/-}$ is comparable to the *Shaker-1*$^{+/-}$ mouse. From P9 onwards the size of the MET current in the *Shaker 1*$^{-/-}$ is significantly smaller and steady decreases in size. P<0.05, 2-way ANOVA, Šidák post-test. Values are mean ± S.D, (n=cells). *Shaker-1*$^{+/-}$ control (black), *Shaker 1*$^{-/-}$ (pink).

It was expected that as there is no effect on the resting open probability in the conditional knockout of myosin 7a that this would also be the case in the *Shaker-1* mouse. However, Figure 3.11 shows the steady increase of the resting open probability in the *shaker 1*$^{-/-}$ mouse, from very small at +99mV in the P5 *shaker 1*$^{-/-}$ mouse compared to the P5 control mouse (P=0.01, 2-way ANOVA, Šidák post-test) to a size that is comparable to the control mice at P10 (P=0.99, 2-way ANOVA, Šidák post-test). The resting open probability is significantly smaller

in the *shaker 1*$^{-/-}$ mouse at P5 at -124mV and +99mV and at P8 at +99mV, although it is not statistically significantly smaller at P7. This could be explained by the large amount of variation in the recordings at P7.

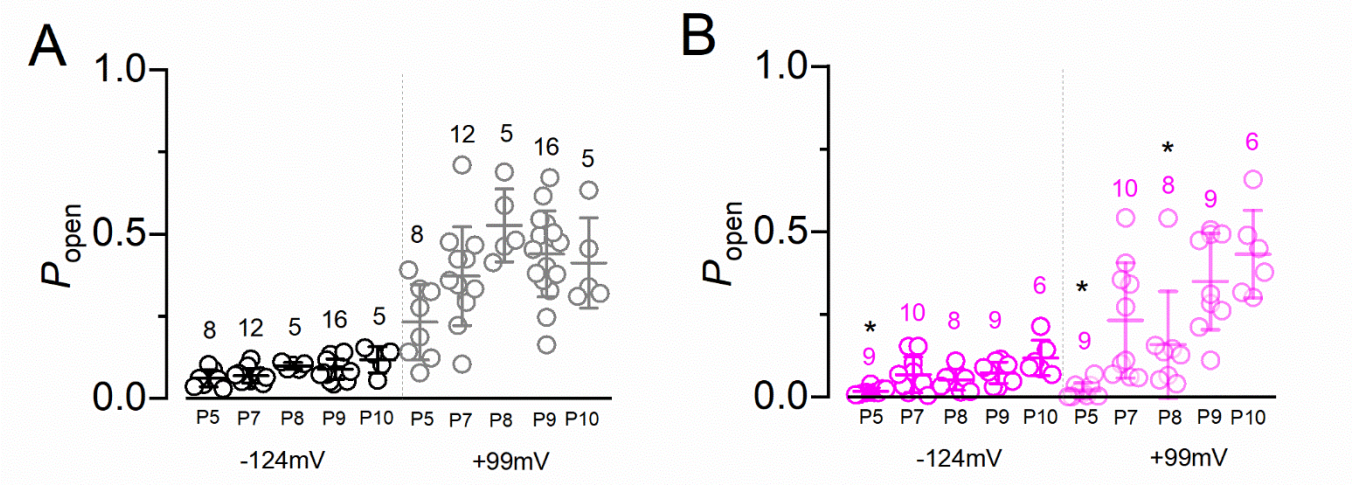

Figure 3.11- Average resting open probability from *Shaker-1* OHCs from P5-P10

(A) size of MET resting open probability from control *Shaker-1*$^{+/-}$ at -124mV and +99mV at P5 and P7 to P10. (B) size of resting open probability from littermate *Shaker 1*$^{-/-}$ mice at -124mV and +99mV at P5 and P7 to P10. In the control mice the open probability stays relatively constant across the ages. In the *Shaker 1*$^{-/-}$ mice there is a steady increase in the open probability from P5-P10. P<0.05, 2-way ANOVA, Šidák post-test. Statistical significance was measured between genotypes. Values are mean ± S.D, (n=cells). *Shaker-1*$^{+/-}$ control (black), *Shaker 1*$^{-/-}$ (pink).

3.2.4 Inner hair cell MET current is affected by the *Shaker-1* mutation

We also looked at the MET current in IHCs to compare them to what we see in the OHCs. IHCs are longer and more prone to breaking, so stimulating the hair bundle repeatedly at increasing voltages makes it very difficult to get reliable recordings. Therefore, for IHCs recordings, the hair bundle was only stimulated at one voltage (-124mV). Figure 3.12 shows that the size of the MET current in the *shaker 1*$^{-/-}$ mouse is similar to the control at P8/9 and is smaller in the *shaker 1*$^{-/-}$ mice at P12/13. Figure 3.13 shows that there is no significant difference between the MET current size at P8/9 (P=0.45, 2-way ANOVA, Šidák post-test, Figure 3.13). However, it is significant at P12-13 (P=0.05, 2-way ANOVA, Šidák post-test,

Figure 3.13). Measuring the MET current at an older time point could show whether the decline in MET current size continues.

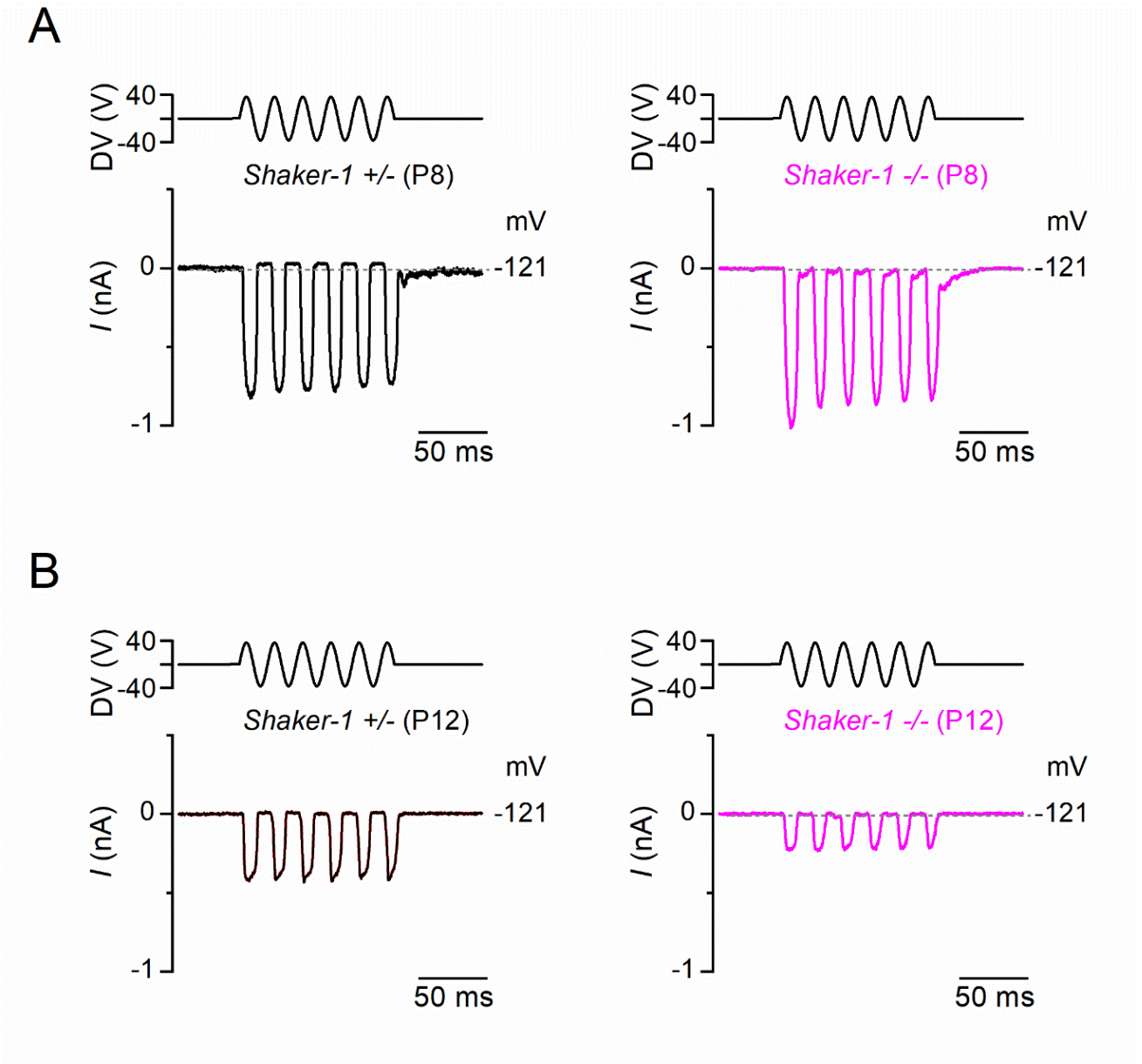

Figure 3.12- MET current in *Shaker-1* IHCs at P8/9 and P12/13

(A) Saturating MET current in apical coil IHCs from P8 control *Shaker-1*$^{+/-}$ and P8 *Shaker 1*$^{-/-}$ mice in response to the sine wave stimuli at -124mV and +99mV. (B) Saturating MET current in apical coil IHCs from P12 control *Shaker-1*$^{+/-}$ and P12 *Shaker 1*$^{-/-}$ mice in response to the sine wave stimuli at -124mV and +99mV. *Shaker-1*$^{+/-}$ control (black), *Shaker 1*$^{-/-}$ (pink). Experiment carried out by Adam Carlton and reproduced with consent.

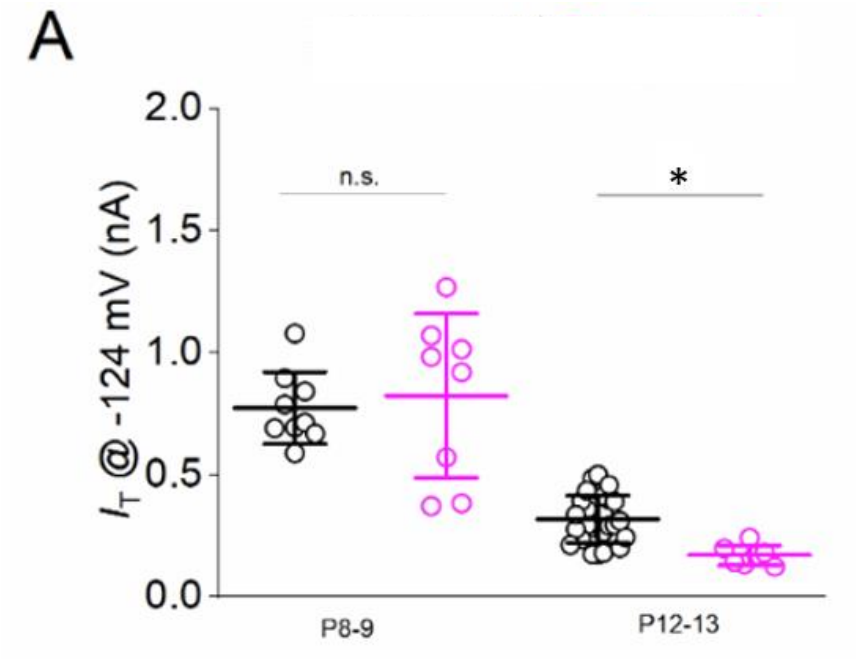

Figure 3.13- Average IHC MET current size at P8-9 and P12-13

(A) MET current size at -124mV from P8-9 control *Shaker-1*$^{+/-}$ (n=9 (4)) and littermate *Shaker 1*$^{-/-}$ (n=8 (4)) mice and P12-13 control *Shaker-1*$^{+/-}$ (n=29 (11)) and littermate *Shaker 1*$^{-/-}$ (n=7 (3)) mice. P<0.05, 2-way ANOVA, Šidák post-test. Values are mean ± S.D, (n=cells (animals)). *Shaker-1*$^{+/-}$ control (black), *Shaker 1*$^{-/-}$ (pink). Experiment carried out by Adam Carlton and reproduced with permission.

The resting open probability was also investigated in the IHCs to determine whether the increase in resting open probability size seen in the OHCs would also be seen in the IHCs. At P8-9 the resting open probability in the IHCs is significantly smaller in the *shaker 1*$^{-/-}$ mouse, compared to the control mouse (P=0.002, 2-way ANOVA, Šidák post-test, Figure 3.14), then at P12-13 the resting open probability increases to be comparable to the control mouse (P=0.97, 2-way ANOVA, Šidák post-test, Figure 3.14). This increase in resting open probability over time in the IHCs is similar to what is seen in the OHCs, albeit at a later time point.

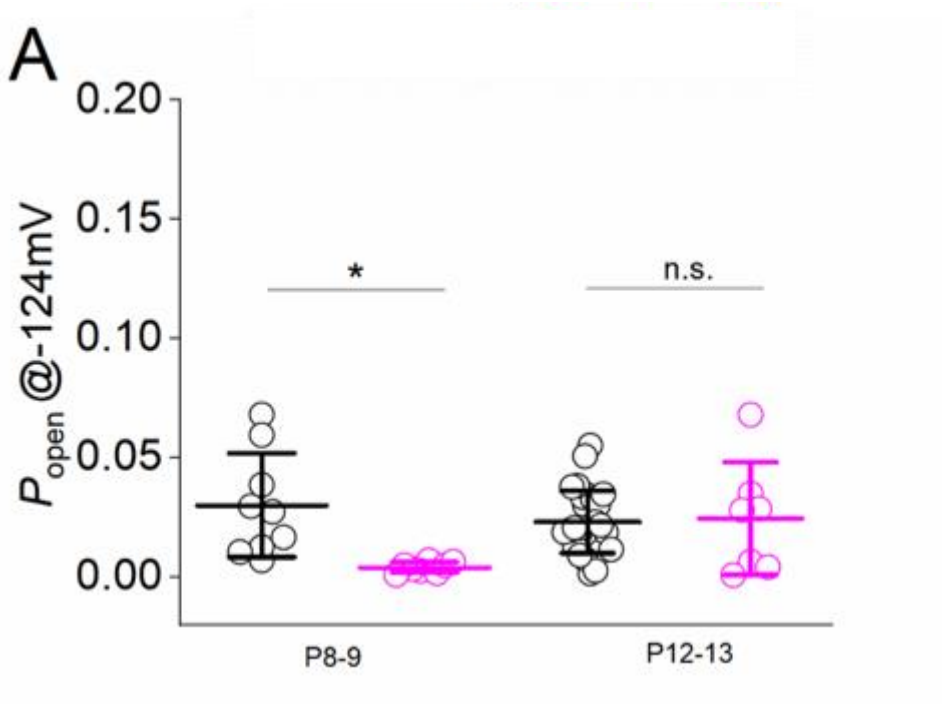

Figure 3.14- Average MET resting open probability in IHCs at P8-9 and P12-13

(A) resting open probability at -124mV from P8/9 control *Shaker-1*$^{+/-}$ (n=9 (4)) and littermate *Shaker 1*$^{-/-}$ mice (n=8 (4)) and P12-13 control *Shaker-1*$^{+/-}$ (n=29 (11)) and littermate *Shaker 1*$^{-/-}$ mice (n=7 (3)). At P8/9 the resting open probability is significantly smaller in the *Shaker 1*$^{-/-}$ mouse. At P12/13 the resting open probability in the *Shaker 1*$^{-/-}$ is similar to the size in the control mouse. P<0.05, students t -test. Values are mean ± S.D, (n=cells (animals)). *Shaker-1*$^{+/-}$ control (black), *Shaker 1*$^{-/-}$ (pink). Experiment carried out by Adam Carlton and reproduced with permission.

3.2.5 Effect of reducing intracellular calcium on the OHC MET current in the *Shaker-1* mouse at P9

The calcium sensitivity of the MET current was measured in the OHCs using intracellular solution containing either 0.1mM or 5mM of BAPTA. The 5mM BAPTA intracellular solution removes calcium from the internal environment of the cell. Removing calcium from the internal environment reduces adaptation of the MET channel and increases the size of the resting open probability. This allows investigation into whether the calcium sensitivity of the MET channel is affected by the *Shaker-1* mutation. Figure 3.15 illustrates the effect BAPTA has on the size of the resting open probability.

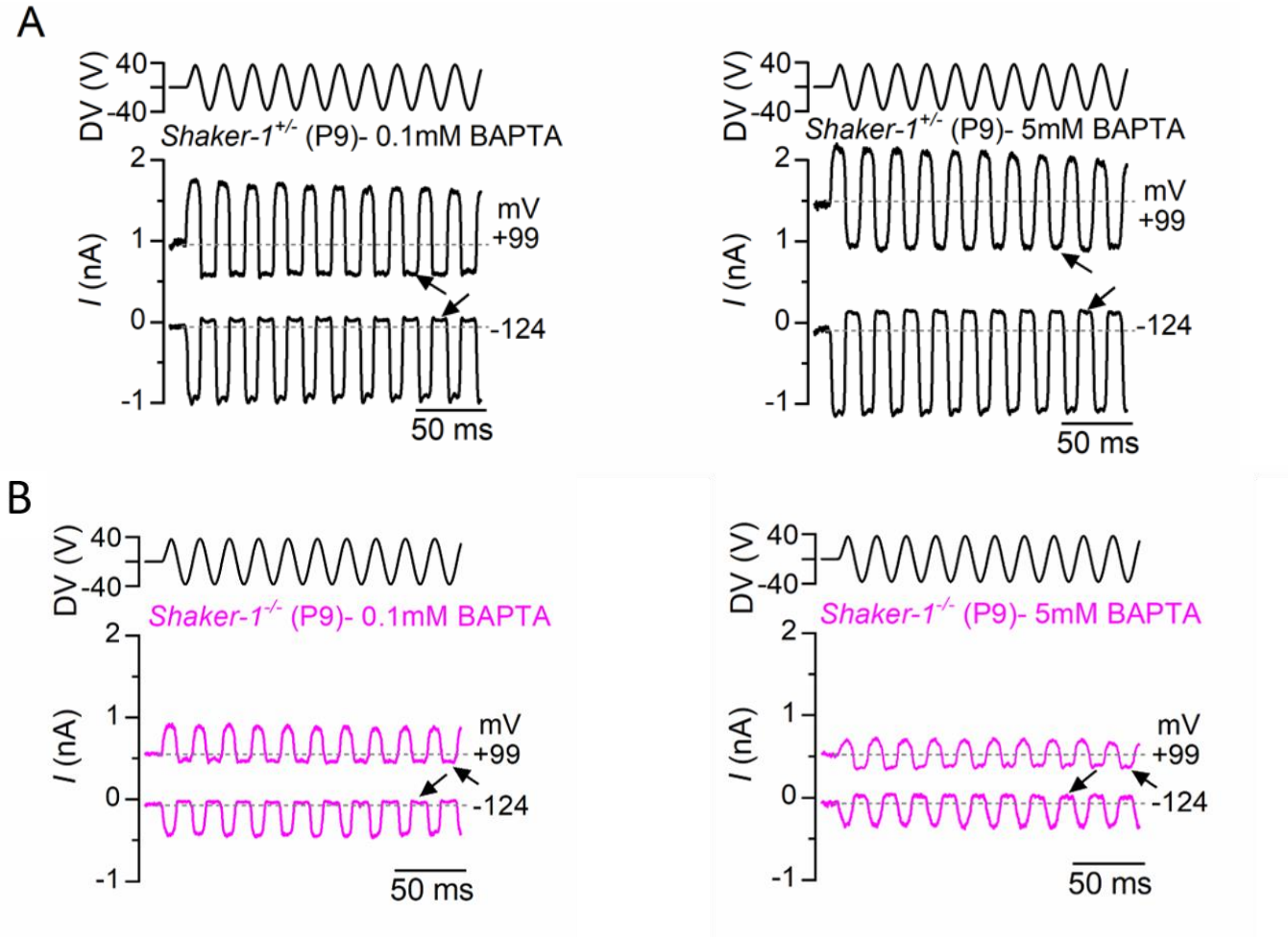

Figure 3.15- Resting open probability in P9 *Shaker-1* OHCs in the presence of different concentrations of BAPTA

The resting open probability (Po) of the MET current in OHCs from both genotypes at the holding potentials (A) -121mV and (B) +99mV at P9 in the presence of 5mM BAPTA in the intracellular solution. *Shaker-1*$^{+/-}$ control (black), *Shaker 1*$^{-/-}$ (pink).

In the control mice, using an intracellular solution containing 5mM BAPTA did not significantly increase the size of the resting open probability at -124mV (P=0.15; 2-way ANOVA, Šidák post-test) or +99mV (P=0.45; 2-way ANOVA, Šidák post-test). In the *Shaker 1*$^{-/-}$ mouse, using a 5mM BAPTA intracellular solution caused a small increase in the size of the resting open probability which was statistically significant at -124mV (P=0.05; 2-way ANOVA, Šidák post-test) but not at +99mV (P=0.37; 2-way ANOVA, Šidák post-test, Figure 3.16). This could be due to the larger variation in data points at +99mV than at -124mV.

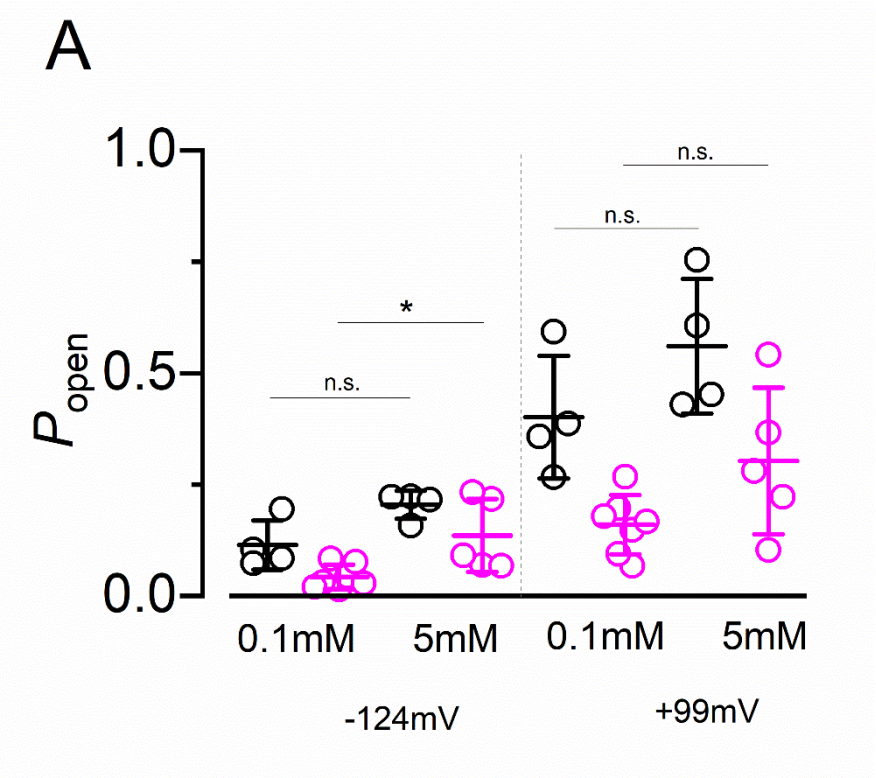

Figure 3.16- Average resting open probability in P9 *Shaker-1* OHCs in the presence of different concentrations of BAPTA

(A) Average resting open probability at P9 from control *Shaker-1*$^{+/-}$ (0.1mM n=4 (4), 5mM n=4 (4)) and littermate *Shaker 1*$^{-/-}$ mice (0.1mM n=7 (5), 5mM n=5 (5)) at -124mV and +99mV in the presence of 0.1mM and 5mM BAPTA. In both the control and *Shaker 1*$^{-/-}$ mice using 5mM BAPTA did not cause an increase in the size of the resting open probability, except in the *Shaker 1*$^{-/-}$ mouse at -124mV. $P<0.05$, 2-way ANOVA, Šidák post-test. Values are mean ± S.D, (n=cells (animals)). *Shaker-1*$^{+/-}$ control (black), *Shaker 1*$^{-/-}$ (pink).

The lack of significance in this experiment could be due to low n numbers and high variation in the data. More recordings were not taken due to a lack of time to do further experiments. There is a trend toward a higher resting open probability with the 5mM BAPTA intracellular solution, so increasing the n numbers could make the results of this experiment more significant. Overall, as the 5mM BAPTA didn't increase the open probability in the control mice, it is difficult to conclude anything from this experiment.

3.2.6 Localization of harmonin isn't affected by the *Shaker-1* mutation

As discussed in the previous chapter, myosin 7a is closely associated with harmonin in the MET current machinery. To investigate whether the *Shaker-1* mutation affects the localisation of harmonin, immunostaining was carried out in the *Shaker-1* mouse for harmonin at P15 (Figure 3.17). In the *shaker* $1^{-/-}$ mouse at P15 harmonin still localises to the stereocilia, suggesting that the *Shaker-1* mutation doesn't affect localisation of harmonin.

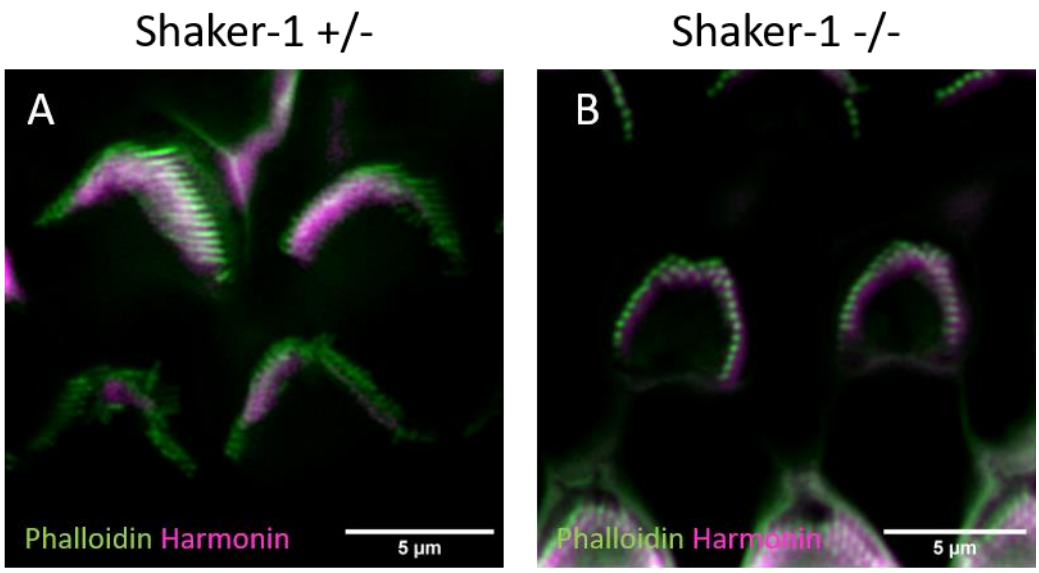

Figure 3.17- The *Shaker-1* mutation doesn't affect the localisation of harmonin

Immunostaining apical coil OHCs from (A) *Shaker-*$1^{+/-}$ (n=5) and (B) *Shaker-*$1^{-/-}$ (n=2) mice with phalloidin and harmonin. Harmonin can be seen in the OHC stereocilia in both the control and *Shaker-*$1^{-/-}$ mouse images. Images are summed intensity projections of a confocal z stack image.

3.3 Discussion

This chapter covers a detailed investigation into the effect of the *Shaker-1* mutation on mechanotransduction and the morphology of the hair bundle. The *Shaker-1* mutation is a point mutation in the area of the myosin 7a protein that binds to actin. It is already known that the *Shaker-1* mutation affects the morphology of the hair bundle, but so far no work has been done on how mechanotransduction is affected in this mouse.

The *Shaker-1* mutation causes hearing impairment in these mice, as seen in the increased ABR threshold at P18. However, the mice were not completely deaf at this age. ABR's at an older age point would show whether the hearing continues to deteriorate as the mouse ages.

The *Shaker-1* mutation also affects the morphology of the hair bundle, suggesting that myosin 7a protein is needed for proper development of the hair bundle. With the mutated myosin 7a protein there is a progressive disappearance of the hair bundle. At P6 there is shortening of the second and third stereocilia in the OHCs and by P12 the third row of stereocilia has disappeared completely. At one month, the morphology of the OHC hair bundle looks quite similar to the P12 OHC hair bundle. This suggests that that the rate of stereocilia loss slows down after P12. SEM at older ages is needed to see if the hair bundle loses the final row of stereocilia.

In the IHCs the hair bundle looks normal at P6. At P12 there are some hair bundles that look disorganised, but most have a normal morphology. At one month old the second and third row of stereocilia have disappeared. It seems that the progression of degeneration is slower in the IHCs than in the OHCs.

The *Shaker-1* mutation also affects the MET current. At P5, P7 and P8 the size of the MET current in the *shaker* $1^{-/-}$ mouse was comparable to the control mouse. However, from P9 to P10 there was a steady decline in the size of the MET current. This demonstrates that the *Shaker-1* mutation affects the MET current in hair cells. When the resting open probability was measured, it was observed that the resting open probability was close to zero at P5-P8 in the *shaker* $1^{-/-}$ mouse. However, at P9 and P10 the size of the resting open probability returned to a normal size. This effect was unexpected, and it is unclear why the resting open probability would be close to zero at the younger ages and then increase to a normal sized resting open probability as the mouse ages.

This increase in resting open probability size as the mouse ages is also seen in the IHCs, with the resting open probability being very close to zero at P8-9. Then at P12-13 the *shaker 1*$^{-/-}$ mice had a normal sized resting open probability. As this effect is seen in both the OHCs and IHCs it seems more likely that this is a real phenotype.

The increase in MET current size from P5 to a normal level at P10 was surprising and it is not clear what mechanism is behind this finding. One hypothesis is that this effect is linked to the Tmc1 and Tmc2 proteins. These are both proteins thought to make up the MET channel. Tmc2 is expressed early in development and is replaced by tmc1 from the end of the first postnatal week (Kawashima et al., 2011). The timing of the replacement of tmc2 by tmc1 seems to match with the timing of the changes in resting open probability in the *shaker 1*$^{-/-}$ mouse. If this is the case, then it suggests that myosin 7a has a role in the exchange between tmc2 and tmc1. It is not clear what that role could be or if there is another mechanism responsible altogether.

To try and understand the effect of the *Shaker-1* mutation on the MET channel and resting open probability, a high concentration of BAPTA was used to measure calcium sensitivity of the MET channel at P9. Whilst the presence of BAPTA did increase the size of the resting open probability in the *Shaker 1*$^{-/-}$ mouse at -124mV, there was no change in resting open probability in the control mice at either voltage. This lack of sensitivity could be due to the low n numbers used in this experiment, and the large variation seen in the data. Unfortunately, there was not enough time during the project to increase the n numbers to see if the results would reach significance. As the 5mM BAPTA did not increase the resting open probability size in the controls it was not possible to reach any conclusions regarding calcium sensitivity from this experiment.

The last aspect of this investigation was to look at how the *Shaker-1* mutation affects the localisation of harmonin. In the *shaker 1*$^{-/-}$ mouse there was no change to the localisation of harmonin compared to the control mouse at P15. This suggests that the mutation in myosin 7a is not needed for the transport of harmonin to the upper tip link density.

In conclusion, the *Shaker-1* mutation affects hearing, mechanotransduction and morphology of the hair bundle. This demonstrates that the *Shaker-1* mutation affects the function of

myosin 7a and that myosin 7a is necessary for normal hearing and for normal development of the hair bundle. Myosin 7a is also necessary for the normal function of the MET channel.

Chapter 4 - Electrophysiological properties and morphology of hair cells in a conditional myosin 7a knockout mouse

4.1 Introduction

4.1.1 Role of myosin 7a in hearing

Data from the constitutive myosin 7a knockout mice has shown that myosin 7a has a vital role in hearing. In the constitutive knockout mouse model, from P3, there is disorganisation of the bundle, and the normal horse-shoe shape is lost. In the constitutive knockout there was also an abnormal gating of the MET channel and the resting open probability was close to zero at hyperpolarising potentials (Kros et al., 2002). This suggested that myosin 7a is involved in the initial development of the hair bundle and gating the MET channel.

So far, all the information we have gathered about myosin 7a is based on data from constitutive myosin 7a knockout models. It is possible that the phenotypes seen in the constitutive knockout mouse are related to widespread degeneration of the hair bundles rather than the role of myosin 7a itself. We have hypothesised that using a conditional knockout to investigate the function of myosin 7a would give results that can be more clearly interpreted. The conditional knockout would also help separate the role myosin 7a might have in maintaining the hair bundle from its role in hair cell development.

Some preliminary work carried out in the Marcotti lab on conditional knockouts used myosin 7a floxed mice crossed with myosin-15 cre (see Methods for details). Myosin-15 is a hair cell specific protein that is only expressed from P4, so the hair bundle is, initially, allowed to develop normally. This should avoid any phenotypes caused by disorganisation and degeneration of the hair bundle.

Work by Carberlotto *et al.* (2011) on another Usher 1 protein, sans (Ush1g), showed that the phenotypes in the constitutive knockout are different to the phenotypes seen in a conditional knockout. For the constitutive mouse model they used a strain where the mutation in the Ush1g gene arose spontaneously in the A/J mouse strain (Kikkawa et al., 2003). For the conditional knockout, a $Ush1g^{fl/fl}$ mouse was generated by targeting exon 2 of the gene. This mouse was then crossed with a PGK-cre mouse, this meant that the protein would only be knocked out from P4.

In the mouse with a constitutive knockout of sans there was profound postnatal disorganisation of the hair bundle. Also, the size and sensitivity of the MET current was strongly reduced. However, in the conditional knockout, where the sans protein was knocked

out from P4, there were still some morphological defects to the stereocilia, and the MET current was slightly smaller. However, there was no change to the sensitivity of the MET current after stimulation of the hair bundle. This demonstrates that not all the phenotypes in the constitutive knockout are directly related to the role of the sans protein (Caberlotto et al., 2011). Following on from this study it seemed possible that the phenotypes described from the other Usher 1 constitutive protein knockouts, such as myosin 7a, might also be due to secondary degeneration of the hair bundle.

One hypothesis for the role of myosin 7a that was investigated in this work, is that myosin 7a is needed to transport other proteins involved in mechanotransduction to the upper tip link density. For example, harmonin is known to form a complex with myosin 7a and it is possible that myosin 7a has a role in transporting harmonin along the stereocilia (Bahloul et al., 2010). Immunohistochemical staining was carried out to investigate what effect the conditional knockout of myosin 7a would have on harmonin localisation.

This work aimed to better understand the role of myosin 7a by using a conditional knockout of myosin 7a. A combination of electrophysiological and morphological studies were carried out to investigate what effect a conditional knockout of myosin 7a has on the hair cells.

4.1.2 Tecta mice

In order to understand how the knockout of myosin 7a affects the function and maintenance of the hair bundle as the mouse ages, it was important to carry out electrophysiological recordings past the onset of hearing (P12). This allowed us to measure the MET current at a range of ages and determine whether there is a decrease in MET size or resting open probability size. However, at the onset of hearing, the tectorial membrane (TM) becomes attached to the tallest stereocilia of OHCs (see Figure 4.1). The tectorial membrane (TM) is a piece of extracellular matrix that sits on top of the organ of corti and is essential for hearing. When performing electrophysiology, the TM has to be removed to allow access to the hair

cells. However, this causes damage to the OHC bundle and makes is exceedingly difficult to get reliable MET current recordings.

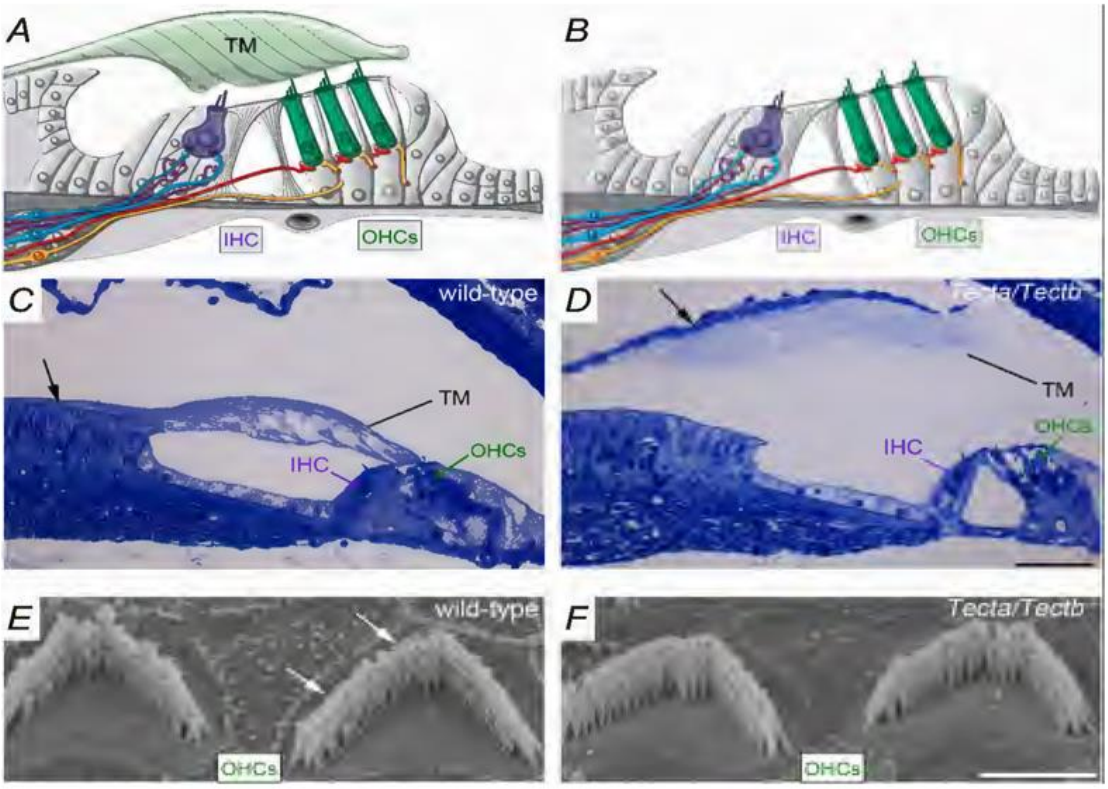

Figure 4.1- Tecta-/- mice are missing the tectorial membrane

(A,B)-Diagram showing the organ of corti in the WT and Tecta$^{-/-}$ mouse. (C,D) Toluidine blue staining of apical semi-thin sections. In the WT the TM is attached to the spiral limbus, whereas, in the Tecta$^{-/-}$ mouse the TM is detached. (E,F) Scanning electron microscopy images of OHCs from WT and Tecta$^{-/-}$ mice. In WT mice there is extra material on the tips of the taller rows of stereocilia (indicated by the arrows). However, this is not seen in the Tecta$^{-/-}$ cells (Jeng et al., 2021)

To get around this problem the *Myo-7a*$^{fl/fl}$*:Myo15-cre*$^{+/-}$ mouse was crossed with the Tecta$^{-/-}$ knock-out mouse. The Tecta$^{-/-}$ mice have a functional-null mutation to the *tecta* gene. The tecta protein is a major component of the TM and without it the TM doesn't form correctly (J.-Y. Jeng et al., 2021). Without the TM, MET current recordings can be obtained past the onset of hearing.

Jeng *et al.*, 2021 investigated the properties of the Tecta mice to ensure the physiological data obtained from them are still comparable to control mice. Electrophysiological recordings from hair cells were taken to investigate whether the hair cells in Tecta$^{-/-}$ mice mature as normal.

Mature IHCs have two characteristic ion channels: $I_{K,f}$ and $I_{K,n}$. In the IHCs of Tecta$^{-/-}$ mice both channels were normal. Mature OHCs also express the $I_{K,n}$ ion channel and this channel was found to be present in the Tecta$^{-/-}$ mouse OHCs. This shows that the hair cells in the Tecta$^{-/-}$ mice are functionally mature.

The membrane properties of hair cells were also measured to ensure they act as normal. It was found that the Tecta$^{-/-}$ mice have a normal resting membrane potential and produce normal voltage responses in current clamp recording conditions. OHCs could also produce a large MET current when stimulated and showed a normal resting open probability (J.-Y. Jeng et al., 2021).

4.2 Results

4.2.1 Conditional knockout of myosin 7a affects hearing thresholds

In order to determine whether the conditional knock-out (cKO) of myosin 7a causes deafness, ABR and DPOAE recordings were carried out on *Myo-7a$^{fl/fl}$:Myo15-cre$^{+/-}$* and *Myo-7a$^{fl/fl}$* mice at P20, P25-26 and P31-31.

Auditory brain stem responses (ABR's) measure the summed electrical response of neurons in the auditory pathway to sound stimuli. The hearing threshold is categorised as the lowest sound intensity which generates an ABR waveform.

At P20, there was no difference in response to clicks or burst-tones between 3 and 24kHz between the *Myo-7a$^{fl/fl}$:Myo15-cre$^{+/-}$* mice and the control mice. However, at 30kHz the ABR frequency was significantly higher in the *Myo-7a$^{fl/fl}$:Myo15-cre$^{+/-}$* mice ($P<0.01$, 2-way ANOVA, Šidák post-test).

At P25, the hearing threshold was increased at all frequencies ($P<0.05$, 2-way ANOVA, Šidák post-test) except 30kHz ($P=0.10$, 2-way ANOVA, Šidák post-test). The lack of statistical significance could be due to a lower n number at this time point. At P30 the mice showed a severe hearing impairment at all frequencies tested ($P<0.05$, 2-way ANOVA, Šidák post-test; Figure 4.2).

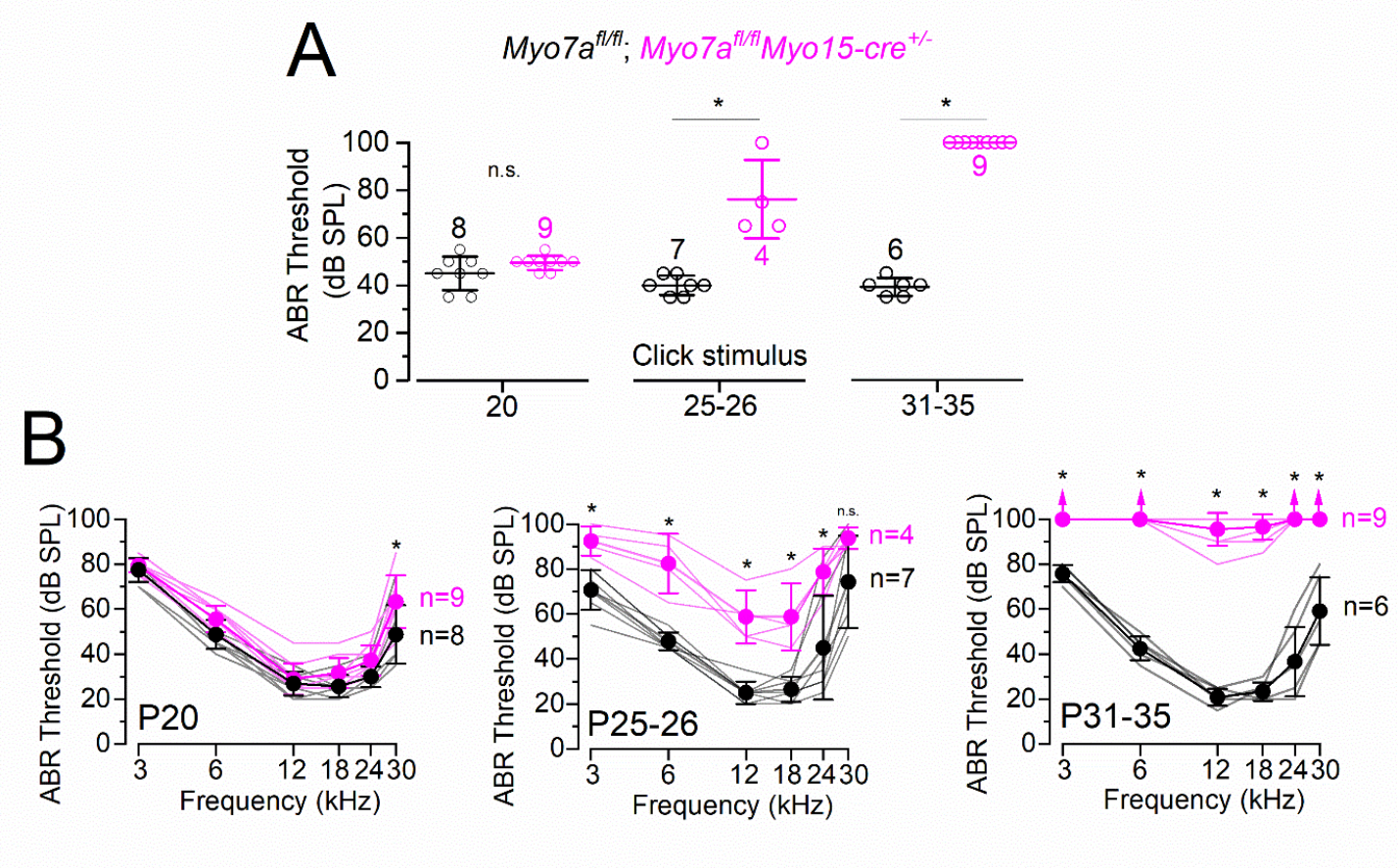

Figure 4.2- Myosin 7a conditional knock-out mice have progressively increased ABR thresholds from P25 to P31

(A) Mean ABR thresholds for clicks from control *Myo7a*$^{fl/fl}$ and littermate *Myo7a*$^{fl/fl}$*:Myo15-cre*$^{+/-}$ mice at P20, P25-26 and P31-35. Response to click is normal in the cKO mice at P20. At P25-26 the cKO mice have an elevated threshold. At P31-35 the cKO mice have no response to click stimuli. (B) ABR thresholds for frequency-specific pure tone stimulation from 3kHz to 30kHz from control *Myo7a*$^{fl/fl}$ and littermate *Myo7a*$^{fl/fl}$*:Myo15-cre*$^{+/-}$ mice. At P20 there is no change in ABR threshold at any frequency in the cKO mice. P25-26 the cKO mice have an increased ABR threshold at all frequencies tested. At P31-35 there is no ABR response at the lowest and highest frequencies and a very small response at 12 and 10 kHz. $P<0.05$, post-hoc Sidak's test following two-way ANOVA. Values are mean ± S.D, (n=animals). *Myo7a*$^{fl/fl}$ control (black), *Myo7a*$^{fl/fl}$*:Myo15-cre*$^{+/-}$ (pink). Experiment carried out by Walter Marcotti and reproduced with consent.

Alongside ABRs, DPOAEs were recorded to measure the activity of the OHCs. DPOAEs are the distortion productions of sound produced in the inner ear. This distortion is the result of electromotility of OHCs. This makes DPOAEs a good readout for the activity of OHCs.

For the DPOAEs we saw a similar progressive loss of function as seen in the ABRs. At P20 there was no change in DPOAE threshold between the conditional knock-out and control mice. At P25-26 the DPOAE threshold is increased at 24kHz in the *Myo-7a$^{fl/fl}$:Myo15-cre$^{+/-}$* mice ($P<0.02$, 2-way ANOVA, Šidák post-test). At P31 the DPOAE threshold was significantly increased in the *Myo-7a$^{fl/fl}$:Myo15-cre$^{+/-}$* mice at frequencies from 12-24kHz ($P<0.05$, 2-way ANOVA, Šidák post-test; Figure 4.3).

These results show that myosin 7a is essential for hearing and the conditional knock-out of myosin 7a causes a progressive decline in function of inner and outer hair cells between P20 and P31.

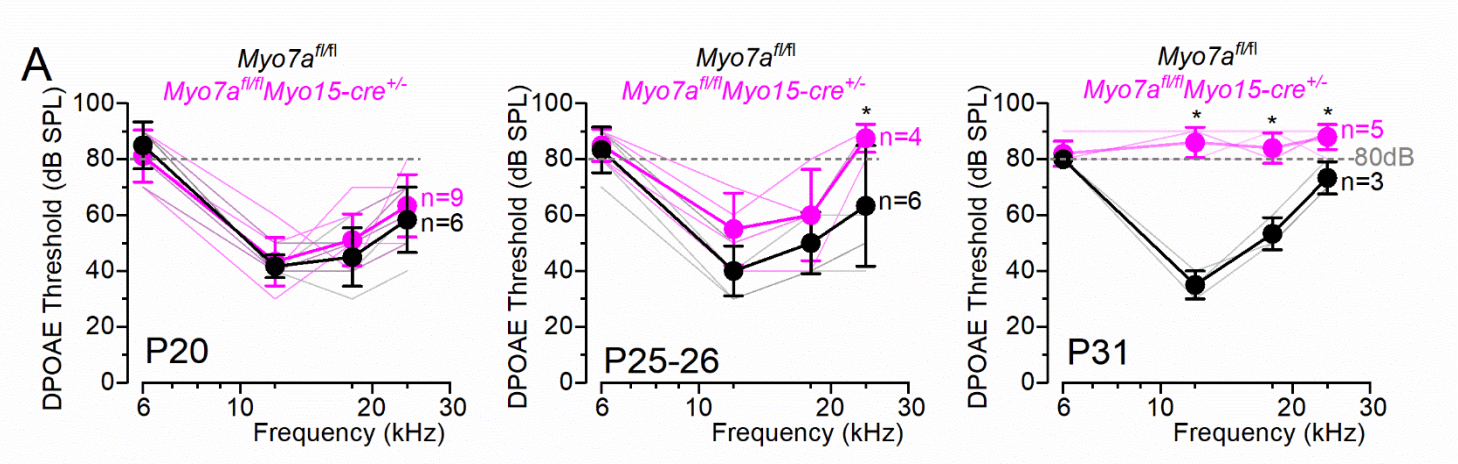

Figure 4.3- DPOAEs from myosin 7a conditional knock-out mice

(A) DPOAE thresholds for control *Myo7a$^{fl/fl}$* and littermate *Myo7a$^{fl/fl}$:Myo15-cre$^{+/-}$* mice at P20, P25-26 and P31. The frequencies tested were 6 kHz, 12 kHz, 18kHz and 24kHz. The dashed line indicates the upper limit of the system (80 dB SPL). At P20 the DPOAE threshold in the cKO mouse was similar to the threshold in the control mouse. At P25-26 the cKO mice had a slightly increased DPOAE threshold at 24kHz. At P31 the DPOAE threshold in the cKO mice was greatly elevated. $P<0.05$, post-hoc Sidak's test following two-way ANOVA. Values are mean ± S.D, (n=animals). *Myo7a$^{fl/fl}$* control (black), *Myo7a$^{fl/fl}$:Myo15-cre$^{+/-}$* (pink). Experiment carried out by Walter Marcotti and reproduced with consent.

4.2.2 Conditional knockout is successful at knocking out myosin 7a

To confirm the knockout of myosin 7a, an apical section of cochlea (6-12kHz) from a *Myo-7a$^{fl/fl}$:Myo15-cre$^{+/-}$* and *Myo-7a$^{fl/fl}$* mouse was stained with an anti-myosin 7a antibody, DAPI was also used to stain the nucleus of the hair cell. At P13 there was greatly decreased myosin 7a staining in the cell body of the hair cell compared to the control cochlea, but there was still some staining present in the stereocilia (Figure 4.4). The staining in the stereocilia could be explained by a slower turnover of myosin 7a in the stereocilia than in the cell body of the hair cell, meaning that myosin 7a remains in the stereocilia for longer than in the cell body.

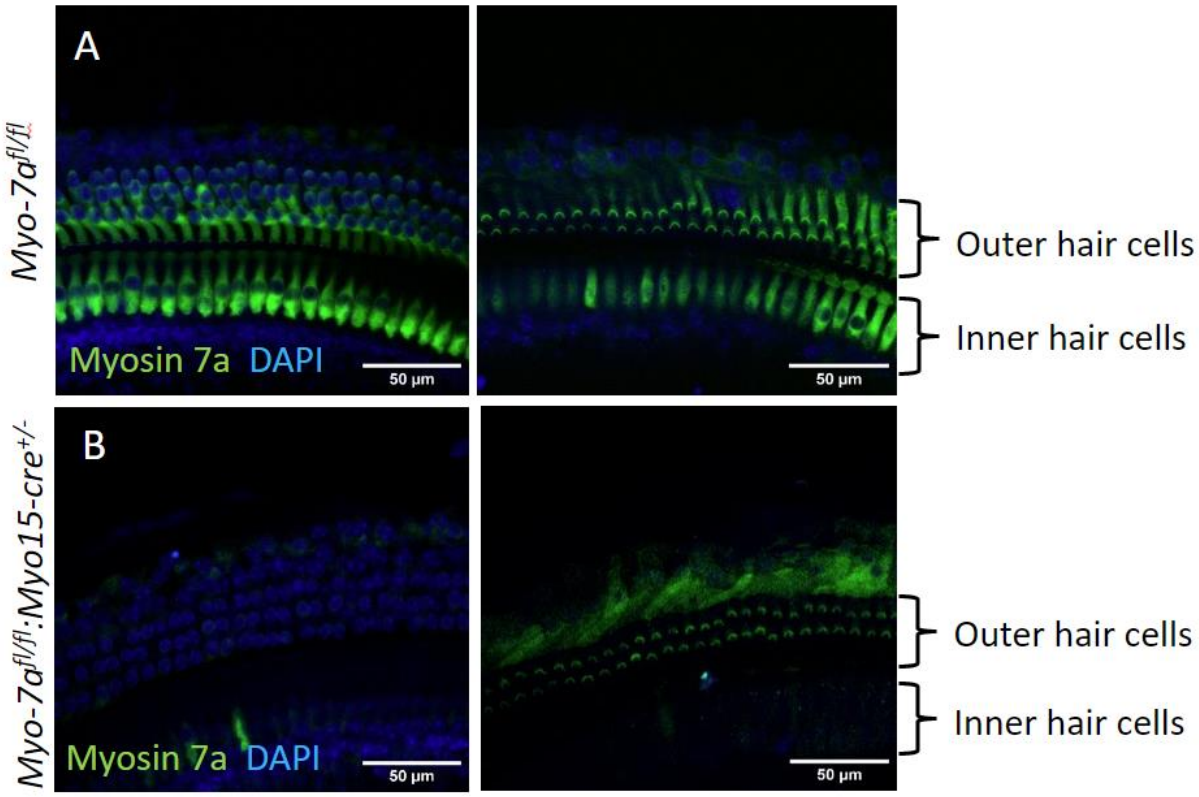

Figure 4.4- Immunostaining showing knockout of myosin 7a in conditional knock-out mouse cochlea at P13

Immunostaining for myosin 7a (green) and DAPI (blue) on an apical cochlea coil at P13 from (A) control *Myo7a$^{fl/fl}$* (n=2) and (B) littermate *Myo7a$^{fl/fl}$:Myo15-cre$^{+/-}$* (n=2) mice At P13 there is some myosin 7a staining in the stereocilia of the cKO mice. Images are summed intensity projections of a confocal z stack image.

At P20 there was no myosin 7a staining in the cell body or stereocilia of the *Myo-7a$^{fl/fl}$:Myo15-cre$^{+/-}$* mouse (Figure 4.5). These results show that the conditional knockout is effective at knocking out myosin 7a at P20.

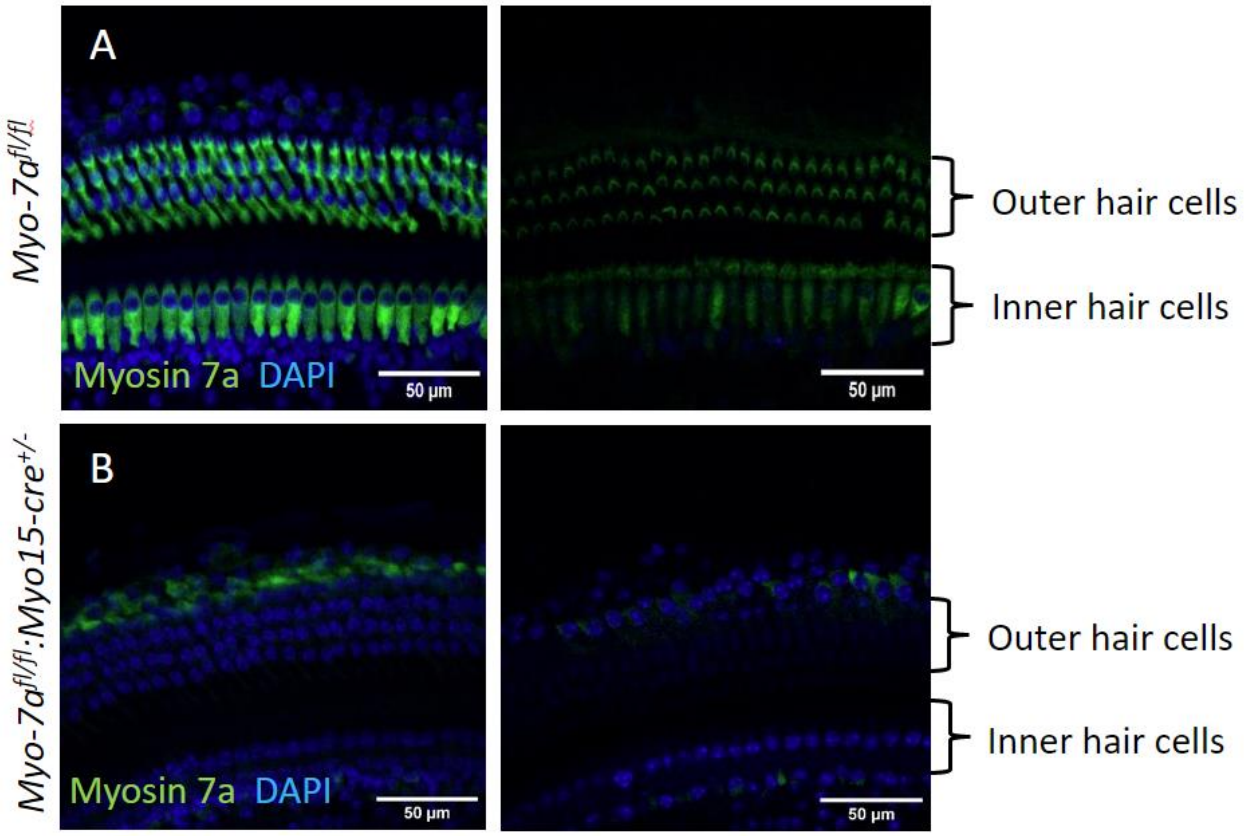

Figure 4.5- Immunostaining showing knockout of myosin 7a in conditional knock-out mouse cochlea at P20

Immunostaining for myosin 7a (green) and DAPI (blue) on an apical cochlea coil at P20 from (A) control *Myo7a$^{fl/fl}$* (n=3) and (B) littermate *Myo7a$^{fl/fl}$:Myo15-cre$^{+/-}$* (n=4) mice. At P20 there is no myosin 7a staining in the cKO mice. Images are summed intensity projections of a confocal z stack image.

4.2.3 Conditional knock-out of myosin 7a does not affect bundle morphology until later in life

In mouse models with a constitutive knockout of myosin 7a the hair bundle degenerates very rapidly. To compare this to the conditional knockout, the morphology of the hair bundles in the apical coil were examined using scanning electron microscopy (SEM) at P15, P30 and 5-8 months. At both P15 and P30 there was no obvious change to the morphology of the inner or outer hair cell's hair bundle in the *Myo7a$^{fl/fl}$:Myo15-cre$^{+/-}$* mouse (Figure 4.6). This is contrasted to the rapid disorganisation of the hair bundle seen in constitutive knockouts of myosin 7a at this age (Kros *et al.*, 2002). These results also suggest that hearing impairment seen at this age is due to the knockout of myosin 7a, rather than degeneration of the hair bundle.

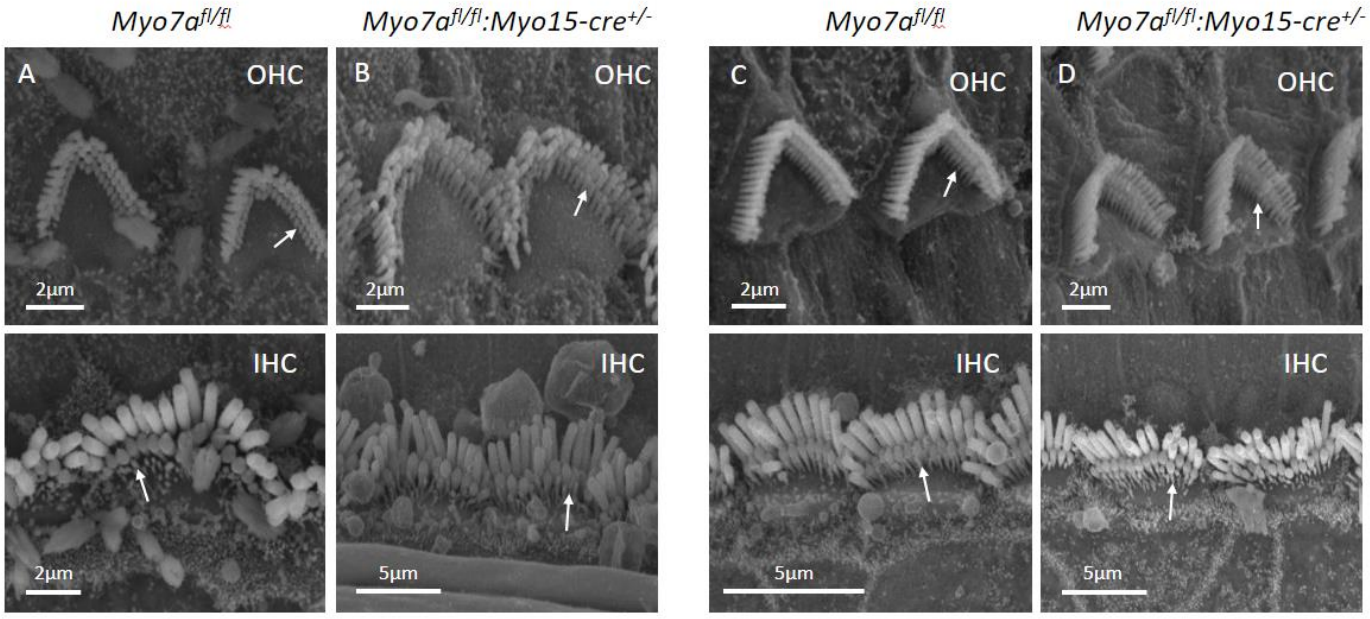

Figure 4.6- SEM of inner and outer hair cells in P15 and P30 conditional knock-out mouse

Scanning electron micrograph of apical coil of (A,B) P15 control *Myo7a$^{fl/fl}$* (n=8) and littermate *Myo7a$^{fl/fl}$:Myo15-cre$^{+/-}$* mice (n=8) and (C,D) P30 control *Myo7a$^{fl/fl}$* (n=4) and littermate *Myo7a$^{fl/fl}$:Myo15-cre$^{+/-}$* mice (n=5). Arrows indicate normal morphology in both genotypes with all three rows of stereocilia present in the IHCs and OHCs.

In order to look at whether the morphology of the hair bundle degenerates as the mouse ages, SEM was carried out on 5-8 month old mice. In these mice there was a clear degeneration of the hair bundle in the *Myo7a*$^{fl/fl}$*:Myo15-cre*$^{+/-}$ mouse. Almost all of the hair bundles were missing and there was fusion of the remaining IHC hair bundles (Figure 4.7). This suggests that the knockout of myosin 7a doesn't initially affect the hair bundle but myosin 7a could have a role in maintaining the bundle as the mouse ages.

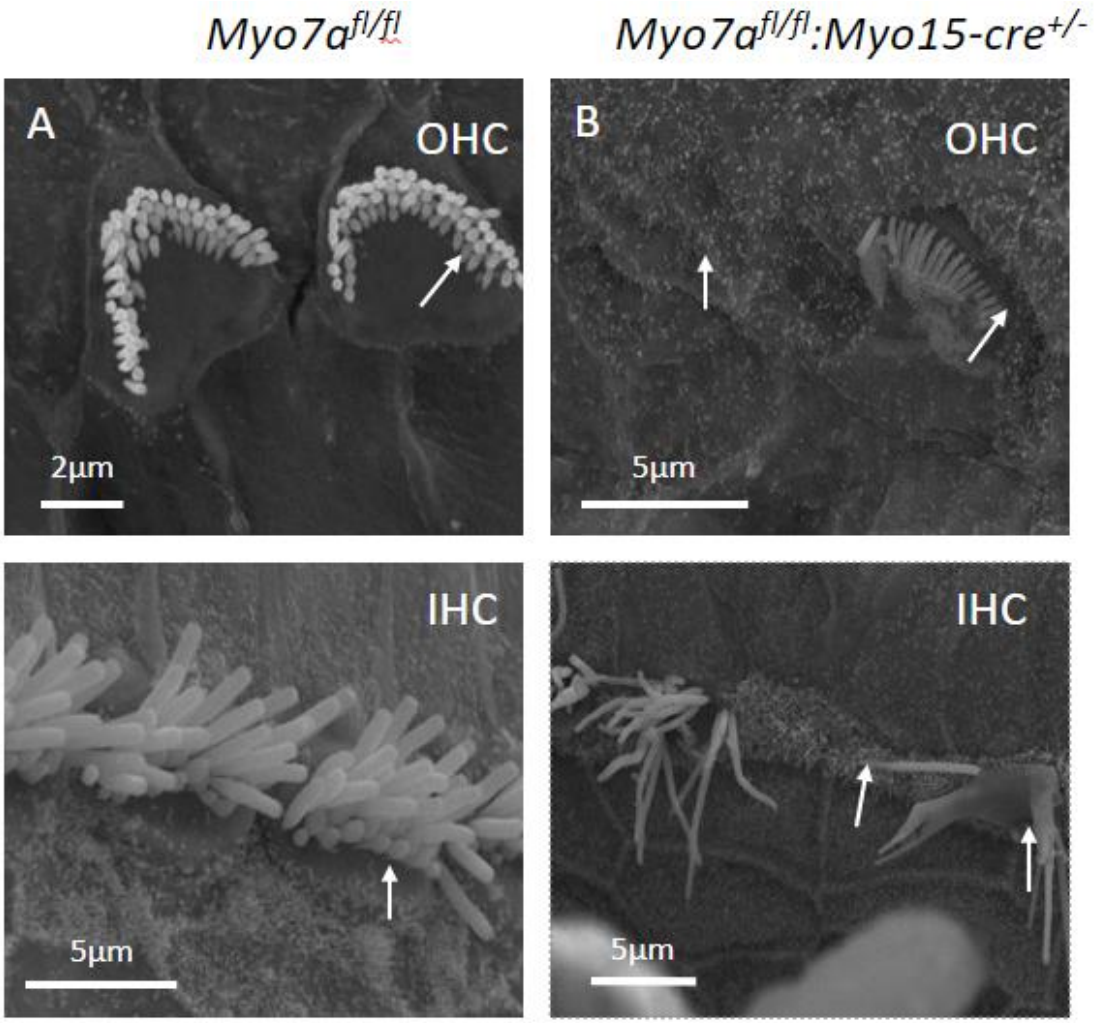

Figure 4.7- SEM of inner and outer hair cells in 5-8 month old conditional knock-out mice

SEM of apical coil of (A) control *Myo7a*$^{fl/fl}$ (n=3) and (B) littermate *Myo7a*$^{fl/fl}$*:Myo15-cre*$^{+/-}$ mice (n=2) at 5-8 months. In the *Myo7a*$^{fl/fl}$ images the arrows indicate the normal morphology of the IHCs and OHCs with all three rows of stereocilia present. In the *Myo7a*$^{fl/fl}$*:Myo15-cre*$^{+/-}$ images the arrows indicate missing and disorganised stereocilia. In the IHCs the arrows also indicate fusing of stereocilia.

4.2.4 Conditional knockout of myosin 7a causes progressive loss of the outer hair cell MET current

Due to the localisation of myosin 7a in the upper tip link density, and previous work that has shown that MET channel gating is affected in a constitutive knockout of myosin 7a (Kros *et al.*, 2002), we investigated whether the MET current would be affected in the conditional knockout. To measure the size of the MET current, the hair bundle was stimulated using a piezo driven fluid jet, as described previously. To look at the progression of MET current reduction the MET current was measured at a range of ages, from P7 to P27. The *Tecta*$^{-/-}$*: Myo7a*$^{fl/fl}$*:Myo15-cre*$^{+/-}$ was used for any MET current experiments over the onset of hearing (P12) as this mouse does not have a tectorial membrane. This allows for access to the hair bundles past the onset of hearing without damaging them by removing the TM. Mice with no TM are deaf, but they mature as normal and can still generate a large MET current (Jeng *et al.*, 2021).

In the P7-11 and P12-P16 age ranges there was no difference in size of MET current between the control *Myo7a*$^{fl/fl}$ mice and *Myo7a*$^{fl/fl}$*:Myo15-cre*$^{+/-}$ mice at any of the holding potentials tested (Figure 4.8)

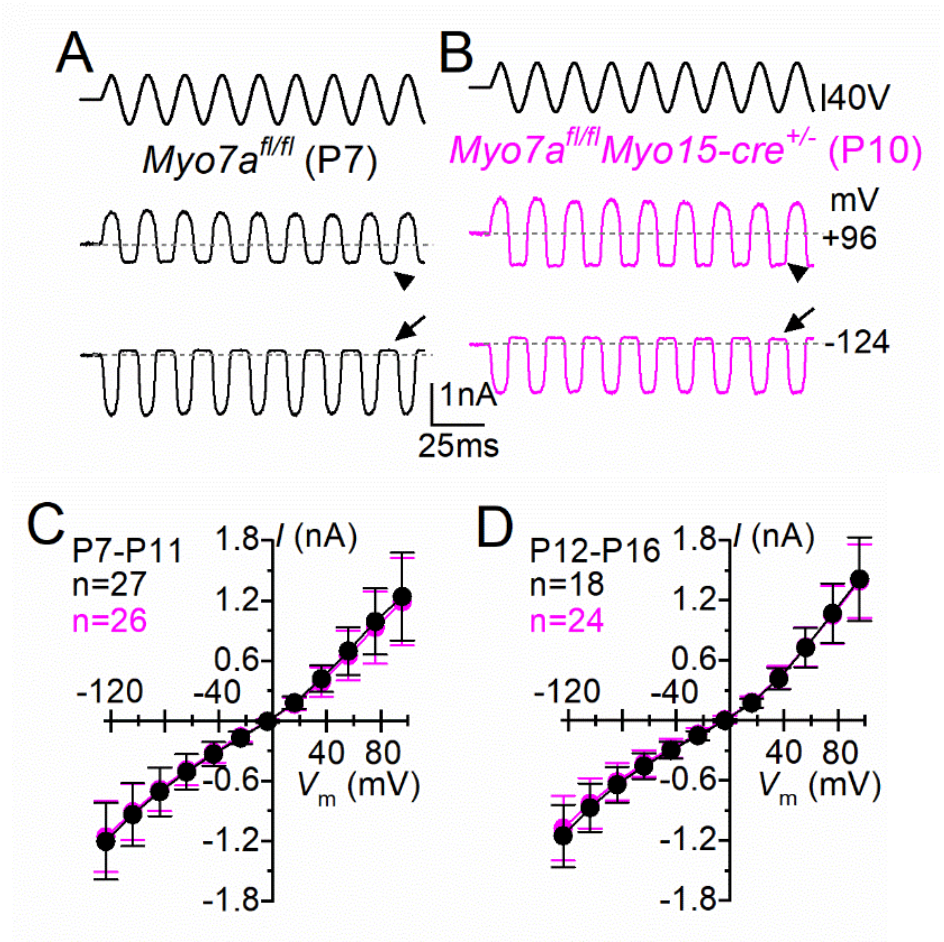

Figure 4.8- MET current size in myosin7a conditional knock-out OHCs at P7-16

(A) saturating MET current in apical coil OHCs from P7 control *Myo7a*$^{fl/fl}$ and (B) P10 *Myo7a*$^{fl/fl}$*:Myo15-cre*$^{+/-}$ mice in response to the sine wave stimuli at -124mV and +99mV. (C) average MET current-voltage curves from P7-11 control *Myo7a*$^{fl/fl}$ (n=27 (15)) and littermate *Myo7a*$^{fl/fl}$*:Myo15-cre*$^{+/-}$ (n=26 (14)) mice. (D) average MET current-voltage curves from P12-16 control *Myo7a*$^{fl/fl}$ (n=18 (15)) and littermate *Myo7a*$^{fl/fl}$*:Myo15-cre*$^{+/-}$ (n=24 (15)) mice. Current-voltage curves were obtained by stimulated the hair bundles while stepping the membrane potential from -124mV to +99mV in 20mV steps. Values are mean ± S.D, (n=cells (animals)). *Myo7a*$^{fl/fl}$ control (black), *Myo7a*$^{fl/fl}$*:Myo15-cre*$^{+/-}$ (pink).

Figure 4.9 shows no significant decrease MET current size at P17-21 in the *Myo7a*$^{fl/fl}$*:Myo15-cre*$^{+/-}$ mouse. AT P24-27 the MET current is much smaller in the *Myo7a*$^{fl/fl}$*:Myo15-cre*$^{+/-}$ mice mouse compared to the control mouse.

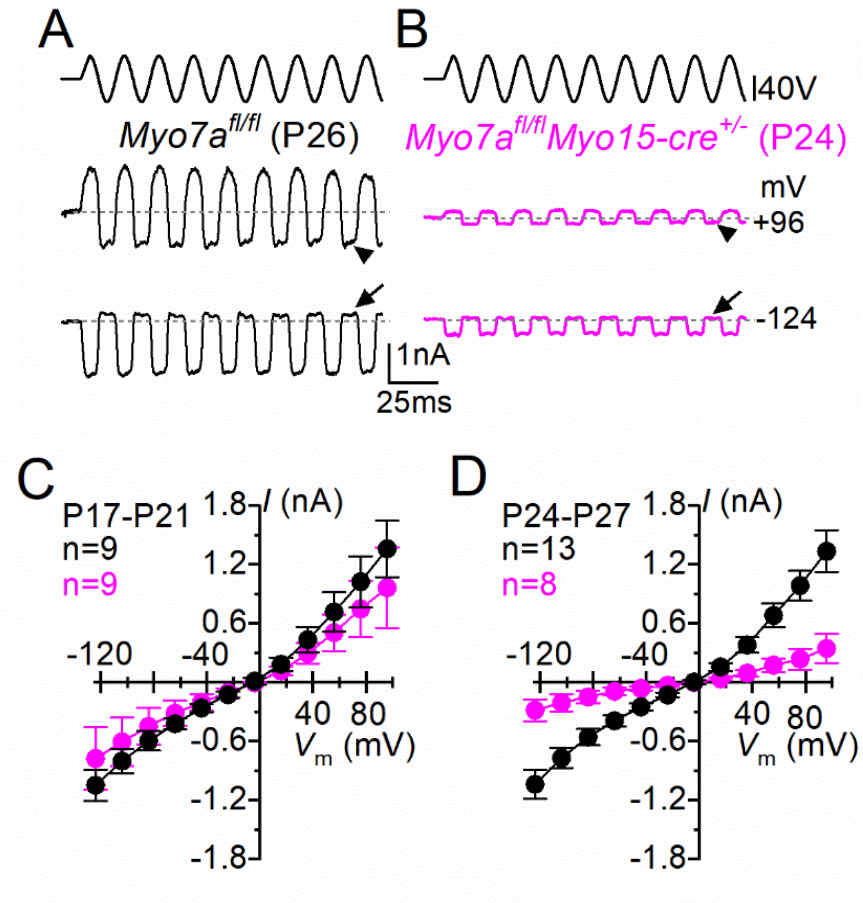

Figure 4.9- MET current size in myosin7a conditional knock-out OHCs at P17-27

(A) saturating MET current in apical coil OHCs from P26 control *Myo7a*$^{fl/fl}$ and (B) P24 *Myo7a*$^{fl/fl}$*:Myo15-cre*$^{+/-}$ mice in response to the sine wave stimuli at -124mV and +99mV. (C) average MET current-voltage curves from P17-21 control *Myo7a*$^{fl/fl}$ (n=9 (7)) and littermate *Myo7a*$^{fl/fl}$*:Myo15-cre*$^{+/-}$ (n=9 (7)) mice. (D) average MET current-voltage curves from P24-27 control *Myo7a*$^{fl/fl}$ (n=13 (11)) and littermate *Myo7a*$^{fl/fl}$*:Myo15-cre*$^{+/-}$ (n=8 (6)) mice. Current-voltage curves were obtained by stimulating the hair bundles while stepping the membrane potential from -124mV to +99mV in 20mV steps. Values are mean ± S.D, (n=cells (animals). *Myo7a*$^{fl/fl}$ control (black), *Myo7a*$^{fl/fl}$*:Myo15-cre*$^{+/-}$ (pink).

Between the ages of P17-21 the decrease in MET current size in the *Myo7a$^{fl/fl}$:Myo15-cre$^{+/-}$* mice, compared to the control mice, is not significant at -124mV (P=0.24, 2-way ANOVA, Šidák post-test) or at +99mV (P=0.16, 2-way ANOVA, Šidák post-test). At P24-27 there was a significant decrease in the size of the MET current, compared to the control mice at both 124mV (P<0.01, 2-way ANOVA, Šidák post-test) and at +99mV (P<0.01, 2-way ANOVA, Šidák post-test) (Figure 4.10). The time point when the decrease in MET current size is seen corresponds to when the increase in ABR threshold is seen between P20 and P30.

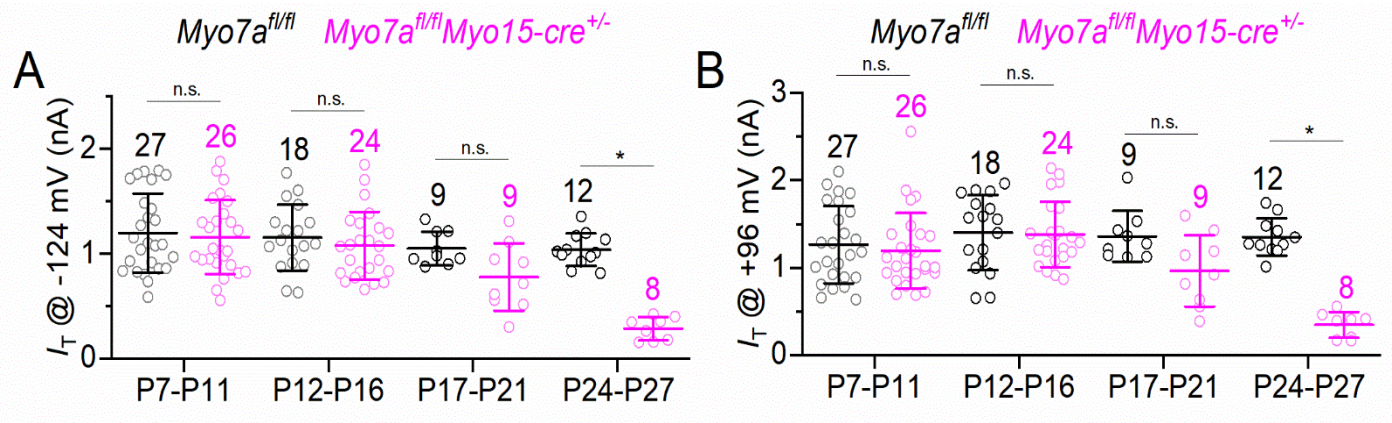

Figure 4.10- MET current size in myosin 7a conditional knock-out OHCs at -121mV and +96mV

(A) maximal size of the MET current in control and *Myosin7a$^{fl/fl}$:Myo15-cre$^{+/-}$* mice at (A) -124mV and (B) +96mV at P7-11, P12-16, P17-21 and P24-27. P<0.05, post-hoc Sidak's test following two-way ANOVA. Values are mean ± S.D, (n=cells). *Myo7a$^{fl/fl}$* control (black), *Myo7a$^{fl/fl}$:Myo15-cre$^{+/-}$* (pink).

In the constitutive knockout of myosin 7a it was shown that the MET channels of the OHCs have a resting open probability of zero (Kros *et al.*, 2002). To compare this to the conditional knockout the resting open probability was measured in the same way as described previously. Despite the reduction in MET current size, the size of the resting open probability was not statistically significantly different between the control and mutant mice at -124mV or +96mV from P7-P27 (Figure 4.11). This demonstrates that although the MET current is smaller, the channels are still able to function around their normal resting open probability.

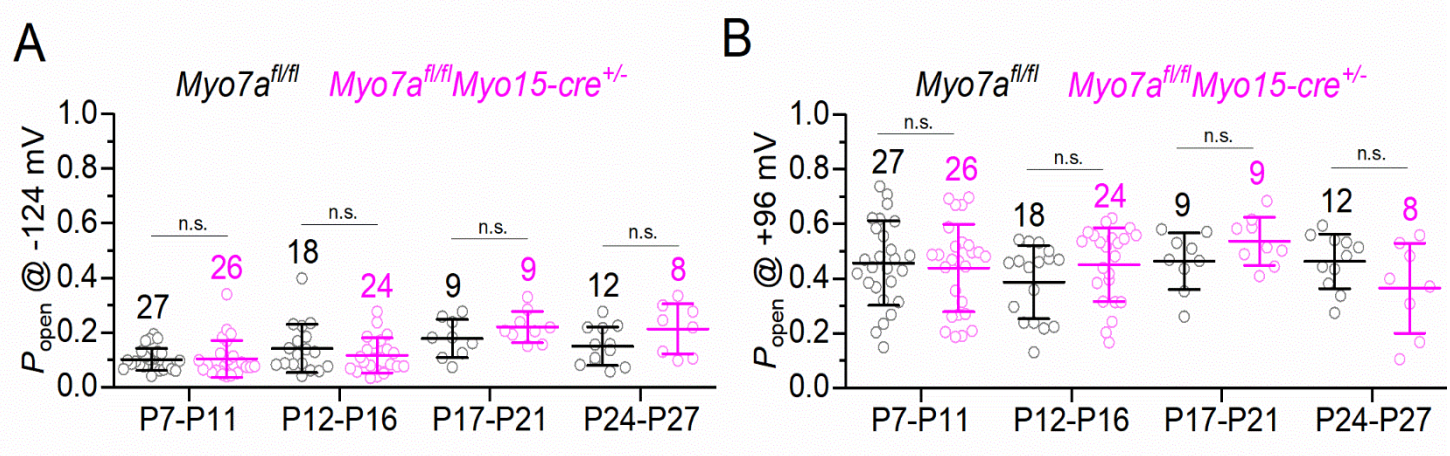

Figure 4.11- Open resting probability in myosin-7a conditional knock-out OHCs

The resting open probability (Po) of the MET current in OHCs from control and *Myo7a$^{fl/fl}$:Myo15-cre$^{+/-}$* mice at the holding potentials (A) -121mV and (B) +99mV. The Po was not significantly different between the two genotypes at any of the ages investigated with P<0.05, post-hoc Sidak's test following two-way ANOVA. Values are mean ± S.D, (n=cells). *Myo7a$^{fl/fl}$* control (black), *Myo7a$^{fl/fl}$:Myo15-cre$^{+/-}$* (pink).

4.2.5 Reducing the intracellular calcium concentration does not affect resting open probability in myosin 7a conditional knockout mice

To investigate the effect of the myosin 7a knockout on the calcium sensitivity of the MET channel, MET current recordings were measured using an intracellular solution containing 5mM of the calcium chelator 1,2-Bis(2-aminophenoxy)ethane-*N*,*N*,*N*′,*N*′-tetraacetic acid (BAPTA) (solution composition detailed in Methods). Using an intracellular solution containing 5mM of BAPTA reduces the calcium concentration inside the cell. Reducing the calcium concentration decreases adaptation of the MET channel, increasing the resting open probability (Figure 4.12). As stated previously, as these experiments were carried out in mice older than P12, the *Tecta$^{-/-}$: Myo7a$^{fl/fl}$:Myo15-cre$^{+/-}$* mouse line was used.

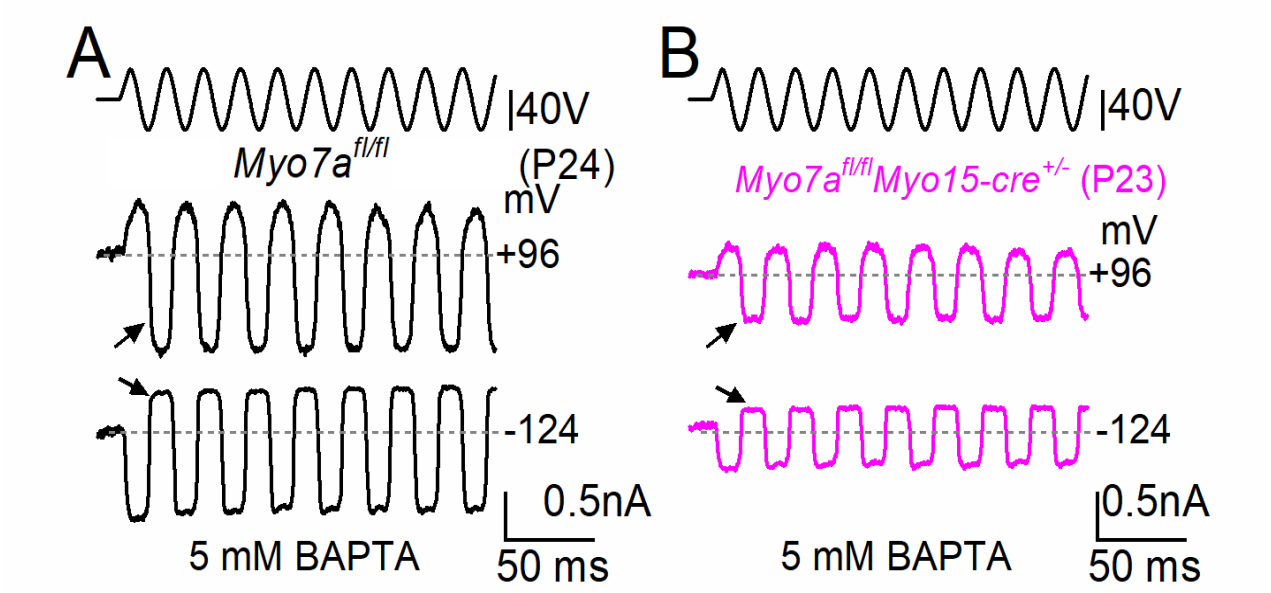

Figure 4.12- Resting open probability in the presence of 5mM BAPTA in P23-24 myosin-7a conditional knock-out OHCs

The resting open probability (Po) of the MET current in OHCs from (A) control and (B) *Myosin7a$^{fl/fl}$:Myo15-cre$^{+/-}$* at -121mV and +99mV holding potential at P9 in the presence of 5mM BAPTA in the intracellular solution. Arrows indicate saturating inhibitory current. *Myo7a$^{fl/fl}$* control (black), *Myo7a$^{fl/fl}$:Myo15-cre$^{+/-}$* (pink).

In both the *Myo-7a$^{fl/fl}$:Myo15-cre$^{+/-}$* and control mice the size of the resting open probability was not significantly different between the control and conditional knock-out mice at either P20-21 or P23-24 when 0mM BAPTA or 5mM BAPTA intracellular solution was used ($p>0.05$, 2-way ANOVA, Šidák post-test, Figure 4.13). This seems to suggest that the calcium sensitivity of the MET channel was not affected by the knockout of myosin 7a. However, the 5mM also BAPTA didn't cause a significant increase in resting open probability when compared to the 0mM BAPTA intracellular solution for either genotype at both ages ($p>0.05$, 2-way ANOVA, Šidák post-test). Except for the *Myo-7a$^{fl/fl}$:Myo15-cre$^{+/-}$* mice at P23-24, where there was a significant increase in resting open probability at +99mV ($p=0.04$, 2-way ANOVA, Šidák post-test). As the 5mM BAPTA didn't increase open probability as expected it is very difficult to gain any meaningful conclusion from this experiment. It is possible that increasing the n numbers in this experiment would lead to a significant result, but more work is needed to determine whether the myosin 7a conditional knockout affects calcium sensitivity.

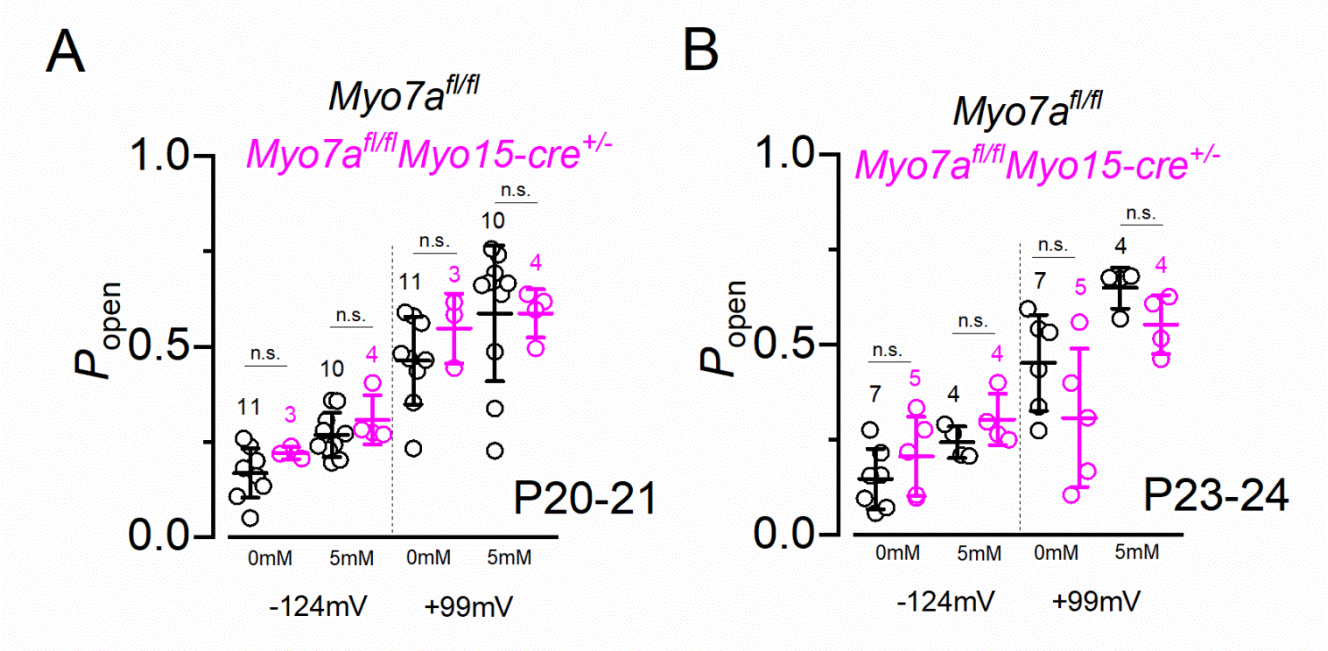

Figure 4.13- Resting current in myosin-7a conditional knock-out OHCs in the presence of 5mM BAPTA

The resting open probability (Po) of the MET current in OHCs from control *Myo7a$^{fl/fl}$* and *Myo7a$^{fl/fl}$:Myo15-cre$^{+/-}$* at the holding potentials of -121mV and+99mV at (A) P20-21 and (B) P23-24 in the presence of 0mM BAPTA and 5mM BAPTA intracellular solution. P<0.05, post-hoc Sidak's test following two-way ANOVA. Values are mean ± S.D, (n=cells). *Myo7a$^{fl/fl}$* control (black), *Myo7a$^{fl/fl}$:Myo15-cre$^{+/-}$* (pink).

4.2.6 Conditional myosin 7a knock-out causes OHCs to revert to an immature phenotype

Basolateral currents from apical coil OHCs (6-12kHz region) from myosin 7a conditional knock-out mice were recorded at P19-21 and P35-44. Hyperpolarizing and depolarizing voltage steps were applied in increasing steps of 10mV starting at the holding potential of -84mV.

At P20 there was no significant difference in the size of the basolateral potassium current between the *Myo-7a$^{fl/fl}$:Myo15-cre$^{+/-}$* and control mice. Also, there was no difference in the size of the I_K current (p=0.66, students t-test) or the $I_{K,n}$ current (p=0.98, students t-test) (for details on how currents are measured see Methods 2.7.5) (Figure 4.14). This demonstrates that the hair cells initially develop normal biophysical properties.

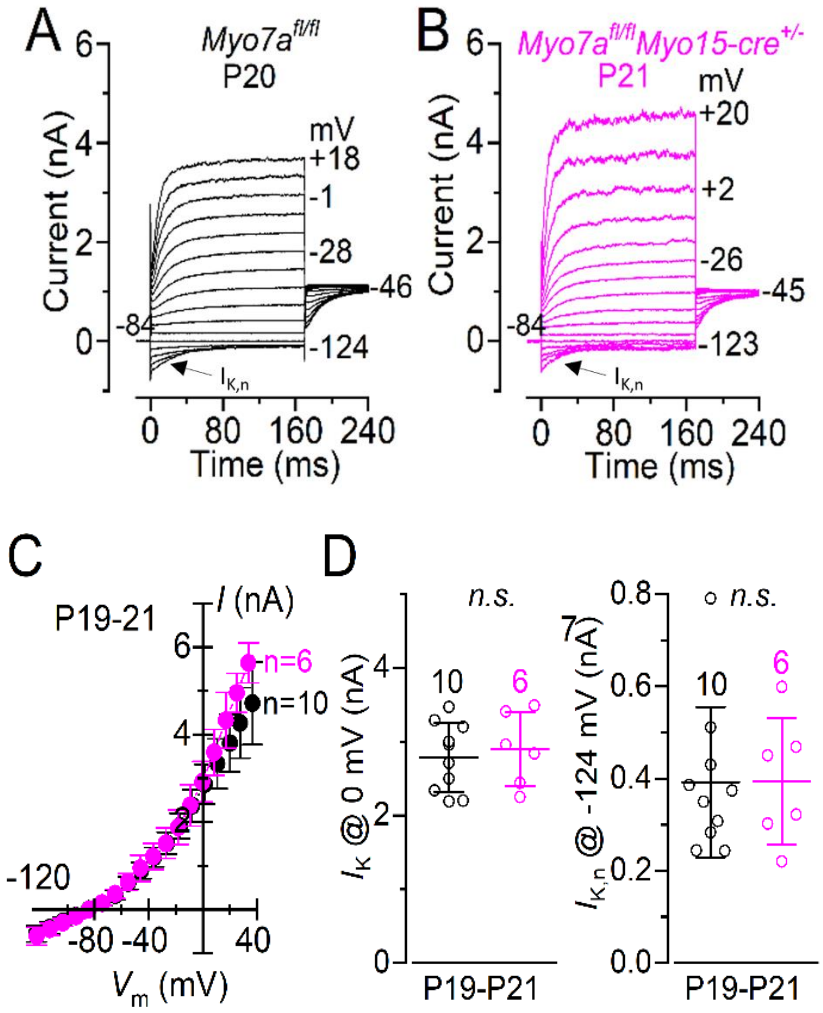

Figure 4.14- Basolateral potassium currents from P20-21 myosin-7a conditional knock-out OHCs

Voltage responses from OHCs of (A) control *Myo7a*$^{fl/fl}$ and (B) *Myo7a*$^{fl/fl}$*:Myo15-cre*$^{+/-}$ mice. Arrows indicate $I_{K,n}$ current. (C) average current-voltage curves from P19-21 control *Myo7a*$^{fl/fl}$ (n=10 (7)) and littermate *Myo7a*$^{fl/fl}$*:Myo15-cre*$^{+/-}$ (n=6 (4)) mice. D, Average I_K and $I_{K,n}$ current from P19-21 control *Myo7a*$^{fl/fl}$ (n=10 (7)) and littermate *Myo7a*$^{fl/fl}$*:Myo15-cre*$^{+/-}$ (n=6 (4)) mice. P<0.05, student t-test. Values are mean ± S.D, (n=cells (animals)). *Myo7a*$^{fl/fl}$ control (black), *Myo7a*$^{fl/fl}$*:Myo15-cre*$^{+/-}$ (pink).

At P35-45, however, the size of the basolateral potassium current was smaller in the *Myo-7a*$^{fl/fl}$*:Myo15-cre*$^{+/-}$ mice compared to the control mice. Also, the I_K current was much smaller ($p<0.008$, students t-test, Figure 4.15) and the $I_{K,n}$ current was reduced to 0nA (Figure 4.15). These characteristics are indicative of a pre-hearing state, demonstrating that the loss of myosin 7a causes the hair cells to revert back to a more immature phenotype.

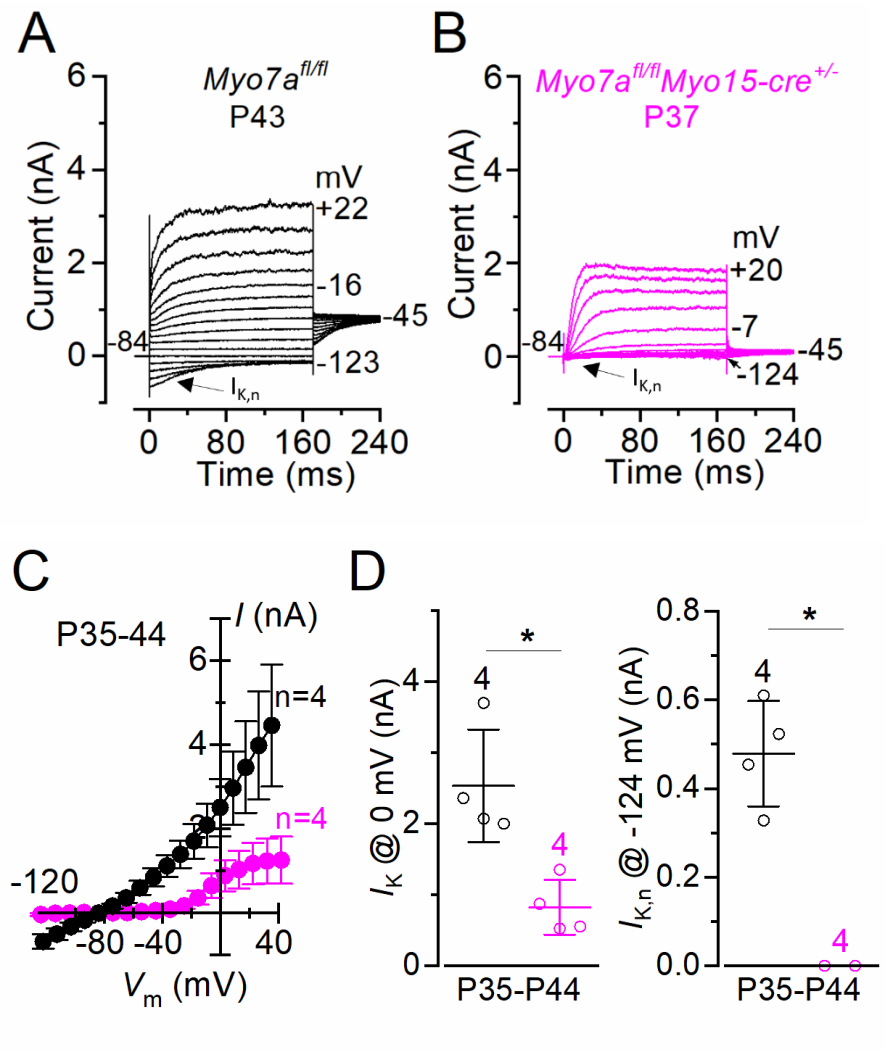

Figure 4.15- Basolateral potassium currents in P37-43 myosin 7a conditional knock-out OHCs

Voltage responses from OHCs of control (A) *Myo7a$^{fl/fl}$* and (B) Myo*7a$^{fl/fl}$:Myo15-cre$^{+/-}$* mice. Arrows indicate $I_{K,n}$ current. (C) average current-voltage curves from P35-44 control *Myo7a$^{fl/fl}$* (n=4 (3)) and littermate *Myo7a$^{fl/fl}$:Myo15-cre$^{+/-}$* (n=4 (3)) mice. (D) Average I_K and $I_{K,n}$ current from P35-44 control *Myo7a$^{fl/fl}$* (n=4 (3)) and littermate *Myo7a$^{fl/fl}$:Myo15-cre$^{+/-}$* (n=4 (3)) mice. P<0.05, students t-test. Values are mean ± S.D, (n=cells (animals)). *Myo7a$^{fl/fl}$* control (black), *Myo7a$^{fl/fl}$:Myo15-cre$^{+/-}$* (pink).

4.2.7 Localization of harmonin is not affected in in conditional knockout mouse

As myosin 7a forms a complex with harmonin it was hypothesised that knocking out myosin 7a could affect the localisation of harmonin. To investigate this an apical section of the cochlea was stained with antibodies for harmonin and phalloidin to stain the actin of the cell. At P32 there was no difference in harmonin staining between the control and *Myo-7a$^{fl/fl}$:Myo15-cre$^{+/-}$* mice. In both samples harmonin was located to the stereocilia of the inner

and outer hair cells (Figure 4.16). This suggests that myosin 7a is not required for the transport of harmonin to the stereocilia.

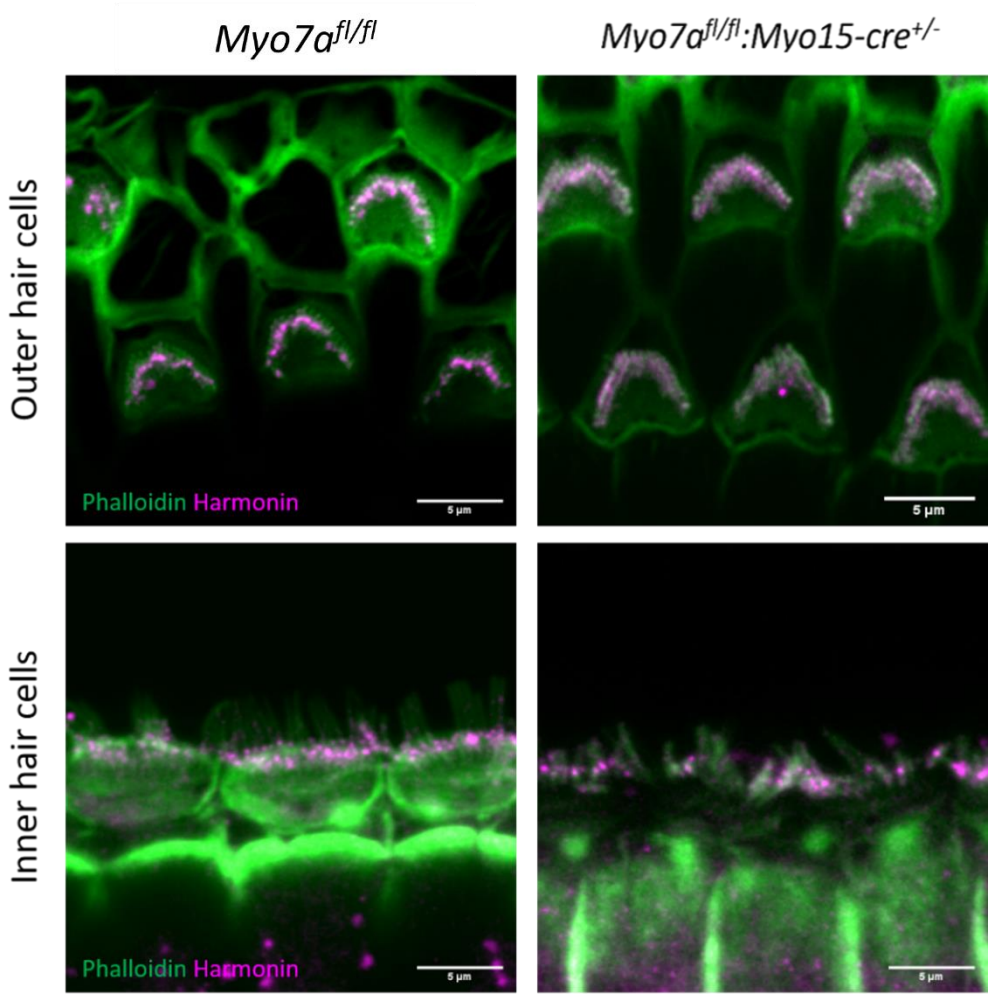

Figure 4.16- Immunostaining showing that the localisation of harmonin is not affected by the conditional knockout of myosin 7a at P32

Immunostaining for phalloidin (green) and harmonin (pink) on an apical cochlea coil at P32 from control *Myo7a*$^{fl/fl}$ (n=3) and littermate *Myo7a*$^{fl/fl}$*:Myo15-cre*$^{+/-}$ (n=3) mice. Images are summed intensity projections of a confocal z stack image.

4.3 Discussion

In this chapter a detailed investigation was carried out into the role of myosin 7a in mechanotransduction in a conditional knockout. As seen in the constitutive knockout, the conditional knockout of myosin 7a causes the mice to have a severe hearing impairment. This is demonstrated by the progressive increase in ABR and DPOAE thresholds in the conditional knockout mice between P20 and P30. From the ABR and DPOAE data it seems that the hearing impairments are seen first in the basal coil hair cells. At P20 the ABR threshold was normal for all frequencies, except for 30kHz where it was significantly higher. At P25-26 the DPOAE thresholds are also significantly higher at 24kHz. Then at P31-35 the ABR and DPOAE thresholds are higher at all frequencies tested. This could suggest that any problems with MET current are occurring earlier in the basal region of the cochlea, compared to the apical region. As most experiments were carried out on the apical region, any early changes in MET current would not be detected.

The onset of the hearing impairment in the conditional knockout correlates to the complete absence of myosin 7a at P20. At P13 there is still evidence of myosin 7a staining in the stereocilia of inner and outer hair cells, demonstrating that the turnover of myosin 7a is slower in the stereocilia than in the cell body of the hair cell.

It has been shown that in the constitutive knockout of myosin 7a there is rapid degeneration of the hair bundle at P3, which could contribute to hearing defects seen in these mice (Kros et al., 2002). However, in the conditional knockout, there is no degeneration of the hair bundle up to at least P30, demonstrating that the hearing impairment seen is due to the knockout of myosin 7a, rather than degeneration of the hair bundle.

When the bundle morphology was investigated at 5-8 months old there was severe degeneration of inner and outer hair cell bundles. Most bundles were lost and the remaining stereocilia were fused and disorganised. This suggests that myosin 7a could have a role in maintaining the hair bundle later in life. Previous work has also shown that the MET current is needed to maintain the hair bundle, therefore this degeneration could be a secondary effect caused by the loss of MET current in the cell (Corns et al., 2018).

The increase in hearing threshold also correlates with a decrease in MET current size in the conditional knockout mice. At P20 there is no change in either the ABR threshold or MET

current size in the conditional knockout mouse, then at P24-27 there is an increase in ABR threshold and a decrease in MET current size. The maintenance of the MET current up to P24, even though myosin 7a is knocked out at P4, could be explained by the slower turnover of myosin 7a in the hair bundle, shown by the immunostaining data.

In contrast to the constitutive knockout, where the OHCs show a resting open probability of zero, up to P27 the size of the resting open probability in OHCs is not significantly different between the conditional knockout and control mice. This suggests that, even though the MET current is smaller, the channels are still functional and there is enough tip link tension to produce a resting open probability of comparable size to the control.

As there is no change to bundle morphology or resting open probability, different properties of the MET channel were explored to try and explain the loss of MET current and hearing in the conditional knockout mice. Investigation of the basolateral currents of the OHCs showed that, at P20 the biophysical properties of the cell were normal. However, by P35 the cell had reverted back to a more immature phenotype, with a smaller overall current size, smaller I_K current, and no $I_{K,n}$ current. Previous work has shown that a functional MET current is needed to maintain the presence of adult-like ion channels in the basolateral membrane (Corns *et al.*, 2018). It is possible that the loss of the MET current is driving the cell to revert to a pre-hearing phenotype.

Another property of the MET channel that was investigated was the effect of reducing the intracellular calcium concentration on the resting open probability. It is thought that intracellular calcium regulates adaptation of the MET channel, and removing intracellular calcium increases the resting open probability by decreasing adaptation (Fettiplace, 2017).

The calcium chelator BAPTA was used in the intracellular solution to remove calcium and investigate the effect of reduced intracellular calcium on the MET channel. There was no difference in resting open probability between the conditional knockout and control mouse. However, there was also no significant change in resting open probability between the 0mM BAPTA and 5mM BAPTA recordings. So, while there is a trend towards a greater resting open probability with the 5mM intracellular solution, no conclusions on calcium sensitivity should be taken from this experiment.

Also, there was no change in the localisation of harmonin, a protein that is closely associated with myosin 7a in the upper tip link density. This suggests that myosin 7a is not required for the localisation of harmonin in the stereocilia.

Overall, this chapter shows that myosin 7a is vital for hearing and proper function of the MET channel. It is possible that myosin 7a has a role in maintaining the hair bundle, but this needs more investigations to confirm. As there are no observable changes in bundle morphology up to P30, we can be confident that the phenotypes seen here are directly related to the knockout of myosin 7a.

Chapter 5 -The role of clarin-2 in mechanotransduction

5.1 Introduction

The clarin genes code for proteins that are part of a family of small integral proteins that each have four alpha-helical transmembrane domains. This family of proteins contains occludins, tetraspanins, claudins and connexins. These proteins have a range of role from scaffolding proteins (tetraspanins), components of tight junctions (claudins and occludins) and gap junctions (connexins) (Adato et al., 2002). In humans there are three clarin genes; clarin-1, clarin-2 and clarin-3. Clarin-1 is thought to be involved in F-actin organisation and maturation of synapses (Västinsalo et al., 2011). Clarin-1 is also essential for the proper formation of hair cell hair bundles and mutations to the clarin-1 gene are known to be involved in usher syndrome type 3A (Geller et al., 2009). This disease causes onset of hearing loss during adolescence and vision loss that varies in onset and severity between different patients. Some patients also experience problems with the vestibular system (Bonnet & El-Amraoui, 2012; NIDCD, 2017). Although there are various studies looking at clarin-1, there is little known about the function and role of clarin-2 or clarin-3.

The link between clarin-2 and deafness was discovered during an *N*-ethyl-*N*-nitrosourea (ENU) mutagenesis screen. The *clarinet* mouse model has a tryptophan-to-stop nonsense mutation in the clarin-2 gene (Dunbar et al., 2019). In humans, variations in clarin-2 are associated with hearing loss in adults (Vona et al., 2021).

Using a GFP (green fluorescent protein)-tagged clarin-2 construct delivered to P2 cochlea cultures, it was found that clarin-2 is enriched in the apical stereocilia of auditory hair cells (Dunbar et al., 2019). In the *clarinet* mice, it was also found that they have an elevated hearing threshold at P16 which continues to increase up to P42. This demonstrates that there is early onset hearing loss in this mouse model. This localisation to the stereocilia along with the hearing loss suggests that clarin-2 could have a role in mechanotransduction or hair bundle morphology.

The development of the hair bundle is also affected in the *clarinet* mouse. By P8 the third row of stereocilia in the OHC hair bundle is shorter than in the control mice and by P16 many of the stereocilia in the third row are missing. By P28 the third row of stereocilia in the OHCs has disappeared completely.

When the MET current was measured in OHCs, it was found that in P6-P8 mice the maximal MET current is significantly lower in the *clarinet* mice than in controls. However, there was no change to the open probability of the MET channels (Figure 5.1) (Dunbar et al., 2019). The reduced MET current could suggest that there are fewer MET channels on the OHC stereocilia. However, as there is no change in open probability, the channels that remain are still functional. It is not possible to take ABR recordings at P6-8, so it is not known whether there is a reduction in hearing at this age.

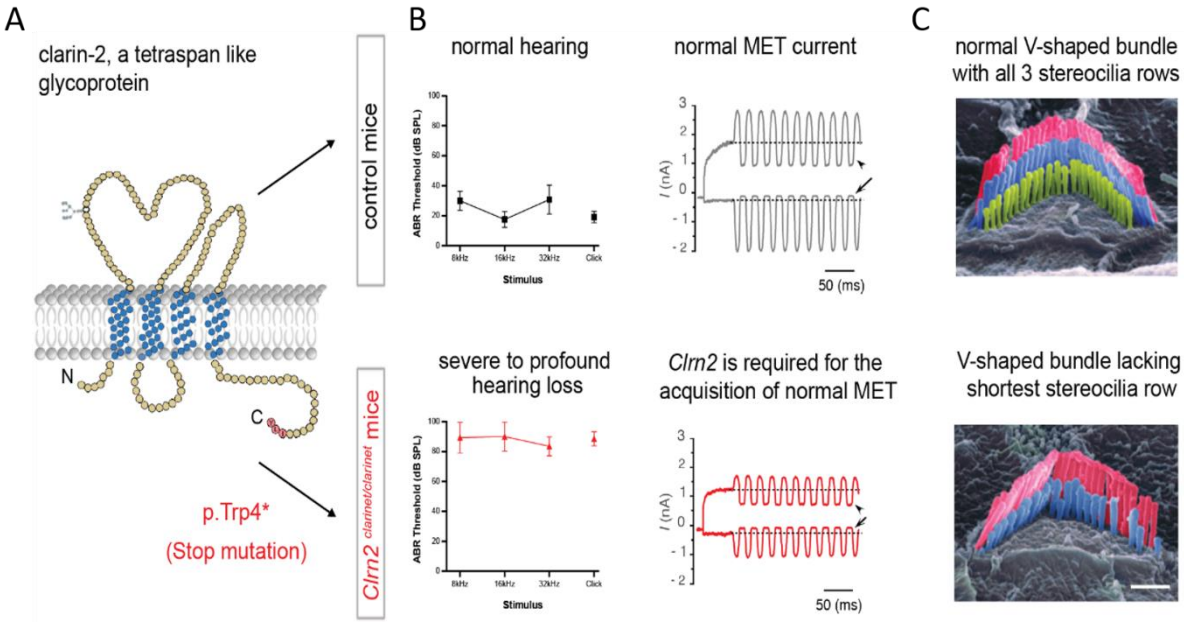

Figure 5.1- Effect of CLRN2 mutation on hearing, MET current and bundle morphology

(A) Diagram of CLRN2 protein showing location of stop mutation. (B) ABR recordings and MET current recordings from a control and *Clrn2*$^{clarinet/clarinet}$ mouse. In *Clrn2*$^{clarinet/clarinet}$ mouse there is an elevated hearing threshold, and the size of the MET current is decreased. (C) SEM of a P28 OHC hair bundle showing the bundle morphology of the control and *Clrn2*$^{clarinet/clarinet}$ mouse. In the *Clrn2*$^{clarinet/clarinet}$ mouse the third row of stereocilia is lost (Dunbar et al., 2019).

In previous work the mouse model used was a constitutive mutation of clarin-2, where the protein is mutated from the beginning of development. The work in this chapter looks at how mechanotransduction is affected in a conditional *Clrn2* knockout mouse model. Here we used a conditional knockout mouse with a floxed clarin-2 gene (*Clrn2*$^{fl/fl}$), crossed with a myosin-15 cre mouse. In this model the cre-recombinase gene expression was driven by the hair cell specific myosin 15 promoter (Caberlotto et al., 2011). The temporal expression of the cre, driven by the myosin-15 promoter, occurs postnatally (~P4 in the cochlea apical coil).

As these conditional knockout mice permit the stereocilia to develop normally, at least initially, we were able to compare the phenotypes seen in the constitutive mutant and conditional knockout mouse. This provided a greater understanding into whether the phenotypes seen in the constitutive mutant are due to the role of clarin-2 in development of the hair cell or are due to loss of stereocilia. In both models there is a severe hearing impairment. However, in the conditional knock-out the mice retain all three rows of stereocilia up to P42 (Figure 5.2). This suggests that the hearing impairment is not due to the loss of the third row of stereocilia (as previously thought).

This chapter aims to investigate the electrophysiological properties of the *Clrn2*$^{fl/fl}$*:Myo15-cre*$^{+/-}$ mice to better understand the role of clarin-2 in mechanotransduction and hearing.

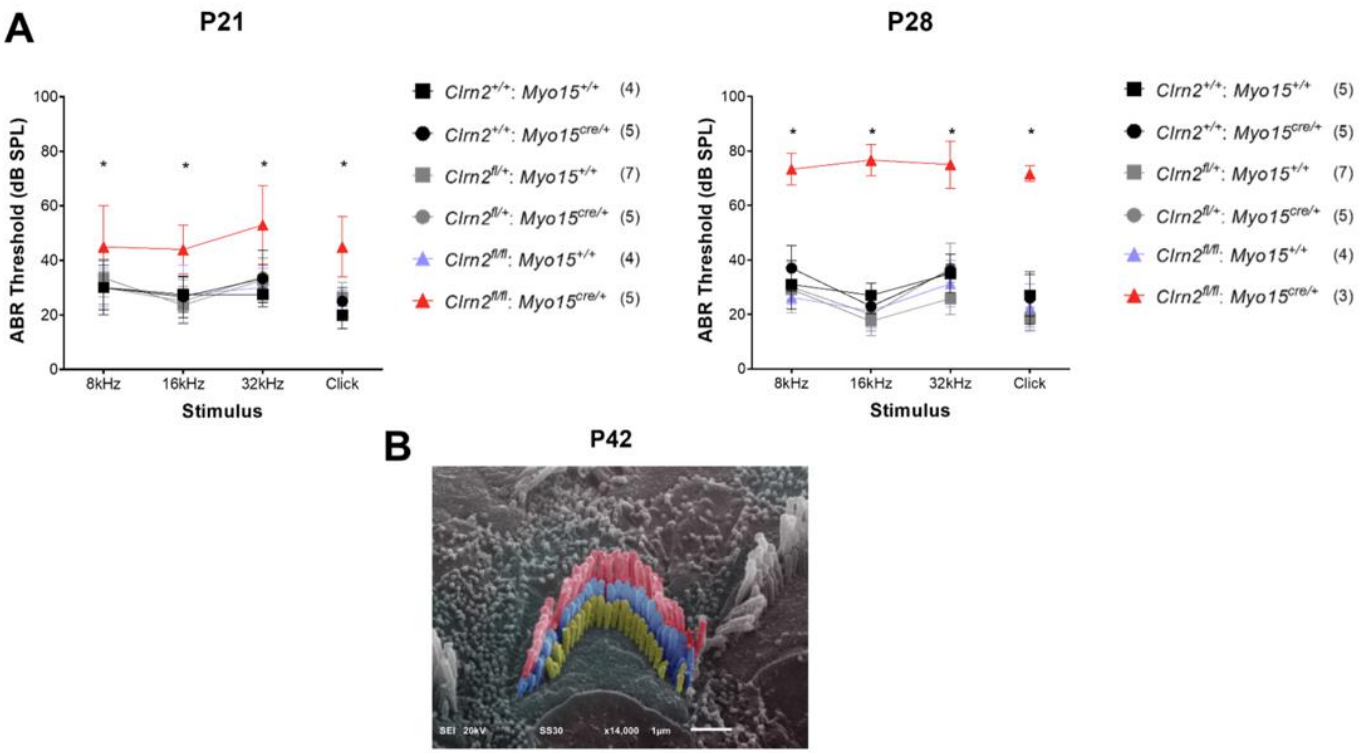

Figure 5.2- Effect of conditional knockout on hearing and bundle morphology

(A) ABR recordings from P21 and P28 control and *CLRN2$^{fl/fl}$:Myo15-cre$^{+/-}$* mice. In the *CLRN2$^{fl/fl}$:Myo15-cre$^{+/-}$* mice there is a slightly increased hearing threshold at P21 and at P28 the mouse is almost completely deaf. (B) SEM of a P42 OHC hair bundle from a *CLRN2$^{fl/fl}$:Myo15-cre$^{+/-}$* mice showing that the bundle morphology is not affected in the *CLRN2$^{fl/fl}$:Myo15-cre$^{+/-}$* mouse (Unpublished data from Mike Bowl, reproduced with consent)

5.2 Results

To further elaborate upon the functional requirement of clarin-2 we investigated the electrophysiological properties of the mechanotransducer current in *Clrn2*$^{fl/fl}$*:Myo15-cre*$^{+/-}$ mice compared to control *Clrn2*$^{fl/fl}$ littermates.

In order to measure the maximal MET current, the difference between the current size at a saturating excitatory direction and saturating inhibitory direction were measured between P7 and P10. This age range was chosen as it is similar to the age range (P6-8) looked at in the constitutive knockout mouse, so a comparison could be made between the two models. While it would have been interesting to look at P16, as this is the age where we see an increase in hearing threshold, this was not possible without creating a mouse model that was missing its tectorial membrane. Above the onset of hearing (P12), removing the tectorial membrane causes damage to the stereocilia. At P7/8 the maximal MET current was not significantly different between the conditional knockout *Clrn2*$^{fl/fl}$*:Myo15-cre*$^{+/-}$ and the control *Clrn2*$^{fl/fl}$ mice at -124mV ($P = 0.96$, 2-way ANOVA, Šidák post-test) or +99mV ($P= 0.74$, 2-way ANOVA, Šidák post-test) (Figure 5.3).

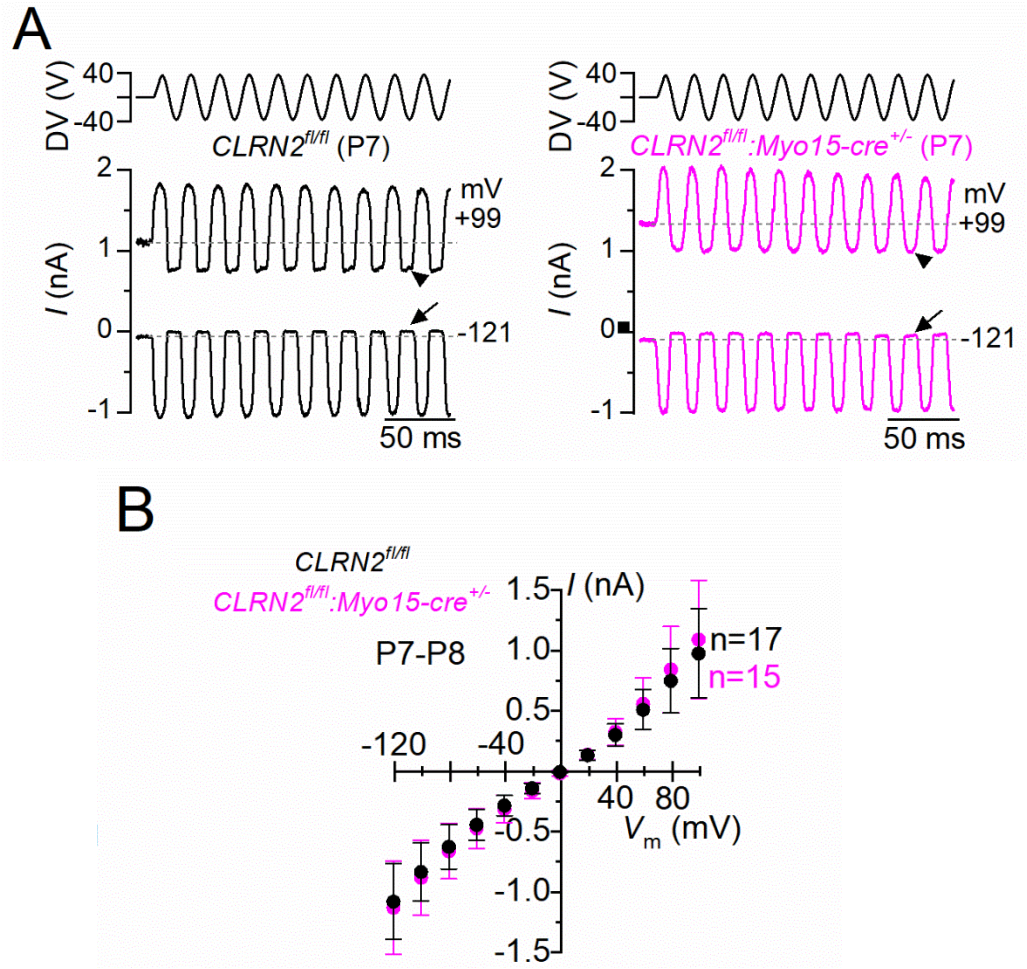

Figure 5.3- MET current size in clarin-2 conditional knock-out OHCs at P7-P8

(A) saturating MET current in apical coil OHCs from P7 control *CLRN2$^{fl/fl}$* and littermate *CLRN2$^{fl/fl}$:Myo15-cre$^{+/-}$* mice in response to the sine wave stimuli at -124mV and +99mV. (B) average MET current-voltage curves from P7 control *CLRN2$^{fl/fl}$* (n=17 (9)) and littermate *CLRN2$^{fl/fl}$:Myo15-cre$^{+/-}$* (n=15 (8)) mice. At P7-8 there is no difference in MET current size between the control and *CLRN2$^{fl/fl}$:Myo15-cre$^{+/-}$* mice. Values are mean ± S.D, (n=cells (animals)). *CLRN2$^{fl/fl}$* control (black), *CLRN2$^{fl/fl}$:Myo15-cre$^{+/-}$* (pink).

At P9 there is no significant decrease in MET current size at -124mV (P = 0.22; 2-way ANOVA, Šidák post-test) or +99mV (P = 0.09; 2-way ANOVA, Šidák post-test, Figure 5.4). However, P10 there was a significant decrease in the maximal current size between the knockout and control mice at -124mV (P = 0.002; 2-way ANOVA, Šidák post-test) and +99mV (P = 0.01; 2-way ANOVA, Šidák post-test, Figure 5.4). Figure 5.5 shows the size of the of MET current in the clarin-2 mouse between P7 and P10.

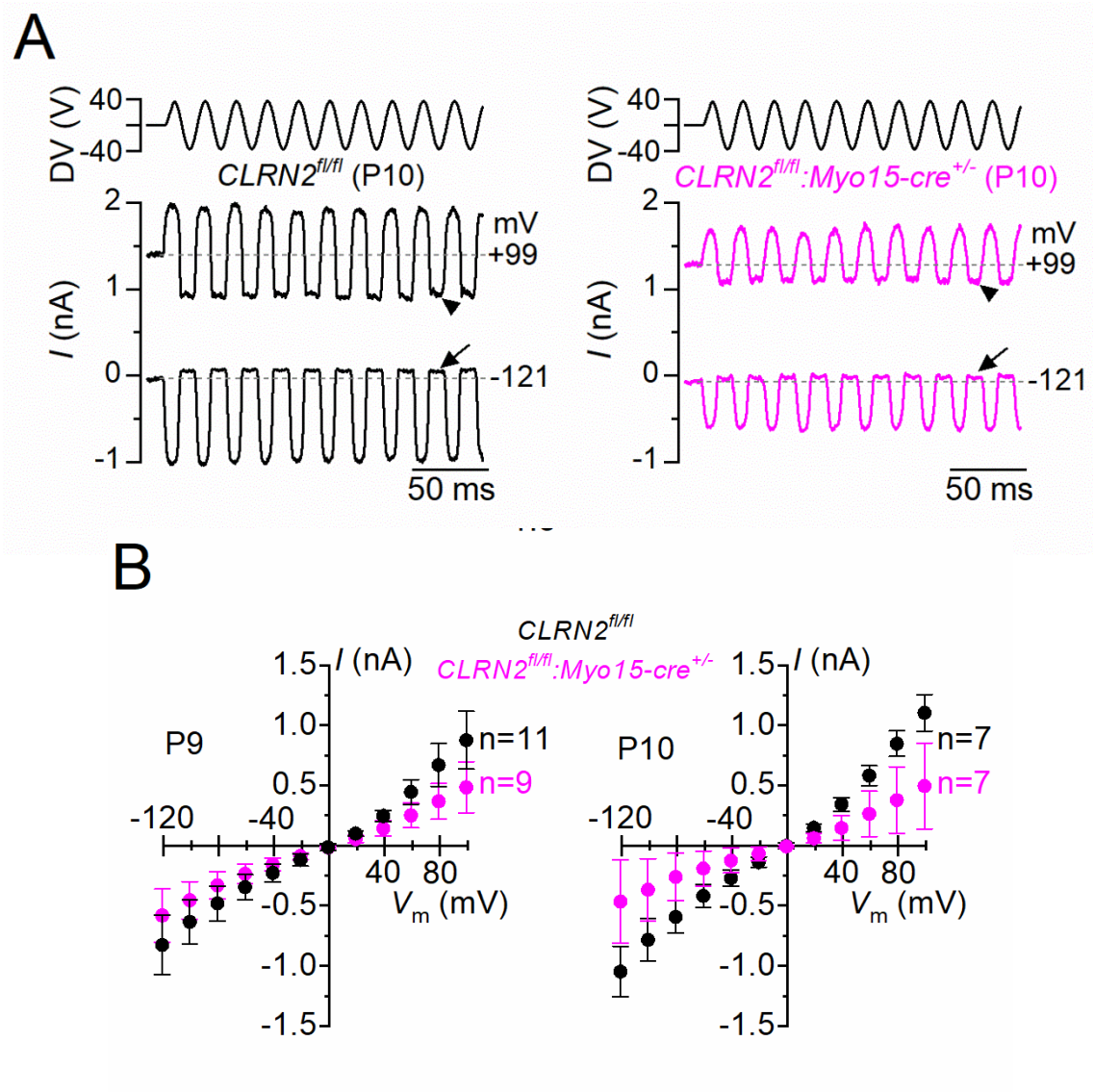

Figure 5.4-MET current size in clarin-2 conditional knockout OHCs at P9 and P10

(A) saturating MET current in apical coil OHCs from P10 control *CLRN2*$^{fl/fl}$ and littermate *CLRN2*$^{fl/fl}$*:Myo15-cre*$^{+/-}$ mice. (B) average MET current-voltage curves from P9 and P10 control *CLRN2*$^{fl/fl}$ (P9 n=11 (5)) (P10 n=7 (5)) and littermate *CLRN2*$^{fl/fl}$*:Myo15-cre*$^{+/-}$ mice (P9 n=7 (5)) (P10 n=7 (4)). At P10 the MET current size is smaller in the *CLRN2*$^{fl/fl}$*:Myo15-cre*$^{+/-}$ mice. Values are mean ± S.D, (n=cells (animals)). *CLRN2*$^{fl/fl}$ control (black), *CLRN2*$^{fl/fl}$*:Myo15-cre*$^{+/-}$ (pink).

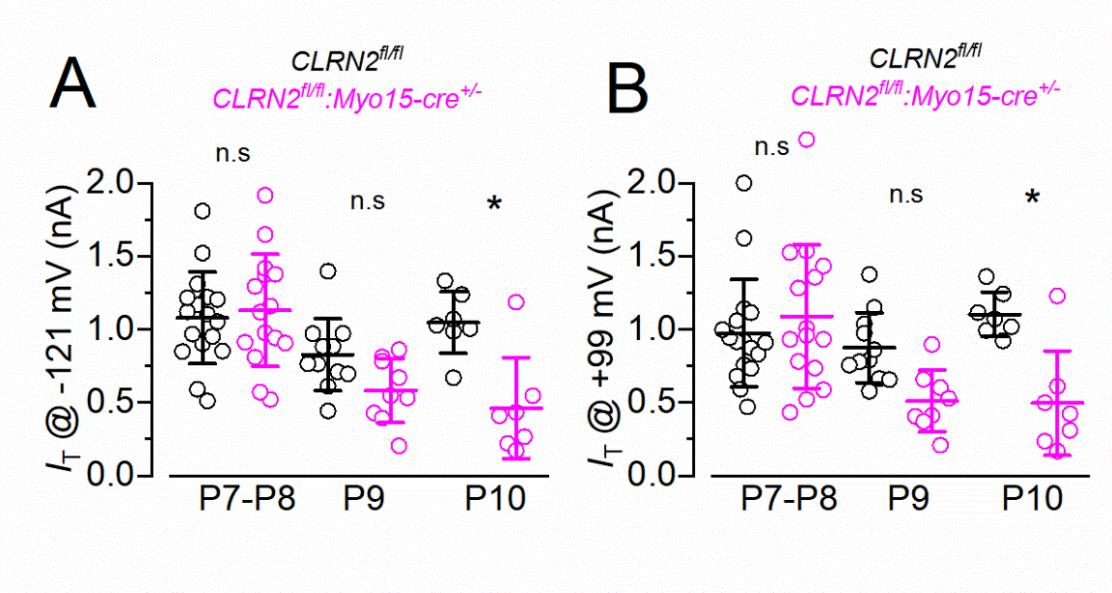

Figure 5.5- Average MET current size in clarin-2 conditional knock-out OHCs

Maximal size of the MET current in *CLRN2$^{fl/fl}$* control (P7-8 n=17 (9), P9 n=11 (5), P10 n=7 (5)) and *CLRN2$^{fl/fl}$:Myo15-cre$^{+/-}$* mice (P7-8 n=15 (8), P9 n=9 (3), P10 n=7 (4)) at (A) -121mV and (B) +99mV at P7-8, P9 and P10. The size of the MET current is significantly reduced at P10. * indicates $P < 0.05$, 2-way ANOVA, Šidák post-test. Values are mean ± S.D, (n=cells (animals)). *CLRN2$^{fl/fl}$* control (black), *CLRN2$^{fl/fl}$:Myo15-cre$^{+/-}$* (pink).

Another important property of the MET channel is the resting open probability. The resting open probability is measured as the difference between the current size at rest and when the hair bundle is being stimulated in a saturated inhibitory direction, taken as a percentage of the maximal current size (see methods). For all age groups between P7-P10 there was no significant decrease in the resting open probability at -121mV or +99mV ($P = 0.99$; two-way ANOVA, Figure 5.6).

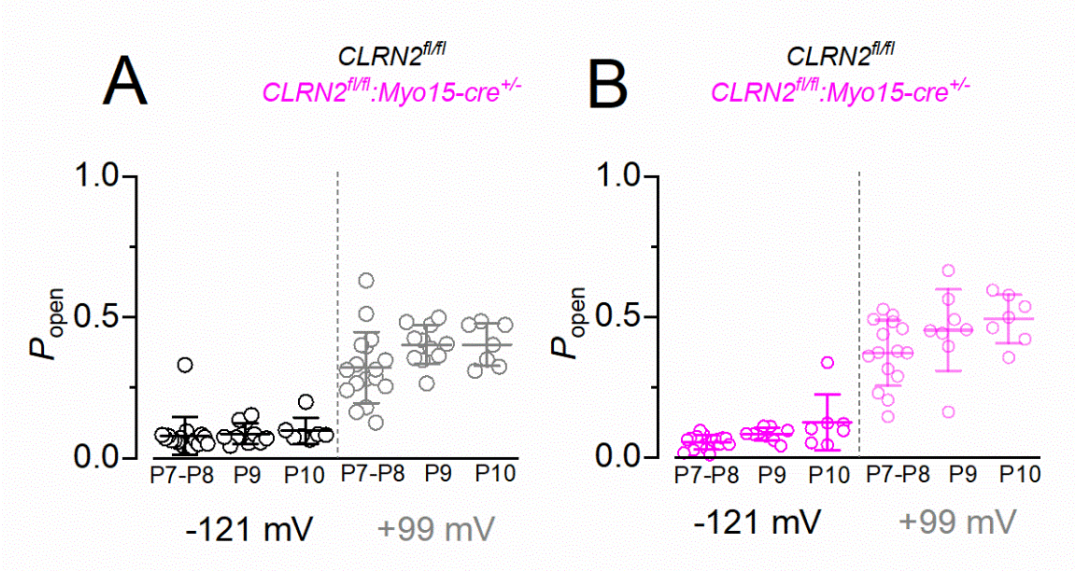

Figure 5.6- Average resting open probability in CLRN2 conditional knock-out OHCs

Resting open probability in (A) *CLRN2*$^{fl/fl}$ control (P7-8 n=17 (9), P9 n=11 (5), P10 n=7 (5)) and (B) *CLRN2*$^{fl/fl}$*:Myo15-cre*$^{+/-}$ mice (P7-8 n=15 (8), P9 n=9 (3), P10 n=7 (4)) at -121mV and +99mV at P7-8, P9 and P10. Values are mean ± S.D, (n=cells (animals)). *CLRN2*$^{fl/fl}$ control (black), *CLRN2*$^{fl/fl}$*:Myo15-cre*$^{+/-}$ (pink).

5.3 Discussion

This chapter has characterised the effect of conditionally deleting *Clrn2*, using a *Myo15*-driven Cre-recombinase, on the mechanotransducer currents elicited in OHCs at P7 to P10. As discussed in the general introduction, the constitutive mutation of a protein can cause degeneration that masks the effect of the mutation. In the *Clrn2*$^{clarinet/clarinet}$ mouse there is a decrease in the size of the MET current at P6-8. It is possible that in the *Clrn2*$^{clarinet/clarinet}$ mouse the loss of MET current is caused by having fewer channels present in the bundle due to loss of the third row of stereocilia, rather than clarin-2 being directly required for MET channel function.

In the conditional knockout there is no loss of stereocilia from the bundle, but there is still a decrease in MET current size, although it wasn't seen until P10. The delay in loss of MET current, compared to the constitutive knockout, could be due to *Clrn2* not being knocked out until ~P4 in the conditional knockout. In the conditional knockout it is possible that *Clrn2* is still present in the cell at P7-P9, and this is why there is no loss of MET current at these time points.

The decrease in MET current size demonstrates that clarin-2 is required for the normal functioning or trafficking of the MET channel. Dunbar *et al.* (2019) hypothesised that the decrease in MET current size could suggest a reduced number of MET channels. Reduced MET current could also be caused by missing or slack tip links, although slack tip links would also affect the resting open probability (Dunbar et al., 2019).

In the *Clrn2*$^{clarinet/clarinet}$ mouse there was no effect on the size of the resting open probability. In the conditional knockout the same thing was observed at all ages investigated (P7-P10). The maintenance of the resting open probability suggests that some MET channels are still present and are able to function in the absence of clarin-2.

In conclusion, both the *Clrn2*$^{clarinet/clarinet}$ mouse and the conditional *Clrn2* knockout mice exhibit a similar reduction in their OHC MET currents, though the loss of current is slightly delayed in the conditional knockout. However, unpublished work from Mike Bowl, showing that no stereocilia are lost up to P42, suggests that the loss of current in the conditional knockout is not due to fewer stereocilia in the hair bundle. As such, this chapter suggests that

clarin-2 is needed for the normal trafficking of the MET channels to the tips of the stereocilia in mature OHCs, but it is not needed to maintain a normal resting open probability.

Chapter 6 - General Discussion

6.1 General discussion

Overall, this project aimed to investigate the function of myosin 7a. Myosin 7a is a vital component of the mechanoelectrical transducer machinery and, when mutated leads to Usher syndrome type 1B. A lot of work has previously been done on the role of myosin 7a in the development and function of the hair cells (Grati & Kachar, 2011; Kros et al., 2002; Self et al., 1998). However, the role of myosin 7a in mechanotransduction is still not fully understood. Thus, the aim of this study was to identify the role of myosin 7a in the development and maintenance of the MET channel using a conditional knockout and the *Shaker-1* model. Having a greater understanding of the role of myosin 7a would also provide insights into how myosin 7a is affected in disease and how it could be targeted for treatment.

6.2 Comparing a constitutive and conditional knockout of myosin 7a

One of the main aims of this project was to determine whether the phenotypes seen in a constitutive knockout of myosin 7a are comparable to what is seen in the conditional knockout. This hypothesis was based on research into a conditional knockout of the sans protein which showed different phenotypes in the constitutive and conditional knockout model (Caberlotto et al., 2011).

It has been shown that in the constitutive knockout of myosin 7a there is rapid degeneration of the hair bundle, which could contribute to hearing defects seen in these mice (Kros et al., 2002). This degeneration is not seen in the conditional knockout up to at least one month old, allowing a more accurate investigation of the role of myosin 7a without widespread degeneration affecting any phenotypes. This suggests that myosin 7a is needed initially for the development of the hair bundle, but once the bundle has developed it is not needed to maintain it.

However, at 5-9 months old most of the hair bundles have disappeared or fused together. The disappearance of the hair bundle at the older age point (5-9 months) could be due to a number of factors. It could suggest that myosin 7a is needed for the long-term survival of the hair bundle after all. It could also be a secondary effect caused by the loss of the MET current, which is known to cause disruption to the hair bundle (Corns et al., 2018). SEM and TEM on

age points between one month and five months could shed some light on this question and give more detail on the progression of loss of the hair bundle.

Previous data from the constitutive knockout mouse showed that in the absence of functional myosin 7a the MET current had abnormal gating and a resting open probability of zero (Kros et al., 2002). This led to the hypothesis that myosin 7a is needed to maintain the tip link tension and the resting open probability. Without sufficient tension in the tip links, the MET channels will not stay open at rest to allow current to enter the cell. However, the work in this PhD project showed that, even though there was a very small MET current, the size of the resting open probability in the conditional knockout mouse was unchanged up to P27. This suggests that there is still enough tension in the tip links, even without myosin 7a, to maintain a resting open probability.

The difference in MET channel recordings between the constitutive and conditional knockout can be explained partly by the disorganisation of the hair bundle seen at P3 in the constitutive knockout mouse. It could also be explained by the presence of an additional, then unknown, mechanotransduction channel. This channel is located at the hair cells apical surface and contains the Piezo2 protein. These MET channels show reverse polarity currents during hair bundle development and after the breakage of tip links (Wu et al., 2017). There is no resting current from these channels at negative membrane potentials and abnormal adaptation of the channels (Marcotti et al., 2014). The discovery of this channel could provide an explanation for the abnormal transducer channel gating seen in the constitutive myosin 7a knockout that is not seen in the conditional knockout.

Overall, this section shows that some of the phenotypes seen in the constitutive knockout are very likely to be due to disorganisation of the hair bundle, caused by the early knockout of myosin 7a. The conditional knockout provides a more accurate picture of the role of myosin 7a in mechanotransduction.

6.3 Comparing a conditional KO of myosin 7a and the *Shaker-1* mouse

The second main aim of this project was to look at how a point mutation of myosin 7a would affect mechanotransduction and compare this to a complete knockout. Figure 6.1 illustrates

the phenotypes seen in the *Shaker-1* and cKO model and when they emerge in each model. The *Shaker-1* mouse has a point mutation in the area of myosin 7a that is involved in binding to actin and could affect the interaction that myosin 7a has with actin. The *Shaker-1* point mutation is more representative of Usher syndrome type 1B as this syndrome is caused by point mutations to myosin 7a rather than by a full knockout of the protein. Using the *Shaker-1* model with the conditional knockout can give a greater understanding of the role of myosin 7a in both development and maintenance of the hair bundle and mechanotransduction.

The pattern of hearing loss is different between the conditional knockout and the *Shaker-1* mouse. In the *Shaker-1* mouse there is hearing impairment from an earlier age (P18) but the decline in hearing is slower. Preliminary data suggests that some hearing is still present at P30, however more work is needed to confirm this result. Whereas, in the conditional knockout, there is no hearing impairment until P25, but then hearing very quickly deteriorates with the mouse being almost completely deaf five days later, at P30.

This is not unexpected as the conditional knockout is a complete knockout of the protein, whereas the *Shaker-1* mouse has only a point mutation and therefore has a less severe hearing phenotype.

Bundle morphology is not affected in the conditional knockout up to P30. Conversely, the *Shaker-1* mice show some degeneration from P5 with shortening of the third and second rows of stereocilia in OHCs and complete loss of the third row by P12. In the *Shaker-1* mouse, IHC bundle morphology is not affected at P12, then by P30 there is loss of the third and second row of stereocilia.

The changes observed in the hair bundle at an early age in the *Shaker-1* mouse is similar to what is seen in the constitutive knockout of myosin 7a (Kros *et al.*, 2002). This shows that when myosin 7a is knocked out or mutated from the beginning of development, the hair bundle shows rapid morphological changes, suggesting that myosin 7a has a vital role in development.

In comparison, when myosin 7a is present for the initial development, and only knocked out at P4, the hair bundle doesn't begin to show signs of morphological changes until much later, around 5-8 months old. If the degeneration at 5-8 months old could be shown to be due to

loss of the MET current, rather than the knockout of myosin 7a, this could suggest that myosin 7a only has a role in bundle morphology in the initial stages of development.

In the *Shaker-1* mouse the size of the OHC MET current starts to decrease from around P8, this is much earlier than the conditional knockout, where MET current starts to decrease from P20. This could be because myosin 7a is knocked out much earlier in the *Shaker-1* mouse, it could also be due to the shortening of the third row of stereocilia in the *Shaker-1* mouse from P6, exacerbating the effect of the mutation. Although, the decrease in MET current size in the conditional knockout, which has a normal bundle morphology, suggests that the reduction in MET current size is a direct effect of the myosin 7a mutation.

The role of myosin 7a in tensioning the tip links and regulating the resting open probability is still a little unclear. In the conditional knockout there is no effect on resting open probability, even when the size of the MET current is very small, suggesting that myosin 7a doesn't have a role in tensioning tip links. The resting open probability is also not affected in the older *Shaker-1* mice (P9-P10), however, the resting open probability is very small at P5 in the *Shaker-1* mouse, suggesting that the *Shaker-1* mutation is affecting the tip link tension. This is an area of research that needs more investigation to fully understand the role of myosin 7a in mechanotransduction and tensioning the tip links.

Calcium sensitivity was measured in both the conditional knockout and the *Shaker-1* mouse. However, in both the conditional knockout mouse and the *Shaker-1* mouse the results were not clear as there was no increase in resting open probability when the 5mM BAPTA intracellular solution was used in all genotypes tested. This result was unexpected as reducing the intracellular calcium concentration should have increased the resting open probability. Increasing the n numbers in this experiment could lead to a statistically significant increase in resting open probability size with 5mM BAPTA. It is difficult to conclude anything from this experiment and more work is needed to determine the role of myosin 7a in regulating calcium sensitivity.

One experiment that could shed some light on the role of myosin 7a in maintaining tip link tension is measuring the effect of 5mM BAPTA on the resting open probability at P5. This would show whether the P5 *Shaker-1* mice can generate a resting open probability by removing calcium from the intracellular environment.

Overall, this section shows that myosin 7a has vital roles in both the early development of the hair bundle and maintaining the MET current in the mature hair cell.

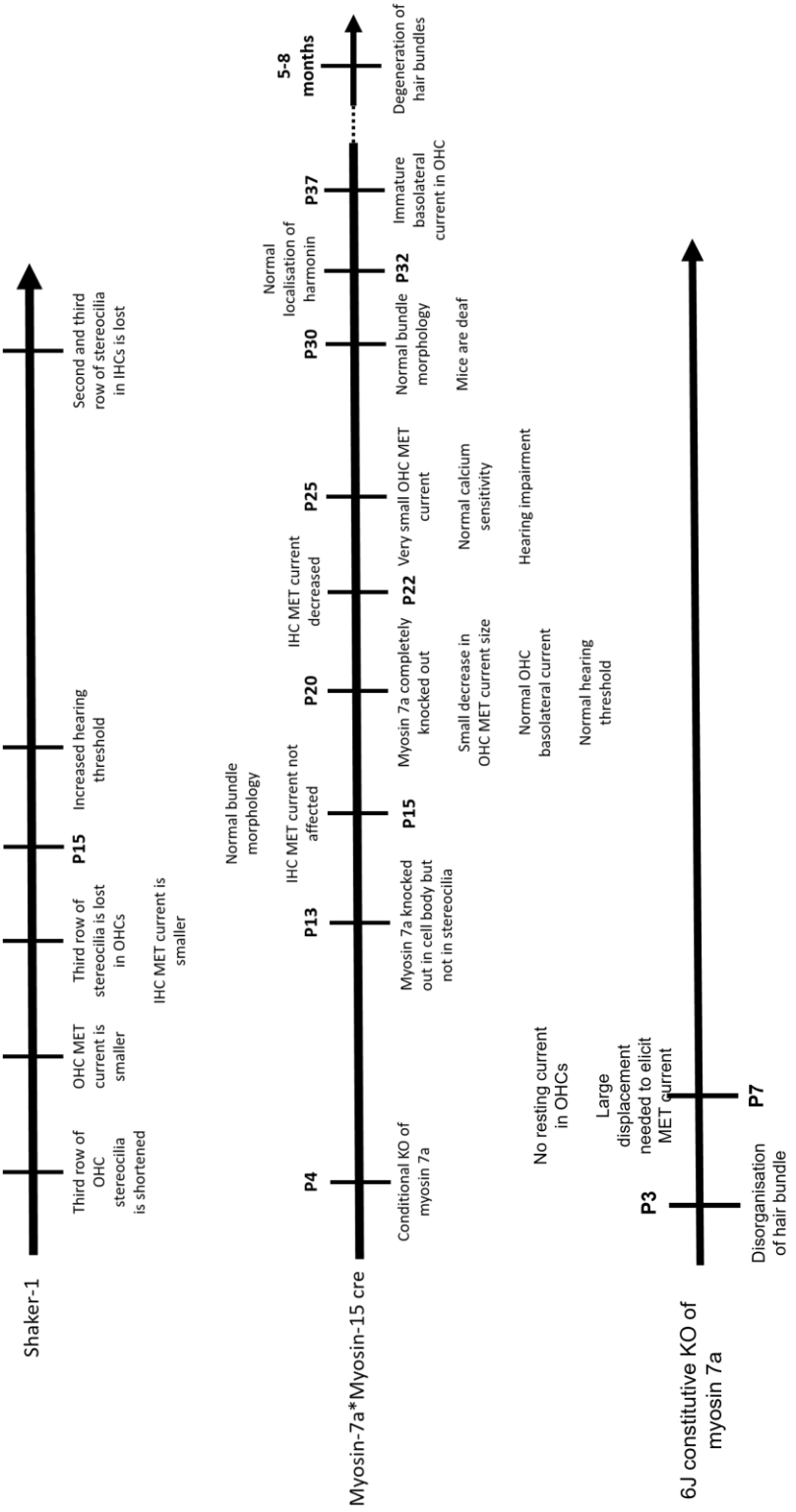

Figure 6.1- Timeline of phenotypes seen in 6J constitutive myosin 7a knockout, conditional myosin 7a knockout and *Shaker-1* mouse

The diagram shows a timeline for the *Shaker-1*, conditional knockout and constitutive knockout mouse, illustrating the emergence of different phenotypes in each model.

6.4 The role of myosin 7a in development and maintenance of hair bundle and mechanotransduction

From this research it seems likely that myosin 7a has a role in both the development of the hair cell, and maintenance of the hair bundle and MET current after the initial development phase.

From the previous work on the constitutive myosin 7a knockout and this work on the *Shaker-1* mouse it is clear that myosin 7a is vital for the proper development of the hair bundle. In both cases there is disorganisation of the hair bundle from an early age. There is also a clear effect on the MET channel with an abnormal MET current in both models (Kros et al., 2002).

However, the work on the conditional knockout demonstrates there is also a role for myosin 7a in the maintenance of the MET current and hair bundle. Without myosin 7a there is a clear, progressive decrease in the size of the MET current between P20 and P27. There is also disorganization of the hair bundle between 5-8 months of age.

Previous work by Corns et al. (2018) showed that in a conditional knockout of myosin 7a the IHC MET current size and resting open probability was lower than in the control mice, which contradicts the finding in OHCs that the resting open probability is not affected (Corns et al., 2018). It is possible that myosin 7a has different roles in the inner and outer hair cells.

This idea is supported by the finding that myosin 7a is expressed in different isoforms in the hair cells. Li et al. (2020) found a canonical isoform of myosin 7a with a transcription start site in exon 2 and another, shorter isoform where the transcription start site is two exons downstream. This paper investigated the different isoforms of myosin 7a by creating a mouse model where only the canonical isoform of myosin 7a is deleted. They found that the levels of myosin 7a were greatly reduced in the IHCs and tonotopically reduced in the OHCs. In the OHCs the levels of myosin 7a were similar in the basal coil, then decreased up the coil and myosin 7a levels was reduced by 50% in apical coil OHCs. This suggests that there is differential expression of the canonical myosin 7a isoform in the inner and outer hair cells (Li et al., 2020).

Li et al. (2020) found that the IHCs at P7-8 had a reduced resting open probability, although the peak size of the MET current was unaffected in this mouse model. Also, there was no

change to peak MET current size or resting open probability in the OHCs at P7-8 (Li et al., 2020). The decrease in resting open probability in the IHCs in the conditional knockout and canonical myosin 7a knockout suggests that myosin 7a is needed to maintain tip link tension in the IHCs. The work in these papers, combined with the work shown in this thesis, suggests that myosin 7a is playing different roles in the inner and outer hair cells. This could be explained by the expression of different isoforms of myosin 7a in each cell type.

6.5 The role of clarin-2 in mechanotransduction

The last aim of the project was related to a different protein that has been linked to deafness, clarin-2. Part of this work was looking at the difference in phenotypes between constitutive and conditional knockouts of deafness related proteins. The constitutive knockout was already investigated by Dunbar et al. (2019) and this project looked at the electrophysiological properties of the conditional knockout. The hypothesis for the *clrn2* mouse was that the size of the MET current would be affected but not the resting open probability, which is similar to what is seen in the constitutive knockout model (Dunbar et al., 2019). This hypothesis was proved to be correct as there was a reduction in the size of the MET current from P9-P10, but there was no change in the size of the resting open probability at any age tested.

In this case, using the conditional knockout alongside the constitutive knockout allowed us to show that the loss of MET current in the *Clrn2*$^{fl/fl}$*:Myo15-cre*$^{+/-}$ mouse is due to the knockout of *clrn2*, rather than the loss of stereocilia. Using both models together in a useful tool in separating the role that a protein may have in mechanotransduction, from its potential role in development of the hair bundle.

6.6 Conclusions and future work

This research has shown that myosin 7a is essential for both the development of the hair bundle and the function of the MET channel. However, the exact role of myosin 7a in mechanotransduction is still not clear. Previous hypotheses that myosin 7a is needed for tensioning of the tip links seem to be disproved by the normal resting open probability in the conditional knockout and older *Shaker-1* mouse. Another hypothesis was that myosin 7a is

needed to transport other proteins along the stereocilia (e.g. Harmonin and Sans), however this project showed that harmonin is still localised to the stereocilia in both the conditional knockout and the *Shaker-1* mouse.

For the future, more work is needed to elucidate the precise role of myosin 7a in mechanotransduction and development. One hypothesis on the role of myosin 7a that was not explored in this thesis, is that myosin 7a is needed to regulate adaptation of the MET current. Investigating the adaptive properties of the MET channel would be an important experiment for the future.

Although there is no obvious change to hair bundle morphology in the conditional knockout of myosin 7a, this does not rule out slight changes to height and width of the stereocilia. These small changes, though not observable in SEM, could affect MET channel function. One way to measure this would be with TEM. This would allow a detailed comparison of the height and width of stereocilia in the conditional knockout model.

Another experiment for the future would be looking at the localisation of other proteins involved in mechanotransduction, such as sans and cadherin-23. Both of these proteins interact closely with myosin 7a and make up part of the mechanotransducer machinery.

Lastly, another experiment that would be useful to understand the mechanism of myosin 7a would be RNA-seq. This experiment would provide information about which pathways inside the cell are affected when myosin 7a is knocked out or mutated.

Bibliography

Adachi, N., Yoshida, T., Nin, F., Ogata, G., Yamaguchi, S., Suzuki, T., Komune, S., Hisa, Y., Hibino, H., & Kurachi, Y. (2013). The mechanism underlying maintenance of the endocochlear potential by the K^+ transport system in fibrocytes of the inner ear. *The Journal of Physiology*, *591*(18), 4459–4472. https://doi.org/10.1113/jphysiol.2013.258046

Adato, A., Vreugde, S., Joensuu, T., Avidan, N., Hamalainen, R., Belenkiy, O., Olender, T., Bonne-Tamir, B., Ben-Asher, E., Espinos, C., Millán, J. M., Lehesjoki, A.-E., Flannery, J. G., Avraham, K. B., Pietrokovski, S., Sankila, E.-M., Beckmann, J. S., & Lancet, D. (2002). USH3A transcripts encode clarin-1, a four-transmembrane-domain protein with a possible role in sensory synapses. *European Journal of Human Genetics*, *10*(6), 339–350. https://doi.org/10.1038/sj.ejhg.5200831

Ahmed, Z. M., Masmoudi, S., Kalay, E., Belyantseva, I. A., Mosrati, M. A., Collin, R. W. J., Riazuddin, S., Hmani-Aifa, M., Venselaar, H., Kawar, M. N., Tlili, A., van der Zwaag, B., Khan, S. Y., Ayadi, L., Riazuddin, S. A., Morell, R. J., Griffith, A. J., Charfedine, I., Caylan, R., … Kremer, H. (2008). Mutations of LRTOMT, a fusion gene with alternative reading frames, cause nonsyndromic deafness in humans. *Nature Genetics*, *40*(11), 1335–1340. https://doi.org/10.1038/ng.245

Ashmore, J. (1994). The G.L. Brown Prize Lecture. The cellular machinery of the cochlea. *Experimental Physiology*, *79*(2), 113–134. https://doi.org/10.1113/expphysiol.1994.sp003746

Ashmore, J. (2019). Outer Hair Cells and Electromotility. *Cold Spring Harbor Perspectives in Medicine* , *9*(7). https://doi.org/10.1101/cshperspect.a033522

Bahloul, A., Michel, V., Hardelin, J.-P., Nouaille, S., Hoos, S., Houdusse, A., England, P., & Petit, C. (2010). Cadherin-23, myosin VIIa and harmonin, encoded by Usher syndrome type I genes, form a ternary complex and interact with membrane phospholipids. *Human Molecular Genetics*, *19*(18), 3557–3565. https://doi.org/10.1093/hmg/ddq271

Basch, M. L., Brown 2nd, R. M., Jen, H.-I., & Groves, A. K. (2016). Where hearing starts: the development of the mammalian cochlea. *Journal of Anatomy*, *228*(2), 233–254. https://doi.org/10.1111/joa.12314

Ben-Yosef, T., Belyantseva, I. A., Saunders, T. L., Hughes, E. D., Kawamoto, K., van Itallie, C. M., Beyer, L. A., Halsey, K., Gardner, D. J., Wilcox, E. R., Rasmussen, J., Anderson, J. M., Dolan, D. F., Forge, A., Raphael, Y., Camper, S. A., & Friedman, T. B. (2003). Claudin 14 knockout mice, a model for autosomal recessive deafness DFNB29 , are deaf due to cochlear hair cell degeneration . *Human Molecular Genetics*, *12*(16), 2049–2061. https://doi.org/10.1093/hmg/ddg210

Berg, J. S., Powell, B. C., & Cheney, R. E. (2001). A millennial myosin census. *Molecular Biology of the Cell*, *12*(4), 780–794. https://doi.org/10.1091/mbc.12.4.780

Berglund, A. M., & Ryugo, D. K. (1987). Hair cell innervation by spiral ganglion neurons in the mouse. *Journal of Comparative Neurology*, *255*(4), 560–570. https://doi.org/10.1002/cne.902550408

Beurg, M., Evans, M. G., Hackney, C. M., & Fettiplace, R. (2006). A large-conductance calcium-selective mechanotransducer channel in mammalian cochlear hair cells. *The Journal of Neuroscience : The Official Journal of the Society for Neuroscience*, *26*(43), 10992–11000. https://doi.org/10.1523/JNEUROSCI.2188-06.2006

Beurg, M., Fettiplace, R., Nam, J.-H., & Ricci, A. J. (2009). Localization of inner hair cell mechanotransducer channels using high-speed calcium imaging. *Nature Neuroscience*, *12*(5), 553–558. https://doi.org/10.1038/nn.2295

Beurg, M., Nam, J.-H., Chen, Q., & Fettiplace, R. (2010). Calcium balance and mechanotransduction in rat cochlear hair cells. *Journal of Neurophysiology*, *104*(1), 18–34. https://doi.org/10.1152/jn.00019.2010

Beurg, M., Xiong, W., Zhao, B., Müller, U., & Fettiplace, R. (2015). Subunit determination of the conductance of hair-cell mechanotransducer channels. *Proceedings of the National Academy of Sciences of the United States of America*, *112*(5), 1589–1594. https://doi.org/10.1073/pnas.1420906112

Blazejczyk, M., Sobczak, A., Debowska, K., Wisniewska, M. B., Kirilenko, A., Pikula, S., Jaworski, J., Kuznicki, J., & Wojda, U. (2009). Biochemical characterization and expression analysis of a novel EF-hand Ca2+ binding protein calmyrin2 (Cib2) in brain indicates its function in NMDA receptor mediated Ca2+ signaling. *Archives of Biochemistry and Biophysics*, *487*(1), 66–78. https://doi.org/https://doi.org/10.1016/j.abb.2009.05.002

Boëda, B., El-Amraoui, A., Bahloul, A., Goodyear, R., Daviet, L., Blanchard, S., Perfettini, I., Fath, K. R., Shorte, S., Reiners, J., Houdusse, A., Legrain, P., Wolfrum, U., Richardson, G., & Petit, C. (2002). Myosin VIIa, harmonin and cadherin 23, three Usher I gene products that cooperate to shape the sensory hair cell bundle. *The EMBO Journal*, *21*(24), 6689–6699. https://doi.org/10.1093/EMBOJ/CDF689

Bonnet, C., & El-Amraoui, A. (2012). Usher syndrome (sensorineural deafness and retinitis pigmentosa): pathogenesis, molecular diagnosis and therapeutic approaches. *Current Opinion in Neurology*, *25*(1).

Borbiro, I., Badheka, D., & Rohacs, T. (2015). Activation of TRPV1 channels inhibits mechanosensitive Piezo channel activity by depleting membrane phosphoinositides. *Science Signaling*, *8*(363), ra15 LP-ra15. https://doi.org/10.1126/scisignal.2005667

Brown, P. G., & Ruben, R. J. (1969). The Endocochlear Potential in the Shaker-1 (sh-1/sh-1) Mouse. *Acta Oto-Laryngologica*, *68*(1–6), 14–20. https://doi.org/10.3109/00016486909121538

Brownell, W. E., Bader, C. R., Bertrand, D., & de Ribaupierre, Y. (1985). Evoked mechanical responses of isolated cochlear outer hair cells. *Science*, *227*(4683), 194 LP – 196. https://doi.org/10.1126/science.3966153

Caberlotto, E., Michel, V., Foucher, I., Bahloul, A., Goodyear, R. J., Pepermans, E., Michalski, N., Perfettini, I., Alegria-Prévot, O., Chardenoux, S., do Cruzeiro, M., Hardelin, J.-P., Richardson, G. P., Avan, P., Weil, D., & Petit, C. (2011). Usher type 1G protein sans is a critical component of the tip-link complex, a structure controlling actin polymerization in stereocilia. *Proceedings of the National Academy of Sciences of the United States of America*, *108*(14), 5825–5830. https://doi.org/10.1073/pnas.1017114108

Calabro, K. R., Boye, S. L., Choudhury, S., Fajardo, D., Peterson, J. J., Li, W., Crosson, S. M., Kim, M.-J., Ding, D., Salvi, R., Someya, S., & Boye, S. E. (2019). A Novel Mouse Model of MYO7A USH1B Reveals Auditory and Visual System Haploinsufficiencies. *Frontiers in Neuroscience*, *13*, 1255. https://doi.org/10.3389/fnins.2019.01255

Cheung, E. L. M., & Corey, D. P. (2006). Ca2+ changes the force sensitivity of the hair-cell transduction channel. *Biophysical Journal*, *90*(1), 124–139. https://doi.org/10.1529/biophysj.105.061226

Coate, T. M., Scott, M. K., & Gurjar, M. (2019). Current concepts in cochlear ribbon synapse formation. *Synapse (New York, N.Y.)*, *73*(5), e22087–e22087. https://doi.org/10.1002/syn.22087

Corns, L. F., Johnson, S. L., Kros, C. J., & Marcotti, W. (2014). Calcium entry into stereocilia drives adaptation of the mechanoelectrical transducer current of mammalian cochlear hair cells. *Proceedings of the National Academy of Sciences of the United States of America*, *111*(41), 14918–14923. https://doi.org/10.1073/pnas.1409920111

Corns, L. F., Johnson, S. L., Kros, C. J., & Marcotti, W. (2016). Tmc1 Point Mutation Affects Ca2+ Sensitivity and Block by Dihydrostreptomycin of the Mechanoelectrical Transducer Current of Mouse Outer Hair Cells. *The Journal of Neuroscience*, *36*(2), 336 LP – 349. https://doi.org/10.1523/JNEUROSCI.2439-15.2016

Corns, L. F., Johnson, S. L., Roberts, T., Ranatunga, K. M., Hendry, A., Ceriani, F., Safieddine, S., Steel, K. P., Forge, A., Petit, C., Furness, D. N., Kros, C. J., & Marcotti, W. (2018). Mechanotransduction is required for establishing and maintaining mature inner hair cells and regulating efferent innervation. *Nature Communications*, *9*(1). https://doi.org/10.1038/s41467-018-06307-w

Cosgrove, D., & Zallocchi, M. (2014). Usher protein functions in hair cells and photoreceptors. *The International Journal of Biochemistry & Cell Biology*, *46*, 80–89. https://doi.org/10.1016/j.biocel.2013.11.001

Coureux, P.-D., Sweeney, H. L., & Houdusse, A. (2004). Three myosin V structures delineate essential features of chemo-mechanical transduction. *The EMBO Journal*, *23*(23), 4527–4537. https://doi.org/10.1038/sj.emboj.7600458

Crawford, A. C., Evans, M. G., & Fettiplace, R. (1991). The actions of calcium on the mechano-electrical transducer current of turtle hair cells. *The Journal of Physiology*, *434*, 369–398. https://doi.org/10.1113/jphysiol.1991.sp018475

Cunningham, C. L., & Müller, U. (2019). Molecular Structure of the Hair Cell Mechanoelectrical Transduction Complex. *Cold Spring Harbor Perspectives in Medicine* , *9*(5). https://doi.org/10.1101/cshperspect.a033167

Cunningham, C. L., Wu, Z., Jafari, A., Zhao, B., Schrode, K., Harkins-Perry, S., Lauer, A., & Müller, U. (2017). The murine catecholamine methyltransferase mTOMT is essential for mechanotransduction by cochlear hair cells. *ELife*, *6*, e24318. https://doi.org/10.7554/eLife.24318

Dallos, P., Wu, X., Cheatham, M. A., Gao, J., Zheng, J., Anderson, C. T., Jia, S., Wang, X., Cheng, W. H. Y., Sengupta, S., He, D. Z. Z., & Zuo, J. (2008). Prestin-based outer hair cell motility is necessary for mammalian cochlear amplification. *Neuron*, *58*(3), 333–339. https://doi.org/10.1016/j.neuron.2008.02.028

Dallos, P., Zheng, J., & Cheatham, M. A. (2006). Prestin and the cochlear amplifier. *The Journal of Physiology*, *576*(Pt 1), 37–42. https://doi.org/10.1113/jphysiol.2006.114652

Deol, M. S. (1956). The anatomy and development of the mutant pirouette, shaker-1 and waltzer in the mouse. *Proceedings of the Royal Society of London. Series B, Biological Sciences*, *145*(919), 206–213. https://doi.org/10.1098/rspb.1956.0028

Doran, M. H., & Lehman, W. (2021). The Central Role of the F-Actin Surface in Myosin Force Generation. *Biology*, *10*(12). https://doi.org/10.3390/BIOLOGY10121221

Dumont, R. A., Lins, U., Filoteo, A. G., Penniston, J. T., Kachar, B., & Gillespie, P. G. (2001). Plasma membrane Ca2+-ATPase isoform 2a is the PMCA of hair bundles. *The Journal of Neuroscience : The Official Journal of the Society for Neuroscience*, *21*(14), 5066–5078. https://doi.org/10.1523/JNEUROSCI.21-14-05066.2001

Dunbar, L. A., Patni, P., Aguilar, C., Mburu, P., Corns, L., Wells, H. R., Delmaghani, S., Parker, A., Johnson, S., Williams, D., Esapa, C. T., Simon, M. M., Chessum, L., Newton, S., Dorning, J., Jeyarajan, P., Morse, S., Lelli, A., Codner, G. F., … Bowl, M. R. (2019). Clarin-2 is

essential for hearing by maintaining stereocilia integrity and function. *EMBO Molecular Medicine*, *11*(9), e10288–e10288. https://doi.org/10.15252/emmm.201910288

Duvall, A. J., & Rhodes, V. T. (1967). Reissner's Membrane: An Ultrastructural Study. *Archives of Otolaryngology*, *86*(2), 143–151. https://doi.org/10.1001/archotol.1967.00760050145004

Effertz, T., Becker, L., Peng, A. W., & Ricci, A. J. (2017). Phosphoinositol-4,5-Bisphosphate Regulates Auditory Hair-Cell Mechanotransduction-Channel Pore Properties and Fast Adaptation. *The Journal of Neuroscience*, *37*(48), 11632 LP – 11646. https://doi.org/10.1523/JNEUROSCI.1351-17.2017

El-Amraoui, A., Sahly, I., Picaud, S., Sahel, J., Abitbol, M., & Petit, C. (1996). Human Usher 1B/Mouse shaker-1 : The Retinal Phenotype Discrepancy Explained By The Presence/Absence of Myosin VIIA in The Photoreceptor Cells . *Human Molecular Genetics*, *5*(8), 1171–1178. https://doi.org/10.1093/hmg/5.8.1171

Elliott, S. J., & Shera, C. A. (2012). The cochlea as a smart structure. *Smart Materials & Structures*, *21*(6), 64001. https://doi.org/10.1088/0964-1726/21/6/064001

Farquhar, M. G., & Palade, G. E. (1963). Junctional complexes in various epithelia. *The Journal of Cell Biology*, *17*(2), 375–412. https://doi.org/10.1083/jcb.17.2.375

Fettiplace, R. (2017). Hair Cell Transduction, Tuning, and Synaptic Transmission in the Mammalian Cochlea. *Comprehensive Physiology*, *7*(4), 1197–1227. https://doi.org/10.1002/cphy.c160049

Fettiplace, R., & Hackney, C. M. (2006). The sensory and motor roles of auditory hair cells. *Nature Reviews Neuroscience*, *7*(1), 19–29. https://doi.org/10.1038/nrn1828

Flock, A., & Cheung, H. C. (1977). Actin filaments in sensory hairs of inner ear receptor cells. *The Journal of Cell Biology*, *75*(2 Pt 1), 339–343. https://doi.org/10.1083/jcb.75.2.339

Flock, Å., Cheung, H. C., Flock, B., & Utter, G. (1981). Three sets of actin filaments in sensory cells of the inner ear. Identification and functional orientation determined by gel electrophoresis, immunofluorescence and electron microscopy. *Journal of Neurocytology*, *10*(1), 133–147. https://doi.org/10.1007/BF01181749

Flores, E. N., Duggan, A., Madathany, T., Hogan, A. K., Márquez, F. G., Kumar, G., Seal, R. P., Edwards, R. H., Liberman, M. C., & García-Añoveros, J. (2015). A non-canonical pathway from cochlea to brain signals tissue-damaging noise. *Current Biology : CB*, *25*(5), 606–612. https://doi.org/10.1016/j.cub.2015.01.009

Frank, M. M., & Goodrich, L. v. (2018). Talking back: Development of the olivocochlear efferent system. *Wiley Interdisciplinary Reviews. Developmental Biology*, *7*(6), e324–e324. https://doi.org/10.1002/wdev.324

Frank, M., & Goodrich, L. (2018). Talking back: development of the olivocochlear efferent system. *Wiley Interdiscip Rev Dev Biol*, *6*. https://doi.org/10.1002/wdev.324

Froud, K. E., Wong, A. C. Y., Cederholm, J. M. E., Klugmann, M., Sandow, S. L., Julien, J.-P., Ryan, A. F., & Housley, G. D. (2015). Type II spiral ganglion afferent neurons drive medial olivocochlear reflex suppression of the cochlear amplifier. *Nature Communications*, *6*(1), 7115. https://doi.org/10.1038/ncomms8115

Furness, D. N., & Hackney, C. M. (1986). High-resolution scanning-electron microscopy of stereocilia using the osmium-thiocarbohydrazide coating technique. *Hearing Research*, *21*(3), 243–249. https://doi.org/https://doi.org/10.1016/0378-5955(86)90222-4

Furness, D. N., Katori, Y., Nirmal Kumar, B., & Hackney, C. M. (2008). The dimensions and structural attachments of tip links in mammalian cochlear hair cells and the effects of exposure to different levels of extracellular calcium. *Neuroscience*, *154*(1), 10–21. https://doi.org/https://doi.org/10.1016/j.neuroscience.2008.02.010

Geller, S. F., Guerin, K. I., Visel, M., Pham, A., Lee, E. S., Dror, A. A., Avraham, K. B., Hayashi, T., Ray, C. A., Reh, T. A., Bermingham-McDonogh, O., Triffo, W. J., Bao, S., Isosomppi, J., Västinsalo, H., Sankila, E. M., & Flannery, J. G. (2009). CLRN1 Is Nonessential in the Mouse Retina but Is Required for Cochlear Hair Cell Development. *PLoS Genetics*, *5*(8), 1000607. https://doi.org/10.1371/JOURNAL.PGEN.1000607

Gentry, H. R., Singer, A. U., Betts, L., Yang, C., Ferrara, J. D., Sondek, J., & Parise, L. v. (2005). Structural and Biochemical Characterization of CIB1 Delineates a New Family of EF-hand-containing Proteins. *Journal of Biological Chemistry* , *280*(9), 8407–8415. https://doi.org/10.1074/jbc.M411515200

Gibson, F., Walsh, J., Mburu, P., Varela, A., Brown, K. A., Antonio, M., Beisel, K. W., Steel, K. P., & Brown, S. D. M. (1995). A type VII myosin encoded by the mouse deafness gene shaker-1. *Nature*, *374*(6517), 62–64. https://doi.org/10.1038/374062a0

Giese, A. P. J., Tang, Y.-Q., Sinha, G. P., Bowl, M. R., Goldring, A. C., Parker, A., Freeman, M. J., Brown, S. D. M., Riazuddin, S., Fettiplace, R., Schafer, W. R., Frolenkov, G. I., & Ahmed, Z. M. (2017). CIB2 interacts with TMC1 and TMC2 and is essential for mechanotransduction in auditory hair cells. *Nature Communications*, *8*(1), 43. https://doi.org/10.1038/s41467-017-00061-1

Gillespie, P. G., & Cyr, J. L. (2004). Myosin-1c, the Hair Cell's Adaptation Motor. *Annual Review of Physiology*, *66*(1), 521–545. https://doi.org/10.1146/annurev.physiol.66.032102.112842

Gillespie, P. G., & Hudspeth, A. J. (1993). Adenine nucleoside diphosphates block adaptation of mechanoelectrical transduction in hair cells. *Proceedings of the National Academy of Sciences of the United States of America*, *90*(7), 2710–2714. https://doi.org/10.1073/pnas.90.7.2710

Gillespie, P. G., Wagner, M. C., & Hudspeth, A. J. (1993). Identification of a 120 kd hair-bundle myosin located near stereociliary tips. *Neuron*, *11*(4), 581–594. https://doi.org/https://doi.org/10.1016/0896-6273(93)90071-X

Glowatzki, E., & Fuchs, P. A. (2002). Transmitter release at the hair cell ribbon synapse. *Nature Neuroscience*, *5*(2), 147–154. https://doi.org/10.1038/nn796

Goldring, A. C., Beurg, M., & Fettiplace, R. (2019). The contribution of TMC1 to adaptation of mechanoelectrical transduction channels in cochlear outer hair cells. *The Journal of Physiology*, *597*(24), 5949–5961. https://doi.org/10.1113/JP278799

Goodyear, R. J., Marcotti, W., Kros, C. J., & Richardson, G. P. (2005). Development and properties of stereociliary link types in hair cells of the mouse cochlea. *Journal of Comparative Neurology*, *485*(1), 75–85. https://doi.org/10.1002/cne.20513

Goutman, J. D., Elgoyhen, A. B., & Gómez-Casati, M. E. (2015). Cochlear hair cells: The sound-sensing machines. *FEBS Letters*, *589*(22), 3354–3361. https://doi.org/10.1016/j.febslet.2015.08.030

Gowri D., N., Ratnayaka, H. S. K., Goodyear, R. J., & Richardson, G. P. (2007). Development of the hair bundle and mechanotransduction. *International Journal of Developmental Biology*, *51*(6–7), 597–608. https://doi.org/10.1387/ijdb.072392gn.

Grati, M., & Kachar, B. (2011). Myosin VIIa and sans localization at stereocilia upper tip-link density implicates these Usher syndrome proteins in mechanotransduction. *Proceedings of the National Academy of Sciences of the United States of America*, *108*(28), 11476–11481. https://doi.org/10.1073/pnas.1104161108

Grillet, N., Xiong, W., Reynolds, A., Kazmierczak, P., Sato, T., Lillo, C., Dumont, R. A., Hintermann, E., Sczaniecka, A., Schwander, M., Williams, D., Kachar, B., Gillespie, P. G., & Müller, U. (2009). Harmonin mutations cause mechanotransduction defects in cochlear hair cells. *Neuron*, *62*(3), 375–387. https://doi.org/10.1016/j.neuron.2009.04.006

Hasson, T., Gillespie, P. G., Garcia, J. A., MacDonald, R. B., Zhao, Y., Yee, A. G., Mooseker, M. S., & Corey, D. P. (1997). Unconventional Myosins in Inner-Ear Sensory Epithelia. *Journal of Cell Biology*, *137*(6), 1287–1307. https://doi.org/10.1083/jcb.137.6.1287

Hasson, T., Walsh, J., Cable, J., Mooseker, M. S., Brown, S. D. M., & Steel, K. P. (1997). Effects of shaker-1 mutations on myosin-VIIa protein and mRNA expression. *Cell Motility*, *37*(2), 127–138. https://doi.org/10.1002/(SICI)1097-0169(1997)37:2<127::AID-CM5>3.0.CO;2-5

Holt, J. R., Gillespie, S. K. H., Provance, D. W., Shah, K., Shokat, K. M., Corey, D. P., Mercer, J. A., & Gillespie, P. G. (2002). A Chemical-Genetic Strategy Implicates Myosin-1c in Adaptation by Hair Cells. *Cell*, *108*(3), 371–381. https://doi.org/https://doi.org/10.1016/S0092-8674(02)00629-3

Homma, K., & Dallos, P. (2011). Dissecting the electromechanical coupling mechanism of the motor-protein prestin. *Communicative & Integrative Biology*, *4*(4), 450–453. https://doi.org/10.4161/cib.4.4.15463

Houdusse, A., & Sweeney, H. L. (2016). How Myosin Generates Force on Actin Filaments. *Trends in Biochemical Sciences*, *41*(12), 989–997. https://doi.org/10.1016/j.tibs.2016.09.006

Housley, G. D., Marcotti, W., Navaratnam, D., & Yamoah, E. N. (2006). Hair Cells – Beyond the Transducer. *The Journal of Membrane Biology*, *209*(2), 89. https://doi.org/10.1007/s00232-005-0835-7

Howard, J., & Hudspeth, A. J. (1987). Mechanical relaxation of the hair bundle mediates adaptation in mechanoelectrical transduction by the bullfrog's saccular hair cell. *Proceedings of the National Academy of Sciences of the United States of America*, *84*(9), 3064–3068. https://doi.org/10.1073/pnas.84.9.3064

Howard, J., & Hudspeth, A. J. (1988). Compliance of the hair bundle associated with gating of mechanoelectrical transduction channels in the Bullfrog's saccular hair cell. *Neuron*, *1*(3), 189–199. https://doi.org/https://doi.org/10.1016/0896-6273(88)90139-0

Jacques, B. E., Puligilla, C., Weichert, R. M., Ferrer-Vaquer, A., Hadjantonakis, A.-K., Kelley, M. W., & Dabdoub, A. (2012). A dual function for canonical Wnt/β-catenin signaling in the developing mammalian cochlea. *Development (Cambridge, England)*, *139*(23), 4395–4404. https://doi.org/10.1242/dev.080358

Jarman, A. P., Grell, E. H., Ackerman, L., Jan, L. Y., & Jan, Y. N. (1994). atonal is the proneural gene for Drosophila photoreceptors. *Nature*, *369*(6479), 398–400. https://doi.org/10.1038/369398a0

Jeng, J. Y., Carlton, A. J., Johnson, S. L., Brown, S. D. M., Holley, M. C., Bowl, M. R., & Marcotti, W. (2021). Biophysical and morphological changes in inner hair cells and their efferent innervation in the ageing mouse cochlea. *The Journal of Physiology*, *599*(1), 269–287. https://doi.org/10.1113/JP280256

Jeng, J.-Y., Harasztosi, C., Carlton, A. J., Corns, L. F., Marchetta, P., Johnson, S. L., Goodyear, R. J., Legan, K. P., Rüttiger, L., Richardson, G. P., & Marcotti, W. (2021). MET currents and otoacoustic emissions from mice with a detached tectorial membrane indicate the extracellular matrix regulates Ca2+ near stereocilia. *The Journal of Physiology*, *599*(7), 2015–2036. https://doi.org/https://doi.org/10.1113/JP280905

Johnson, S. L., Beurg, M., Marcotti, W., & Fettiplace, R. (2011). Prestin-driven cochlear amplification is not limited by the outer hair cell membrane time constant. *Neuron*, *70*(6), 1143–1154. https://doi.org/10.1016/j.neuron.2011.04.024

Kandler, K., Clause, A., & Noh, J. (2009). Tonotopic reorganization of developing auditory brainstem circuits. *Nature Neuroscience*, *12*(6), 711–717. https://doi.org/10.1038/nn.2332

Karniski, L. P., Lötscher, M., Fucentese, M., Hilfiker, H., Biber, J., & Murer, H. (1998). Immunolocalization of sat-1 sulfate/oxalate/bicarbonate anion exchanger in the rat kidney. *American Journal of Physiology-Renal Physiology*, *275*(1), F79–F87. https://doi.org/10.1152/ajprenal.1998.275.1.F79

Kawashima, Y., Géléoc, G. S. G., Kurima, K., Labay, V., Lelli, A., Asai, Y., Makishima, T., Wu, D. K., della Santina, C. C., Holt, J. R., & Griffith, A. J. (2011). Mechanotransduction in mouse inner ear hair cells requires transmembrane channel-like genes. *The Journal of Clinical Investigation*, *121*(12), 4796–4809. https://doi.org/10.1172/JCI60405

Kelly, J. B., & Sally, S. L. (1988). Organization of auditory cortex in the albino rat: binaural response properties. *Journal of Neurophysiology*, *59*(6), 1756–1769. https://doi.org/10.1152/jn.1988.59.6.1756

Kikkawa, Y., Shitara, H., Wakana, S., Kohara, Y., Takada, T., Okamoto, M., Taya, C., Kamiya, K., Yoshikawa, Y., Tokano, H., Kitamura, K., Shimizu, K., Wakabayashi, Y., Shiroishi, T., Kominami, R., & Yonekawa, H. (2003). Mutations in a new scaffold protein Sans cause deafness in Jackson shaker mice. *Human Molecular Genetics*, *12*(5), 453–461. https://doi.org/10.1093/hmg/ddg042

Kikuchi, K., & Hilding, D. A. (1965). The Defective Organ of Corti in Shaker-1 Mice. *Acta Oto-Laryngologica*, *60*(1–6), 287–303. https://doi.org/10.3109/00016486509127014

Kim, H., Kim, M., Im, S.-K., & Fang, S. (2018). Mouse Cre-LoxP system: general principles to determine tissue-specific roles of target genes. *Laboratory Animal Research*, *34*(4), 147–159. https://doi.org/10.5625/lar.2018.34.4.147

Kim, K. X., & Fettiplace, R. (2013). Developmental changes in the cochlear hair cell mechanotransducer channel and their regulation by transmembrane channel-like proteins. *The Journal of General Physiology*, *141*(1), 141–148. https://doi.org/10.1085/jgp.201210913

Koffler, T., Ushakov, K., & Avraham, K. B. (2015). Genetics of Hearing Loss: Syndromic. *Otolaryngologic Clinics of North America*, *48*(6), 1041–1061. https://doi.org/10.1016/j.otc.2015.07.007

Koschak, A., Reimer, D., Huber, I., Grabner, M., Glossmann, H., Engel, J., & Striessnig, J. (2001). α1D (Cav1.3) Subunits Can Form L-type Ca2+ Channels Activating at Negative Voltages. *Journal of Biological Chemistry*, *276*(25), 22100–22106. https://doi.org/10.1074/JBC.M101469200

Kros, C. J., Marcotti, W., van Netten, S. M., Self, T. J., Libby, R. T., Brown, S. D. M., Richardson, G. P., & Steel, K. P. (2002). Reduced climbing and increased slipping adaptation in cochlear hair cells of mice with Myo7a mutations. *Nature Neuroscience*, *5*, 41. http://dx.doi.org/10.1038/nn784

Kros, C. J., Ruppersberg, J. P., & Rüsch, A. (1998). Expression of a potassium current in inner hair cells during development of hearing in mice. *Nature*, *394*(6690), 281–284. https://doi.org/10.1038/28401

Laine, H., Doetzlhofer, A., Mantela, J., Ylikoski, J., Laiho, M., Roussel, M. F., Segil, N., & Pirvola, U. (2007). p19(Ink4d) and p21(Cip1) collaborate to maintain the postmitotic state of auditory hair cells, their codeletion leading to DNA damage and p53-mediated apoptosis. *The Journal of Neuroscience : The Official Journal of the Society for Neuroscience*, *27*(6), 1434–1444. https://doi.org/10.1523/JNEUROSCI.4956-06.2007

Lee, Y.-S., Liu, F., & Segil, N. (2006). A morphogenetic wave of p27Kip1 transcription directs cell cycle exit during organ of Corti development. *Development (Cambridge, England)*, *133*, 2817–2826. https://doi.org/10.1242/dev.02453

Lefèvre, G., Michel, V., Weil, D., Lepelletier, L., Bizard, E., Wolfrum, U., Hardelin, J.-P., & Petit, C. (2008). A core cochlear phenotype in USH1 mouse mutants implicates fibrous links of the hair bundle in its cohesion, orientation and differential growth. *Development*, *135*(8), 1427 LP – 1437. http://dev.biologists.org/content/135/8/1427.abstract

Li, S., Mecca, A., Kim, J., Caprara, G. A., Wagner, E. L., Du, T. T., Petrov, L., Xu, W., Cui, R., Rebustini, I. T., Kachar, B., Peng, A. W., & Shin, J. B. (2020). Myosin-VIIa is expressed in

multiple isoforms and essential for tensioning the hair cell mechanotransduction complex. *Nature Communications*, *11*(1). https://doi.org/10.1038/S41467-020-15936-Z

Liu, C., Glowatzki, E., & Fuchs, P. A. (2015). Unmyelinated type II afferent neurons report cochlear damage. *Proceedings of the National Academy of Sciences of the United States of America*, *112*(47), 14723–14727. https://doi.org/10.1073/pnas.1515228112

Liu, X. Z., Hope, C., Walsh, J., Newton, V., Xiao Mei Ke, Chuan Yu Liang, Li Ron Xu, Jiu Mu Zhou, Trump, D., Steel, K. P., Bundey, S., & Brown, S. D. M. (1998). Mutations in the Myosin VIIA Gene Cause a Wide Phenotypic Spectrum, Including Atypical Usher Syndrome. *The American Journal of Human Genetics*, *63*(3), 909–912. https://doi.org/10.1086/302026

Lohi, H., Kujala, M., Kerkelä, E., Saarialho-Kere, U., Kestilä, M., & Kere, J. (2000). Mapping of Five New Putative Anion Transporter Genes in Human and Characterization of SLC26A6, A Candidate Gene for Pancreatic Anion Exchanger. *Genomics*, *70*(1), 102–112. https://doi.org/https://doi.org/10.1006/geno.2000.6355

Lord, E., & Gates, W. H. (1929). Shaker, a new mutation of the house mouse (Mus musculus). *The Americal Naturalist*, *63*(688), 435–442.

Mahendrasingam, S., Fettiplace, R., Alagramam, K. N., Cross, E., & Furness, D. N. (2017). Spatiotemporal changes in the distribution of LHFPL5 in mice cochlear hair bundles during development and in the absence of PCDH15. *PLOS ONE*, *12*(10), e0185285. https://doi.org/10.1371/journal.pone.0185285

Manor, U., & Kachar, B. (2008). Dynamic length regulation of sensory stereocilia. *Seminars in Cell & Developmental Biology*, *19*(6), 502–510. https://doi.org/10.1016/j.semcdb.2008.07.006

Marcotti, W., Corns, L. F., Desmonds, T., Kirkwood, N. K., Richardson, G. P., & Kros, C. J. (2014). Transduction without tip links in cochlear hair cells is mediated by ion channels with permeation properties distinct from those of the mechano-electrical transducer channel. *The Journal of Neuroscience : The Official Journal of the Society for Neuroscience*, *34*(16), 5505–5514. https://doi.org/10.1523/JNEUROSCI.4086-13.2014

Marcotti, W., Johnson, S. L., Holley, M. C., & Kros, C. J. (2003). Developmental changes in the expression of potassium currents of embryonic, neonatal and mature mouse inner hair

cells. *The Journal of Physiology*, *548*(Pt 2), 383–400. https://doi.org/10.1113/jphysiol.2002.034801

Marcotti, W., Johnson, S. L., & Kros, C. J. (2004a). Effects of intracellular stores and extracellular Ca(2+) on Ca(2+)-activated K(+) currents in mature mouse inner hair cells. *The Journal of Physiology*, *557*(Pt 2), 613–633. https://doi.org/10.1113/jphysiol.2003.060137

Marcotti, W., Johnson, S. L., & Kros, C. J. (2004b). A transiently expressed SK current sustains and modulates action potential activity in immature mouse inner hair cells. *The Journal of Physiology*, *560*(Pt 3), 691–708. https://doi.org/10.1113/jphysiol.2004.072868

Marcotti, W., Johnson, S. L., Rusch, A., & Kros, C. J. (2003). Sodium and calcium currents shape action potentials in immature mouse inner hair cells. *The Journal of Physiology*, *552*(Pt 3), 743–761. https://doi.org/10.1113/jphysiol.2003.043612

Marcotti, W., & Kros, C. J. (1999). Developmental expression of the potassium current IK,n contributes to maturation of mouse outer hair cells. *The Journal of Physiology*, *520 Pt 3*(Pt 3), 653–660. https://doi.org/10.1111/j.1469-7793.1999.00653.x

Marcus, D. C., Wu, T., Wangemann, P., & Kofuji, P. (2002). KCNJ10 (Kir4.1) potassium channel knockout abolishes endocochlear potential. *American Journal of Physiology-Cell Physiology*, *282*(2), C403–C407. https://doi.org/10.1152/ajpcell.00312.2001

Masterton, B., Diamond, I. T., Harrison, J. M., & Beecher, M. D. (1967). Medial superior olive and sound localization. *Science (New York, N.Y.)*, *155*(3770), 1696–1697. https://doi.org/10.1126/science.155.3770.1696-a

Mathur, P., & Yang, J. (2015). Usher syndrome: Hearing loss, retinal degeneration and associated abnormalities. *Biochimica et Biophysica Acta*, *1852*(3), 406–420. https://doi.org/10.1016/j.bbadis.2014.11.020

Mburu, P., Liu, X. Z., Walsh, J., Saw, D., Cope, M., Gibson, F., Kendrick-Jones, J., Steel, K., & Brown, S. (1997). Mutation analysis of the mouse myosin VIIA deafness gene. *Genes and Function*, *1*(3), 191–203. https://doi.org/10.1046/j.1365-4624.1997.00020.x

Meyer, A. C., Frank, T., Khimich, D., Hoch, G., Riedel, D., Chapochnikov, N. M., Yarin, Y. M., Harke, B., Hell, S. W., Egner, A., & Moser, T. (2009). Tuning of synapse number, structure and function in the cochlea. *Nature Neuroscience*, *12*(4), 444–453. https://doi.org/10.1038/nn.2293

Michna, M., Knirsch, M., Hoda, J.-C., Muenkner, S., Langer, P., Platzer, J., Striessnig, J., & Engel, J. (2003). Cav1.3 (alpha1D) Ca2+ currents in neonatal outer hair cells of mice. *The Journal of Physiology*, *553*(Pt 3), 747–758. https://doi.org/10.1113/jphysiol.2003.053256

Naz, S., Giguere, C. M., Kohrman, D. C., Mitchem, K. L., Riazuddin, S., Morell, R. J., Ramesh, A., Srisailpathy, S., Deshmukh, D., Riazuddin, S., Griffith, A. J., Friedman, T. B., Smith, R. J. H., & Wilcox, E. R. (2002). Mutations in a novel gene, TMIE, are associated with hearing loss linked to the DFNB6 locus. *American Journal of Human Genetics*, *71*(3), 632–636. https://doi.org/10.1086/342193

NIDCD. (2017). *Usher syndrome*. https://www.nidcd.nih.gov/health/usher-syndrome

Odermatt, B., & Lagnado, L. (2009). *Ribbon Synapses* (L. R. B. T.-E. of N. Squire, Ed.; pp. 373–381). Academic Press. https://doi.org/https://doi.org/10.1016/B978-008045046-9.00923-2

Oghalai, J. S. (2004). The cochlear amplifier: augmentation of the traveling wave within the inner ear. *Current Opinion in Otolaryngology & Head and Neck Surgery*, *12*(5), 431. https://doi.org/10.1097/01.MOO.0000134449.05454.82

Ogun, O., & Zallocchi, M. (2014). Clarin-1 acts as a modulator of mechanotransduction activity and presynaptic ribbon assembly. *The Journal of Cell Biology*, *207*(3), 375–391. https://doi.org/10.1083/jcb.201404016

Paluch, E. K., Nelson, C. M., Biais, N., Fabry, B., Moeller, J., Pruitt, B. L., Wollnik, C., Kudryasheva, G., Rehfeldt, F., & Federle, W. (2015). Mechanotransduction: use the force(s). *BMC Biology*, *13*, 47. https://doi.org/10.1186/s12915-015-0150-4

Pan, B., Askew, C., Galvin, A., Heman-Ackah, S., Asai, Y., Indzhykulian, A. A., Jodelka, F. M., Hastings, M. L., Lentz, J. J., Vandenberghe, L. H., Holt, J. R., & Géléoc, G. S. (2017). Gene therapy restores auditory and vestibular function in a mouse model of Usher syndrome type 1c. *Nature Biotechnology*, *35*(3), 264–272. https://doi.org/10.1038/nbt.3801

Pan, B., Géléoc, G. S., Asai, Y., Horwitz, G. C., Kurima, K., Ishikawa, K., Kawashima, Y., Griffith, A. J., & Holt, J. R. (2013). TMC1 and TMC2 are components of the mechanotransduction channel in hair cells of the mammalian inner ear. *Neuron*, *79*(3), 504–515. https://doi.org/10.1016/j.neuron.2013.06.019

Pan, N., Jahan, I., Kersigo, J., Kopecky, B., Santi, P., Johnson, S., Schmitz, H., & Fritzsch, B. (2011). Conditional deletion of Atoh1 using Pax2-Cre results in viable mice without differentiated cochlear hair cells that have lost most of the organ of Corti. *Hearing Research*, *275*(1–2), 66–80. https://doi.org/10.1016/j.heares.2010.12.002

Patuzzi, R., & Robertson, D. (1988). Tuning in the mammalian cochlea. *Physiological Reviews*, *68*(4), 1009–1082. https://doi.org/10.1152/physrev.1988.68.4.1009

Pickles, J. O. (2015). *Auditory pathways* (Vol. 129). Elsevier Health Sciences. https://doi.org/10.1016/B978-0-444-62630-1.00001-9

Pickles, J. O., Comis, S. D., & Osborne, M. P. (1984). Cross-links between stereocilia in the guinea pig organ of Corti, and their possible relation to sensory transduction. *Hearing Research*, *15*(2), 103–112. https://doi.org/https://doi.org/10.1016/0378-5955(84)90041-8

Pujol, R., Lavigne-Rebillard, M., & Lenoir, M. (1998). *Development of Sensory and Neural Structures in the Mammalian Cochlea BT - Development of the Auditory System* (E. W. Rubel, A. N. Popper, & R. R. Fay, Eds.; pp. 146–192). Springer New York. https://doi.org/10.1007/978-1-4612-2186-9_4

Purves, D., Augustine, G., & Fitzpatrick, D. (2001). *Neuroscience* (2nd editio). Sinauer Associates. https://www.ncbi.nlm.nih.gov/books/NBK10867/

Raphael, Y., & Altschuler, R. A. (2003). Structure and innervation of the cochlea. *Brain Research Bulletin*, *60*(5), 397–422. https://doi.org/https://doi.org/10.1016/S0361-9230(03)00047-9

Ren, T., He, W., & Gillespie, P. G. (2011). Measurement of cochlear power gain in the sensitive gerbil ear. *Nature Communications*, *2*, 216. https://doi.org/10.1038/ncomms1226

Riazuddin, S., Belyantseva, I. A., Giese, A. P. J., Lee, K., Indzhykulian, A. A., Nandamuri, S. P., Yousaf, R., Sinha, G. P., Lee, S., Terrell, D., Hegde, R. S., Ali, R. A., Anwar, S., Andrade-Elizondo, P. B., Sirmaci, A., Parise, L. v, Basit, S., Wali, A., Ayub, M., … Ahmed, Z. M. (2012). Alterations of the CIB2 calcium- and integrin-binding protein cause Usher syndrome type 1J and nonsyndromic deafness DFNB48. *Nature Genetics*, *44*(11), 1265–1271. https://doi.org/10.1038/ng.2426

Ricci, A. J., Wu, Y. C., & Fettiplace, R. (1998). The endogenous calcium buffer and the time course of transducer adaptation in auditory hair cells. *The Journal of Neuroscience : The Official Journal of the Society for Neuroscience*, *18*(20), 8261–8277. https://doi.org/10.1523/JNEUROSCI.18-20-08261.1998

Sahly, I., El-Amraoui, A., Abitbol, M., Petit, C., & Dufier, J.-L. (1997). Expression of myosin VIIA during mouse embryogenesis. *Anatomy and Embryology*, *196*(2), 159–170. https://doi.org/10.1007/s004290050088

Sato, O., Komatsu, S., Sakai, T., Tsukasaki, Y., Tanaka, R., Mizutani, T., Watanabe, T. M., Ikebe, R., & Ikebe, M. (2017). Human myosin VIIa is a very slow processive motor protein on various cellular actin structures. *The Journal of Biological Chemistry*, *292*(26), 10950–10960. https://doi.org/10.1074/jbc.M116.765966

Saw Jr., D., Steel, K. P., & Brown, S. D. (1997). Shaker mice and a peek into the House of Usher. *Exp Anim*, *46*(1), 1–9. https://doi.org/10.1538/expanim.46.1

Scheffer, D. I., Shen, J., Corey, D. P., & Chen, Z.-Y. (2015). Gene Expression by Mouse Inner Ear Hair Cells during Development. *The Journal of Neuroscience*, *35*(16), 6366 LP – 6380. https://doi.org/10.1523/JNEUROSCI.5126-14.2015

Schnupp, J., Nelken, I., & King, A. (2011). *Auditory neuroscience*. MIT Press.

Schwander, M., Kachar, B., & Müller, U. (2010). Review series: The cell biology of hearing. *The Journal of Cell Biology*, *190*(1), 9–20. https://doi.org/10.1083/jcb.201001138

Self, T., Mahony, M., Fleming, J., Walsh, J., Brown, S. D., & Steel, K. P. (1998). Shaker-1 mutations reveal roles for myosin VIIA in both development and function of cochlear hair cells. *Development (Cambridge, England)*, *125*(4), 557–566. http://www.ncbi.nlm.nih.gov/pubmed/9435277

Shnerson, A., Lenoir, M., van de Water, T. R., & Pujol, R. (1983). The pattern of sensorineural degeneration in the cochlea of the deaf shaker-1 mouse: Ultrastructural observations. *Developmental Brain Research*, *9*(3), 305–315. https://doi.org/https://doi.org/10.1016/0165-3806(83)90028-7

Siththanandan, V. B., & Sellers, J. R. (2011). Regulation of myosin 5a and myosin 7a. *Biochemical Society Transactions*, *39*(5), 1136–1141. https://doi.org/10.1042/BST0391136

Sobin, A., & Flock, Å. (1983). Immunohistochemical Identification and Localization of Actin and Fimbrin in Vestibular Hair Cells in the Normal Guinea Pig and in A Strain of the Waltzing Guinea Pig. *Acta Oto-Laryngologica*, *96*(5–6), 407–412. https://doi.org/10.3109/00016488309132726

Spoendlin, H. (1981). Differentiation of Cochlear Afferent Neurons. *Acta Oto-Laryngologica*, *91*(1–6), 451–456. https://doi.org/10.3109/00016488109138527

Stauffer, E. A., & Holt, J. R. (2007). Sensory Transduction and Adaptation in Inner and Outer Hair Cells of the Mouse Auditory System. *Journal of Neurophysiology*, *98*(6), 3360–3369. https://doi.org/10.1152/jn.00914.2007

Steel, K. P., & Barkway, C. (1989). Another role for melanocytes: their importance for normal stria vascularis development in the mammalian inner ear. *Development*, *107*(3), 453 LP – 463. http://dev.biologists.org/content/107/3/453.abstract

Sun, J. C., van Alphen, A. M., Wagenaar, M., Huygen, P., Hoogenraad, C. C., Hasson, T., Koekkoek, S. K. E., Bohne, B. A., & de Zeeuw, C. I. (2001). Origin of Vestibular Dysfunction in Usher Syndrome Type 1B. *Neurobiology of Disease*, *8*(1), 69–77. https://doi.org/https://doi.org/10.1006/nbdi.2000.0358

Tasaki, I., & Spyropoulos, C. S. (1959). Stria vascularis as source of endocochlear potential. *Journal of Neurophysiology*, *22*(2), 149–155. https://doi.org/10.1152/jn.1959.22.2.149

Tilney, L. G., Tilney, M. S., & DeRosier, D. J. (1992). Actin Filaments, Stereocilia, and Hair Cells: How Cells Count and Measure. *Annual Review of Cell Biology*, *8*(1), 257–274. https://doi.org/10.1146/annurev.cb.08.110192.001353

Várkuti, B. H., Yang, Z., Kintses, B., Erdélyi, P., Bárdos-Nagy, I., Kovács, A. L., Hári, P., Kellermayer, M., Vellai, T., & Málnási-Csizmadia, A. (2012). A novel actin binding site of myosin required for effective muscle contraction. *Nature Structural & Molecular Biology 2012 19:3*, *19*(3), 299–306. https://doi.org/10.1038/nsmb.2216

Västinsalo, H., Jalkanen, R., Dinculescu, A., Isosomppi, J., Geller, S., Flannery, J. G., Hauswirth, W. W., & Sankila, E. M. (2011). Alternative splice variants of the USH3A gene Clarin 1 (CLRN1). *European Journal of Human Genetics*, *19*(1), 30. https://doi.org/10.1038/EJHG.2010.140

Vélez-Ortega, A. C., Freeman, M. J., Indzhykulian, A. A., Grossheim, J. M., & Frolenkov, G. I. (2017). Mechanotransduction current is essential for stability of the transducing stereocilia in mammalian auditory hair cells. *ELife*, *6*, e24661. https://doi.org/10.7554/eLife.24661

Vona, B., Mazaheri, N., Lin, S. J., Dunbar, L. A., Maroofian, R., Azaiez, H., Booth, K. T., Vitry, S., Rad, A., Rüschendorf, F., Varshney, P., Fowler, B., Beetz, C., Alagramam, K. N., Murphy, D., Shariati, G., Sedaghat, A., Houlden, H., Petree, C., … Galehdari, H. (2021). A biallelic variant in CLRN2 causes non-syndromic hearing loss in humans. *Human Genetics*, *140*(6), 915. https://doi.org/10.1007/S00439-020-02254-Z

Vreugde, S., Erven, A., Kros, C. J., Marcotti, W., Fuchs, H., Kurima, K., Wilcox, E. R., Friedman, T. B., Griffith, A. J., Balling, R., Hrabé de Angelis, M., Avraham, K. B., & Steel, K. P. (2002). Beethoven, a mouse model for dominant, progressive hearing loss DFNA36. *Nature Genetics*, *30*(3), 257–258. https://doi.org/10.1038/ng848

Walker, R. G., & Hudspeth, A. J. (1996). Calmodulin controls adaptation of mechanoelectrical transduction by hair cells of the bullfrog's sacculus. *Proceedings of the National Academy of Sciences of the United States of America*, *93*(5), 2203–2207. https://doi.org/10.1073/pnas.93.5.2203

Wan, G., Corfas, G., & Stone, J. S. (2013). Inner ear supporting cells: rethinking the silent majority. *Seminars in Cell & Developmental Biology*, *24*(5), 448–459. https://doi.org/10.1016/j.semcdb.2013.03.009

Wangemann, P., Liu, J., & Marcus, D. C. (1995). Ion transport mechanisms responsible for K+ secretion and the transepithelial voltage across marginal cells of stria vascularis in vitro. *Hearing Research*, *84*(1), 19–29. https://doi.org/https://doi.org/10.1016/0378-5955(95)00009-S

Wangemann, P., & Schacht. (1996). Homeostasic mechanims in the cochlea. *Springer Handbook of Auditory Research: The Cochlea*, 130–185.

Warr, W. B., & Guinan, J. J. (1979). Efferent innervation of the organ of corti: two separate systems. *Brain Research*, *173*(1), 152–155. https://doi.org/https://doi.org/10.1016/0006-8993(79)91104-1

Well, D., Blanchard, S., Kaplan, J., Guilford, P., Gibson, F., Walsh, J., Mburu, P., Varela, A., Levilliers, J., Weston, M. D., Kelley, P. M., Kimberling, W. J., Wagenaar, M., Levi-Acobas, F., Larget-Piet, D., Munnich, A., Steel, K. P., Brown, S. D. M., & Petit, C. (1995). Defective myosin VIIA gene responsible for Usher syndrome type IB. *Nature*, *374*(6517).

Wolfrum, U., Liu, X., Schmitt, A., Udovichenko, I. P., & Williams, D. S. (1998). Myosin VIIa as a common component of cilia and microvilli. *Cell Motility*, *40*(3), 261–271. https://doi.org/10.1002/(SICI)1097-0169(1998)40:3<261::AID-CM5>3.0.CO;2-G

Wu, L., Pan, L., Wei, Z., & Zhang, M. (2011). Structure of MyTH4-FERM Domains in Myosin VIIa Tail Bound to Cargo. *Science*, *331*(6018), 757 LP – 760. https://doi.org/10.1126/science.1198848

Wu, Y.-C., Ricci, A. J., & Fettiplace, R. (1999). Two Components of Transducer Adaptation in Auditory Hair Cells. *Journal of Neurophysiology*, *82*(5), 2171–2181. https://doi.org/10.1152/jn.1999.82.5.2171

Wu, Z., Grillet, N., Zhao, B., Cunningham, C., Harkins-Perry, S., Coste, B., Ranade, S., Zebarjadi, N., Beurg, M., Fettiplace, R., Patapoutian, A., & Müller, U. (2017). Mechanosensory hair cells express two molecularly distinct mechanotransduction channels. *Nature Neuroscience*, *20*(1), 24–33. https://doi.org/10.1038/NN.4449

Xiong, A., Haithcock, J., Liu, Y., Eusner, L., McConnell, M., White, H. D., Belknap, B., & Forgacs, E. (2018). The shaker-1 mouse myosin VIIa deafness mutation results in a severely

reduced rate of the ATP hydrolysis step. *Journal of Biological Chemistry* , *293*(3), 819–829. https://doi.org/10.1074/jbc.M117.810119

Xiong, W., Grillet, N., Elledge, H. M., Wagner, T. F. J., Zhao, B., Johnson, K. R., Kazmierczak, P., & Müller, U. (2012). TMHS is an integral component of the mechanotransduction machinery of cochlear hair cells. *Cell*, *151*(6), 1283–1295. https://doi.org/10.1016/j.cell.2012.10.041

Yamoah, E. N., & Gillespie, P. G. (1996). Phosphate Analogs Block Adaptation in Hair Cells by Inhibiting Adaptation-Motor Force Production. *Neuron*, *17*(3), 523–533. https://doi.org/https://doi.org/10.1016/S0896-6273(00)80184-1

Yang, Y., Baboolal, T. G., Siththanandan, V., Chen, M., Walker, M. L., Knight, P. J., Peckham, M., & Sellers, J. R. (2009). A FERM domain autoregulates Drosophila myosin 7a activity. *Proceedings of the National Academy of Sciences of the United States of America*, *106*(11), 4189–4194. https://doi.org/10.1073/pnas.0808682106

Yu, I. M., Planelles-Herrero, V. J., Sourigues, Y., Moussaoui, D., Sirkia, H., Kikuti, C., Stroebel, D., Titus, M. A., & Houdusse, A. (2017). Myosin 7 and its adaptors link cadherins to actin. *Nature Communications*, *8*. https://doi.org/10.1038/NCOMMS15864

Zhao, B., Wu, Z., Grillet, N., Yan, L., Xiong, W., Harkins-Perry, S., & Müller, U. (2014). TMIE is an essential component of the mechanotransduction machinery of cochlear hair cells. *Neuron*, *84*(5), 954–967. https://doi.org/10.1016/j.neuron.2014.10.041